NAVAL POSTGRADUATE SCHOOL

MONTEREY, CALIFORNIA

THESIS

COMPUTATIONAL FLUID DYNAMICS MODELING OF A SUBMERGED BODY IN A TOW TANK WITH WAVE GENERATION

by

Tara J. Saladin

June 2020

Thesis Advisor: Young W. Kwon
Co-Advisor: Joseph Klamo

Approved for public release. Distribution is unlimited.

THIS PAGE INTENTIONALLY LEFT BLANK

REPORT DOCUMENTATION PAGE			*Form Approved OMB No. 0704-0188*

1. AGENCY USE ONLY *(Leave blank)*	**2. REPORT DATE** June 2020	**3. REPORT TYPE AND DATES COVERED** Master's thesis

4. TITLE AND SUBTITLE
COMPUTATIONAL FLUID DYNAMICS MODELING OF A SUBMERGED BODY IN A TOW TANK WITH WAVE GENERATION

5. FUNDING NUMBERS

6. AUTHOR(S) Tara J. Saladin

7. PERFORMING ORGANIZATION NAME(S) AND ADDRESS(ES)
Naval Postgraduate School
Monterey, CA 93943-5000

8. PERFORMING ORGANIZATION REPORT NUMBER

9. SPONSORING / MONITORING AGENCY NAME(S) AND ADDRESS(ES)
N/A

10. SPONSORING / MONITORING AGENCY REPORT NUMBER

11. SUPPLEMENTARY NOTES The views expressed in this thesis are those of the author and do not reflect the official policy or position of the Department of Defense or the U.S. Government.

12a. DISTRIBUTION / AVAILABILITY STATEMENT
Approved for public release. Distribution is unlimited.

12b. DISTRIBUTION CODE
A

13. ABSTRACT (maximum 200 words)

A computational fluid dynamics (CFD) model of the NPS tow tank with wave generation and a submerged body was created to investigate different methods of solid body modeling using commercial CFD software ANSYS CFX. A comparison of the rigid body method and immersed solid method was performed modeling a submerged rectangular body at different depths and different orientations. The models produced similar results when the body was lower beneath the wave surface with limited fluid-body interaction. As the amount of fluid-body interaction increased, the rigid body method showed increased amounts of wave energy dissipation as compared to the immersed solid method. This disruption of the wave energy resulted in the rigid body method showing lower body forces and moments when compared to the immersed solid model. The increased wave energy dissipation in the rigid body model is likely caused by the different mechanism for modeling body-fluid interaction. Future studies should compare the immersed solid modeling method results to experimental data and develop a CFD model with body motion.

14. SUBJECT TERMS computational fluid dynamics, CFD, wave generation, tow tank	**15. NUMBER OF PAGES** 91
	16. PRICE CODE

17. SECURITY CLASSIFICATION OF REPORT	**18. SECURITY CLASSIFICATION OF THIS PAGE**	**19. SECURITY CLASSIFICATION OF ABSTRACT**	**20. LIMITATION OF ABSTRACT**
Unclassified	Unclassified	Unclassified	UU

NSN 7540-01-280-5500 Standard Form 298 (Rev. 2-89)
Prescribed by ANSI Std. 239-18

THIS PAGE INTENTIONALLY LEFT BLANK

Approved for public release. Distribution is unlimited.

COMPUTATIONAL FLUID DYNAMICS MODELING OF A SUBMERGED BODY IN A TOW TANK WITH WAVE GENERATION

Tara J. Saladin
Lieutenant Commander, United States Navy
BS, Pennsylvania State University, 2008

Submitted in partial fulfillment of the
requirements for the degree of

MASTER OF SCIENCE IN MECHANICAL ENGINEERING

from the

NAVAL POSTGRADUATE SCHOOL
June 2020

Approved by: Young W. Kwon
Advisor

Joseph Klamo
Co-Advisor

Garth V. Hobson
Chair, Department of Mechanical and Aerospace Engineering

THIS PAGE INTENTIONALLY LEFT BLANK

ABSTRACT

A computational fluid dynamics (CFD) model of the NPS tow tank with wave generation and a submerged body was created to investigate different methods of solid body modeling using commercial CFD software ANSYS CFX. A comparison of the rigid body method and immersed solid method was performed modeling a submerged rectangular body at different depths and different orientations. The models produced similar results when the body was lower beneath the wave surface with limited fluid-body interaction. As the amount of fluid-body interaction increased, the rigid body method showed increased amounts of wave energy dissipation as compared to the immersed solid method. This disruption of the wave energy resulted in the rigid body method showing lower body forces and moments when compared to the immersed solid model. The increased wave energy dissipation in the rigid body model is likely caused by the different mechanism for modeling body-fluid interaction. Future studies should compare the immersed solid modeling method results to experimental data and develop a CFD model with body motion.

THIS PAGE INTENTIONALLY LEFT BLANK

TABLE OF CONTENTS

THIS PAGE INTENTIONALLY LEFT BLANK

LIST OF FIGURES

LIST OF TABLES

THIS PAGE INTENTIONALLY LEFT BLANK

ACKNOWLEDGMENTS

I would like to thank Professor Kwon for his continuous encouragement, patience, and optimism throughout my time at NPS. Without his guidance, I would not have learned a fraction of what I did, and this thesis would not exist. I would also like to thank Professor Klamo for constantly expanding my understanding and inspiring me to always strive to improve. The dedication of these individuals and the other NPS faculty to the continuous pursuit of knowledge and the development of students is commendable and something I aspire to as a leader.

THIS PAGE INTENTIONALLY LEFT BLANK

I. INTRODUCTION AND BACKGROUND

A. BACKGROUND AND MOTIVATION

The Department of Defense spends a considerable amount of money supporting testing and evaluation of defense acquisitions. In 2019, $94 billion was appropriated for research, development, test, and evaluation [1]. It was estimated that for 2015 the total cost of testing and evaluation within the Department of Defense was over $9 billion [2]. Test and evaluation is a crucial component of defense acquisition, as it provides information critical to determining if the program is meeting performance objectives. However, realistic modeling and simulation has the potential to significantly decrease test and evaluation costs while maintaining the technical rigor required to satisfy defense acquisition requirements.

Sea-based defense acquisitions often require evaluation of the hydrodynamic behavior of hull forms. Hydrodynamic evaluation often involves constructing various scale models depending on the level of required fidelity and testing them in an environment similar to the planned operating conditions. With increased focus on autonomy, the form of an unmanned underwater vehicle (UUV) may require hydrodynamic testing near the fluid surface while waves are also present. An accurate model of the equivalent environment with surface waves can reduce or remove the requirement to perform physical testing of the hull form.

B. PREVIOUS WORK AND LITERATURE REVIEW

1. Wave Behavior and Modeling

There exist two main concepts for the mathematical study of wave behavior. The most common is linearized wave theory. In linearized wave theory the wavelength is much less than the depth of the water and the wave amplitude is small compared to the wavelength such that the velocity components of the wave potential and the deviation of the free surface and the partial derivatives and any multiple or power thereof are negligible [3]. The alternate concept is nonlinear wave theory, often used to study wave behavior in shallow water. In this case, the deviation of the free surface and its partial derivatives are no longer small enough to be negligible, resulting in higher-order approximations. This

study will focus on linear wave theory. A Stokes wave, shown in Figure 1, is the solution for a two-dimensional symmetric, periodic wave governed by the conservation of mass and Euler's equations [4].

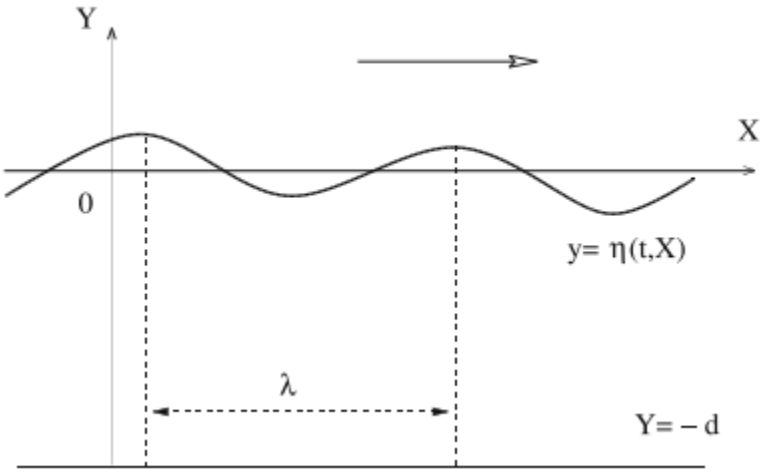

Figure 1. A Stokes wave. Source: [4].

The behavior of particles in a Stokes wave over a flat bed has been described by Constantin [4] based on the location of the particle. A particle initially located on the flat bed will remain at that height. It will initially travel opposing the direction of wave motion, then turn back into the direction of wave motion. It will pass the length of the period, but prior to the completion of the period it will again oppose the direction of wave motion to reach the final location one period past the initial starting point. The motion of a particle initially above the flat bed is similar with the exception that the particle will no longer remain fixed vertically. It will initially travel upward during the first backward motion, then during the ending part of the period the particle will travel downward. In the case of deep-water waves, the particles on the bed are not impacted by the wave; however, the above-bed particle trajectory is applicable and is depicted in Figure 2.

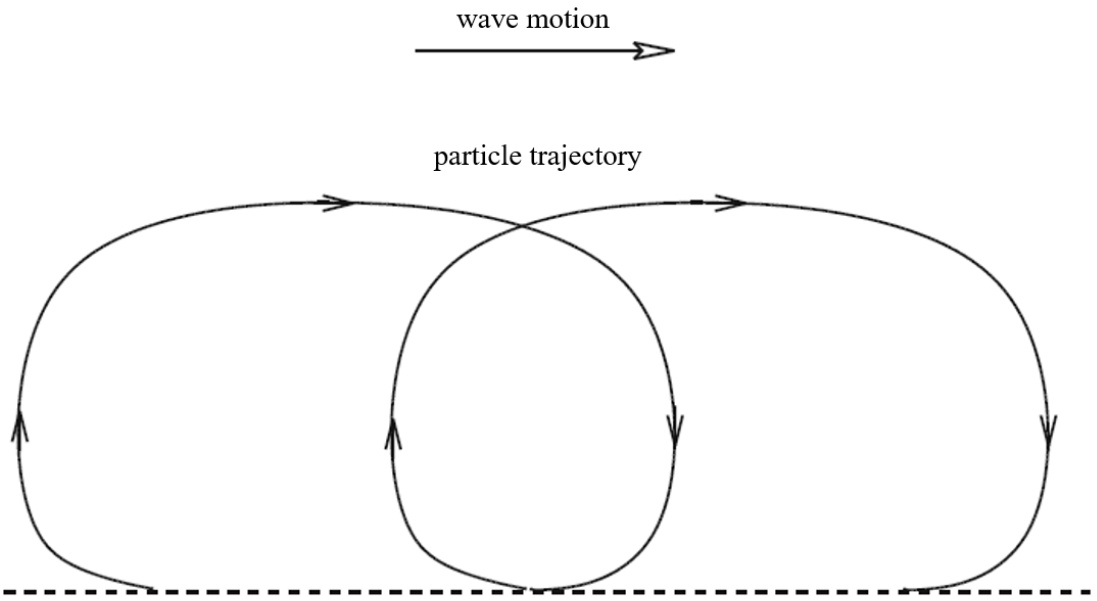

Figure 2. Stokes wave particle trajectory. Source: [4].

Finnegan and Goggins [5] used computational fluid dynamics (CFD) software ANSYS CFX to construct and analyze a two-dimensional model of the waves generated by a flap-type wavemaker in a sloped beach. Prasad et al. [6]. simulated waves in a three-dimensional numerical wave tank with attached turbine using ANSYS CFX and verified the model with experimental data. These studies demonstrated the suitability of commercial CFD software to generate accurate wave generation models.

2. NPS Tow Tank

The Naval Postgraduate School (NPS) tow tank, shown in Figure 3, is 10.97 meters long and equipped with an aluminum tow plate on two rails running the length of the tank.

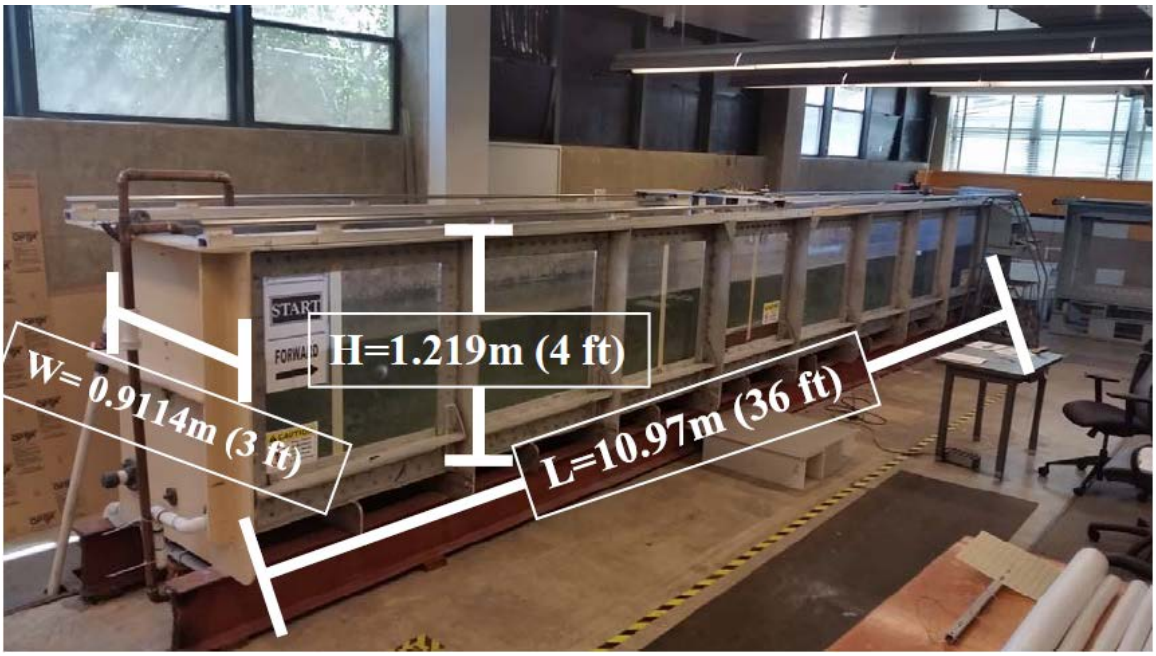

Figure 3. NPS tow tank. Source: [7].

In 2016, wave generation capability was added to the NPS tow tank by Tran [8] through the use of an aluminum wedge attached to a motorized plunger. The wave generation assembly is shown installed in the NPS tow tank in Figure 4. The aluminum wedge is oscillated vertically at an amplitude and frequency specified by the user and provided to the control software to produce the waveforms within the tank.

Figure 4. NPS tow tank wave generation assembly. Source: [9].

In 2017, efforts were made to accurately model the wave generating wedge and NPS tow tank in CFD Finite Element Analysis (FEA) software by Jones [10], [11]. The dimensions for the wedge geometry are shown in Figure 5.

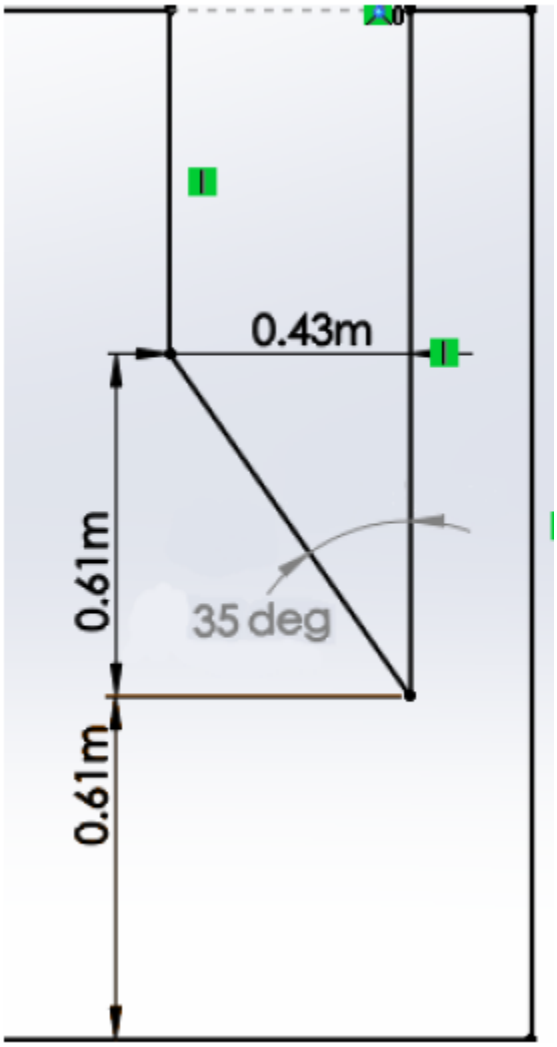

Figure 5. NPS tow tank wave generating wedge geometry. Source: [10].

Jones simulated the wedge wave generation by generating mesh motion of the angled wedge [10]. Wedge displacement was defined in accordance with Equation (1), where z is the wedge displacement, the exponential term models the motor ramp up, a_w is the wedge amplitude, f is the oscillation frequency, and ϕ is the phase.

$$z = \left(1 - e^{-3t^2}\right) a_w \sin\left(2\pi ft + \phi\right) \tag{1}$$

Jones then completed several modelling parametric studies on the mesh size, mesh shape, and transient model time step size to determine a preferred configuration.

Several experiments have been performed to measure wave loading on various submerged bodies within the NPS tow tank. Jones [10], [11] measured the forces on a square submerged body beneath the wave surface. Whitmer [9], [12] measured forces on a cylindrical tube with hemispheric end caps in order to validate the linear superposition of forces and moments from multiple waveforms and measure the low-frequency nonlinear loads. Turner [13], [14] tested hydrodynamic forms with square and rectangular parallel mid-bodies and determined that non-circular hull designs can either reduce or increase the wave-induced loads depending on the aspect ratio when operating near the surface. Suriben [15] tested the forces on cylindrical models with hemispheric and flat-faced endcaps to compare the test results with analytical solutions to assess the importance of viscous effects due to flow separation around the bow.

These experiments are examples of testing done in order to improve understanding of natural behavior and allow comparisons between experimental data and numerical models. Once an accurate model has been developed and validated, this model could then be used to reduce the amount of physical testing necessary to perform trade-off or conceptual studies for a new hydrodynamic form design. The reduction in physical testing would reduce the overall cost of a defense acquisition project.

C. OBJECTIVE

It is desirable to have an accurate model with a relatively short runtime that can be easily modified to change the hydrodynamic form that is being analyzed. This study compares different methods of modeling the submerged body within the NPS tow tank with wave generation to assess the impact different body modeling methods had on the CFD results. Additionally, an assessment of the impact of pitch angle on the submerged body loads was performed.

THIS PAGE INTENTIONALLY LEFT BLANK

II. NUMERICAL ANALYSIS SETUP

A. TOW TANK MODELING AND BOUNDARY CONDITIONS

In order to accomplish a finite element analysis, the simulation domain must be defined. For this analysis, the domain of the NPS tow tank was constructed using SOLIDWORKS 2018. In order to take advantage of symmetric conditions, thereby reducing the model size, only half the width of the tow tank was used in the domain. The wave generating wedge is the front wall of the tank and is constructed consistent with the physical wedge shape. The NPS tow tank SOLIDWORKS domain is shown in Figure 6.

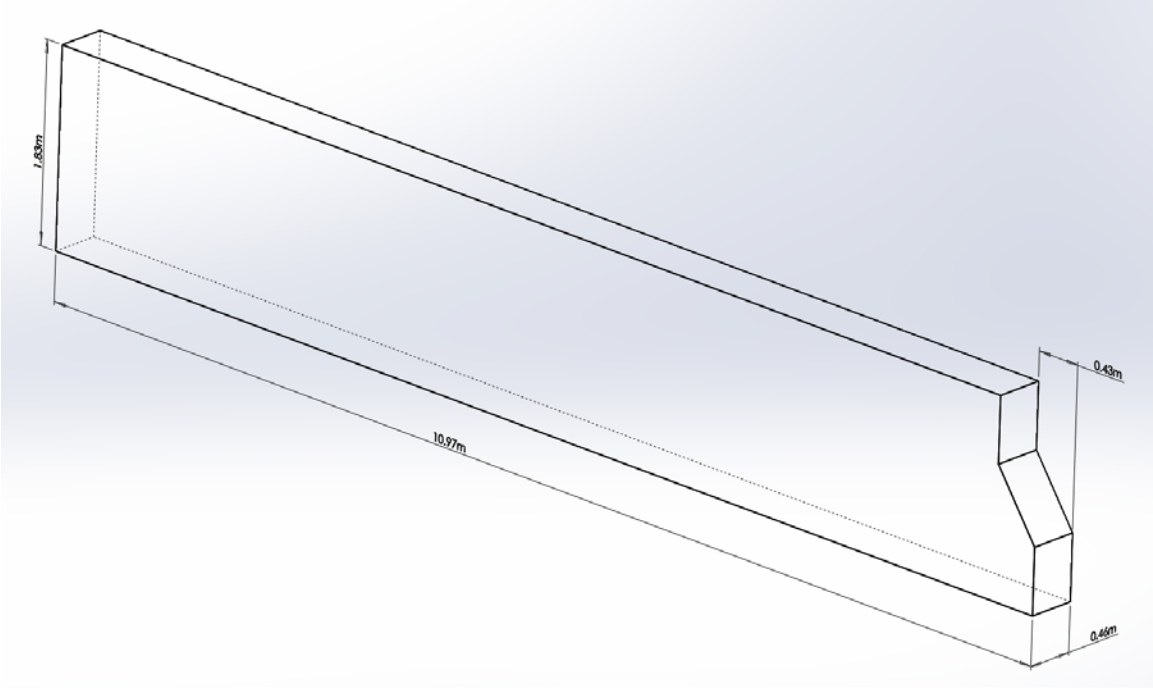

Figure 6. NPS tow tank SOLIDWORKS domain

The SOLIDWORKS model was then imported into ANSYS CFX Version 19.2. The bottom, outer side, and back of the tank were all modeled as smooth, no slip wall boundaries. Smooth boundaries were chosen for these faces as the tow tank is often used to simulate the conditions that would be present in a much larger environment. Therefore, it was desired to minimize the impact surface roughness on these faces causes to the fluid

behavior. The top of the tank was modelled as an opening with no relative pressure gradient. The wedge front of the tank was modeled as a no slip wall with a roughness of 0.01 millimeters. Additionally, the slanted wedge portion was stipulated to have mesh motion consistent to that used by Jones [10] in order to generate the water waves. For all models, a wedge motion amplitude of 0.0254 meters and frequency of 1 Hertz was used. This wedge motion generates a wave with a frequency of 1 Hertz and an average wave amplitude of 0.0175 meters as measured 1 meter downstream of the wedge.

The domain consisted of air at a density of 1.185 kg/m^3 and fresh water at a density of 997.0 kg/m^3 with an initial still water height of 0.9144 meters. The fluids were isothermal at 25°C, a reference pressure of 1 atmosphere was used, and the domain was a buoyant model with gravity set at 9.80665 m/s^2. The transient model was run using 0.01 second time-step increments, consistent with the recommended time-step size determined to yield accurate results by Jones [10]. The models were run for a total time of 12 seconds to prevent wave reflection interference from the back of the tank.

A homogeneous multiphase model was used to represent the fluid interactions, the k-ε turbulence model was used to account for any turbulence, and the transient algorithm used was second order backward Euler as an implicit time-stepping scheme.

B. BODY FORMATION

The model also includes a rectangular body that is submerged within the water beneath the waves at different depths and orientations. The rectangular body is 1.02 meters long, 0.1 meters high, and has a full width of 0.1 meters. However, the body was placed at centerline and again symmetry was used such that the modeled body width was 0.05 meters. The body was located within the tank such that the center of the body was 2.75 meters from the front of the tank and maintained fixed throughout the simulations. In order to model the body within ANSYS CFX, two different methods were used, the rigid body method and the immersed solid method.

1. Rigid Body Method

The rigid body method of body formation uses two-dimensional faces to define the body. The body itself is not meshed, instead the form of the body is removed from the modeled domain in SOLIDWORKS. All meshing is then done around this removed domain, which can make creating a stable mesh difficult, depending on the nature of the body. A model using the rigid body method of body formation is shown in Figure 7 with a detailed view shown in Figure 9. The rigid body method of body formation was used by Jones [10] in his modeling of the NPS tow tank.

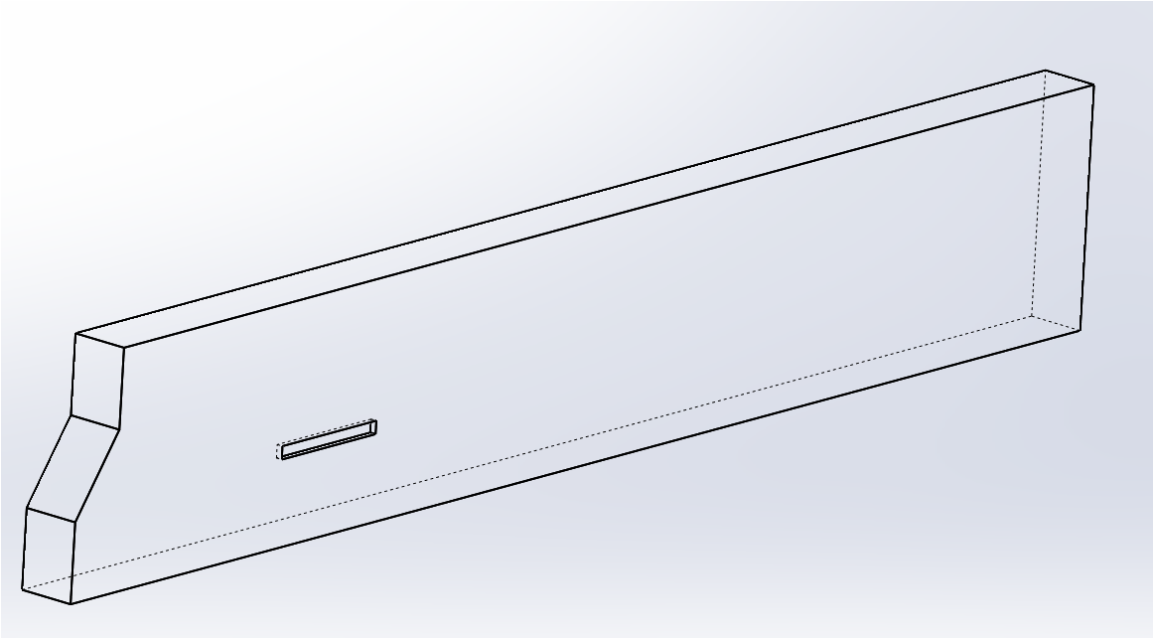

Figure 7. Rigid body method SOLIDWORKS model

2. Immersed Solid Method

The immersed solid method of body formation inserts a separate body within the modelled domain. This was accomplished by importing the SOLIDWORKS NPS tow tank domain and then creating the rectangular body within the tank using ANSYS Design Modeler. The immersed solid is then meshed separately from the domain mesh. The benefit to this method of body formation is that the tank mesh would remain consistent regardless of the body shape placed within the tank. A model using the immersed solid method of

body formation is shown in Figure 8, and a detailed view of the rectangular body is shown in Figure 9.

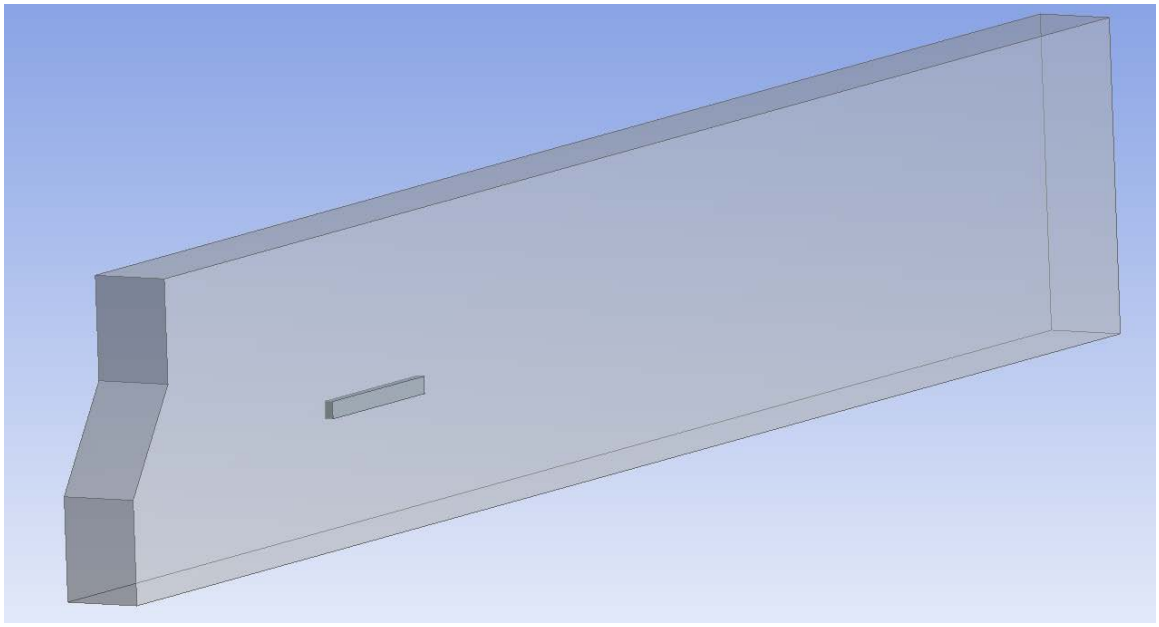

Figure 8. Immersed solid method ANSYS model

A focused comparison of the meshes between the two body forming methods is shown in Figure 9.

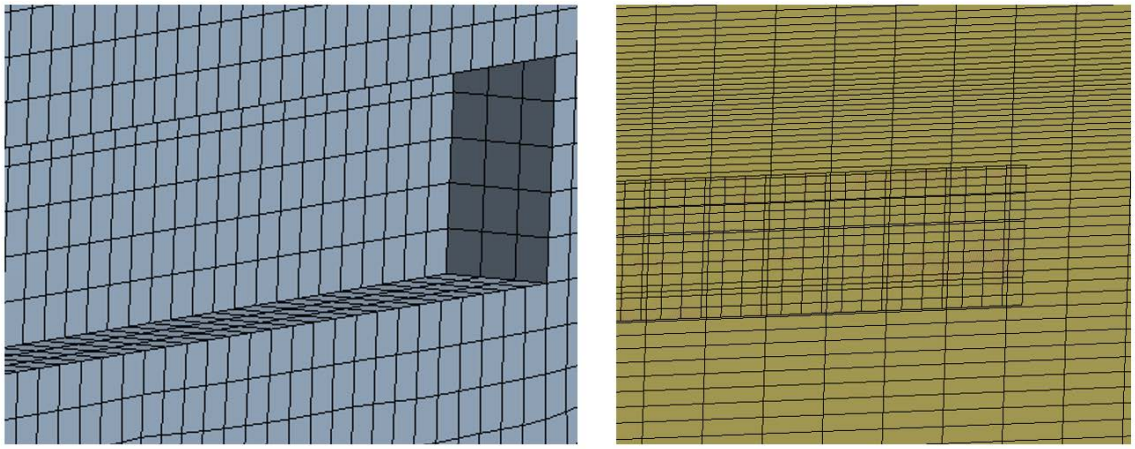

Figure 9. Mesh comparison rigid body method (left) and immersed solid method (right)

C. MODELS

In order to determine the modeled wave behavior and body impacts several variables were changed between models. First, the model had either no body, the rectangular body using the rigid body method, or the rectangular body using the immersed solid method. The second variable changed was the body was either in a high position such that the center of the body was 0.1044 meters beneath the still water surface, or a low position such that the center of the body was 0.2032 meters beneath the still water surface. The high body position yields a non-dimensionalized body depth (body centerline depth divided by model height) of 1.04 and the low body position yields a non-dimensionalized body depth of 2.03. The final variable was the inclination of the body, which was either -15 degrees, horizontal, 7.5 degrees, or 15 degrees from the horizontal. When the body was inclined, the center of the body was maintained at the desired depth. An example of an inclined model is shown in Figure 10.

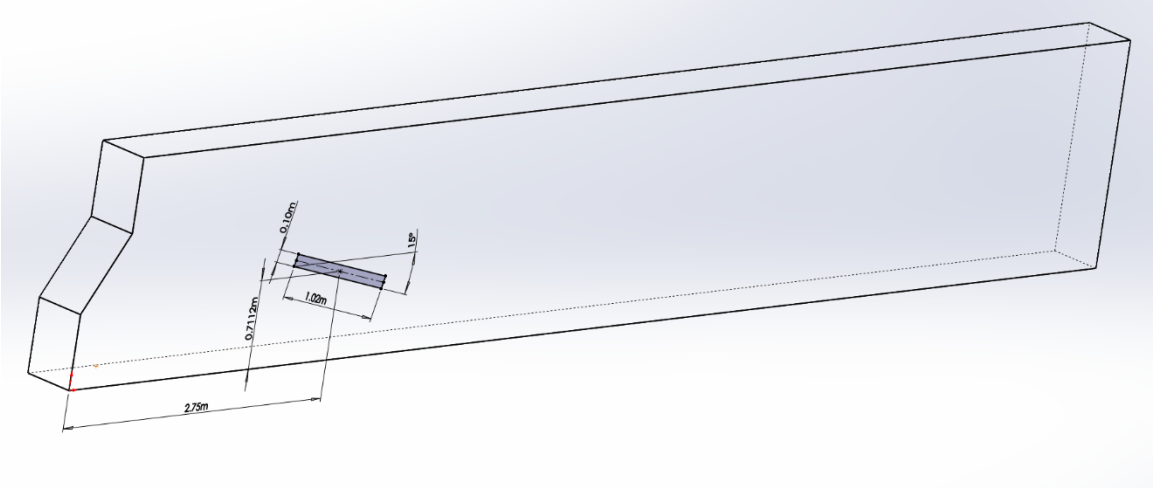

Figure 10. Inclined model at a 15° up angle

The list of models referenced within this paper is as follows:

1. Tank only, no body
2. Rigid body, high position, horizontal
3. Immersed solid, high position, horizontal

4. Rigid body, low position, horizontal
5. Immersed solid, low position, horizontal
6. Rigid body, low position, 15 degrees
7. Rigid body, low position, -15 degrees
8. Rigid body, low position, 7.5 degrees
9. Immersed solid, low position, 7.5 degrees

Each model was run to accumulate transient data on the fluid velocity profile, pressure distribution, wave behavior, and force and moment exerted on the body. The results from these models were compared to assess the accuracy of the modeling method in representing the physical situation. For all models, no validation against experimental data was performed.

There are two different coordinate systems used in the models. The global coordinate frame is for the tank. In this coordinate system, shown in Figure 11, the origin is placed in the inside lower corner of the tank. The negative x-axis extends down the length of the tank, the positive y-axis extends up the height of the tank, and the positive z-axis extends widthwise toward the outer edge of the tank. The coordinate system for the body, shown in Figure 12, maintains all axes in parallel positions to the global coordinate system, regardless of the orientation of the body. However, the body coordinate system the origin is located in the center of the body. The forces and moment on the body are measured with respect to the body coordinate system. All other variables such as fluid particle velocity are measured with respect to the global coordinate system.

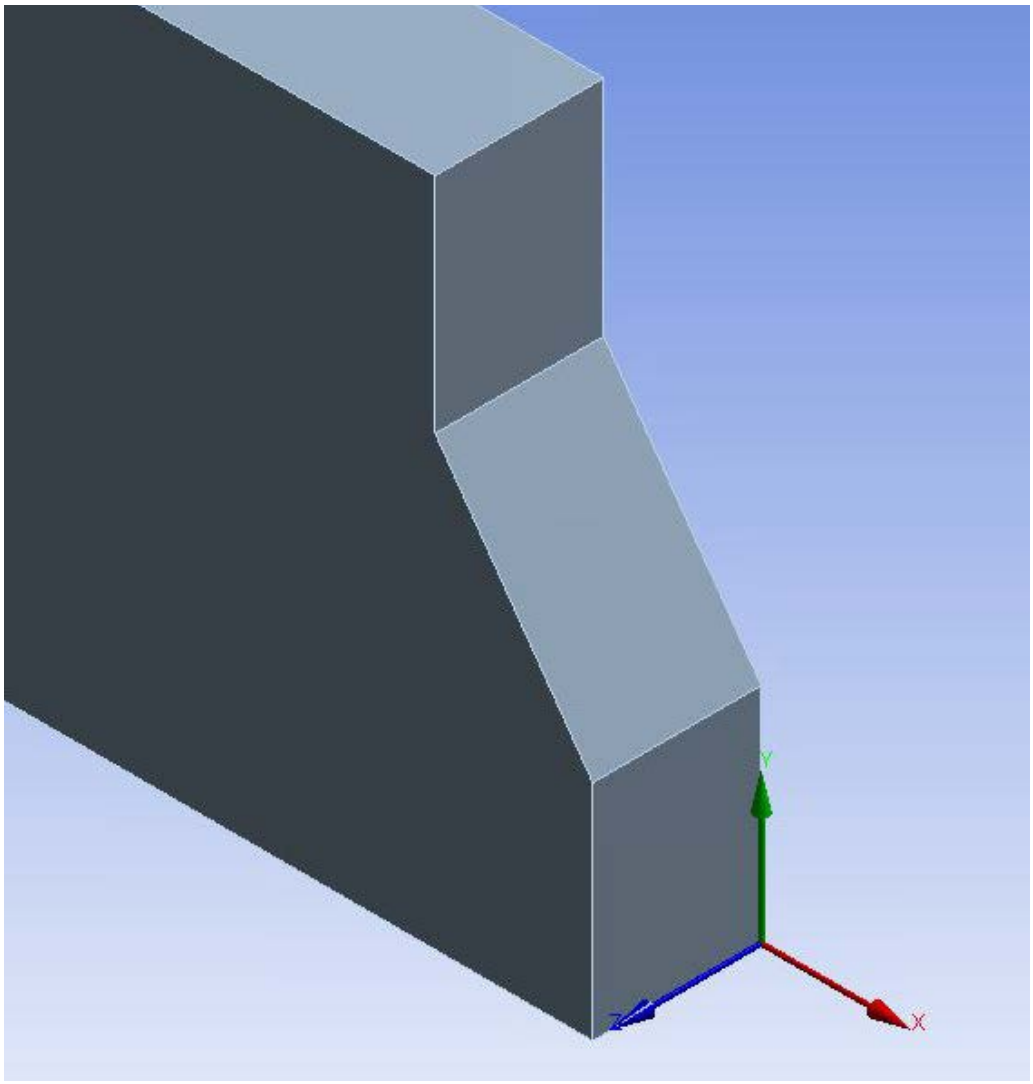

Figure 11. Global coordinate system

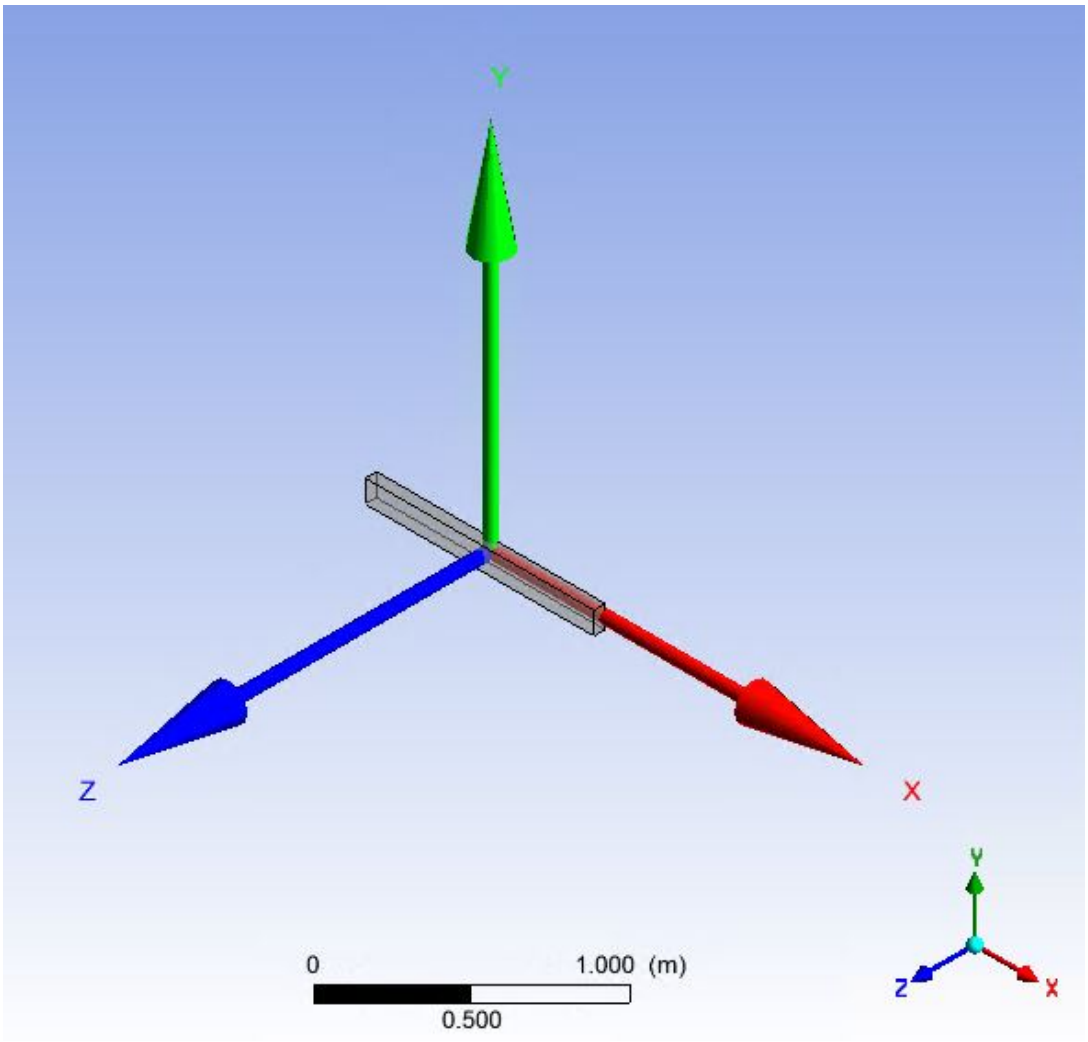

Figure 12. Body coordinate system with global coordinate shown in lower right corner

III. RESULTS AND DISCUSSION

A. COMPARISON OF BODY FORMATION METHOD FOR BODY IN HIGH POSITION

A comparison was performed using the two different methods of body formation while the body was in the same vertical position, denoted as high position, and horizontal orientation. For all models the same wedge motion was used, producing a wave with a frequency of 1 Hertz and amplitude of 0.0175 meters. The intent was to determine if the body formation methods resulted in similar modeling results.

A visual comparison between the two models immediately identified that the immersed solid model demonstrated crisper, more continuous behavior for volume fraction and pressures than the rigid body model. Examples of this are shown in the contour lines for the water volume fraction in Figure 13 and in the dynamic pressure contour lines shown in Figure 14. These images are from the same instant of time in the transient models and as such should show the same condition; however, the rigid body model shows increased dispersion of the water volume fraction and greater dispersion of the dynamic pressure while having lower dynamic pressure values overall.

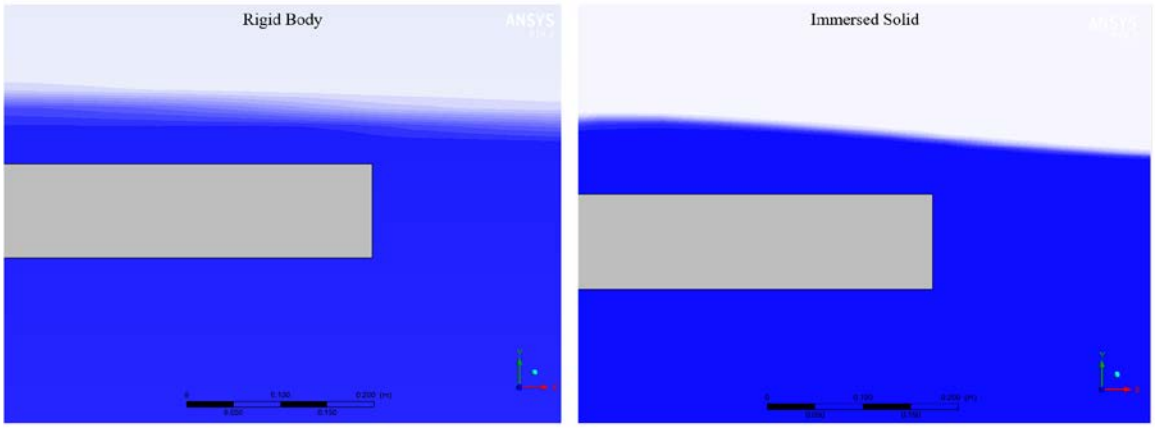

Figure 13. Water volume fraction contour line comparison for body in high position

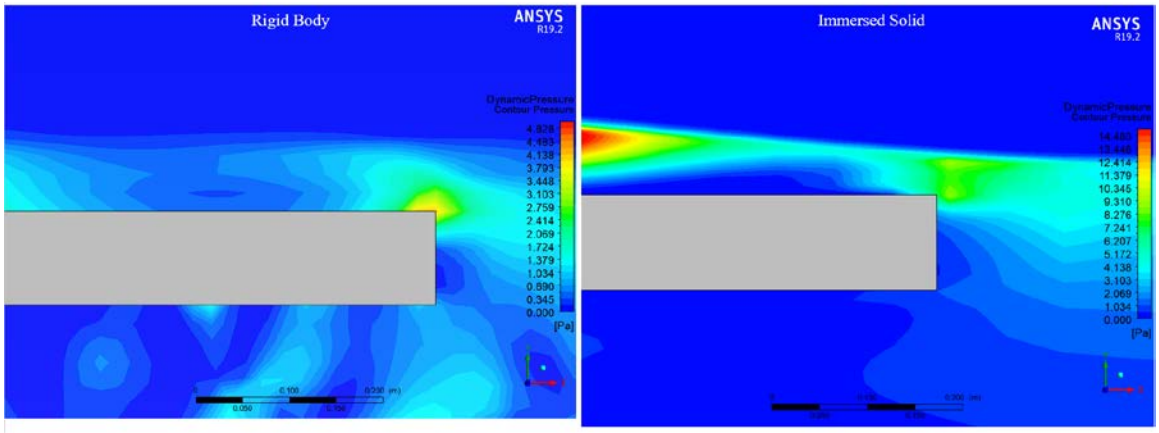

Figure 14. Dynamic pressure contour line comparison for body in high position

The increased cohesion of the immersed solid model was initially perceived as an advantage. However, experimental tests run by Jones [10] with the rectangular body at the same shallow depth as the models demonstrated the waves become steep and incoherent when breaking over the body, shown in Figure 15.

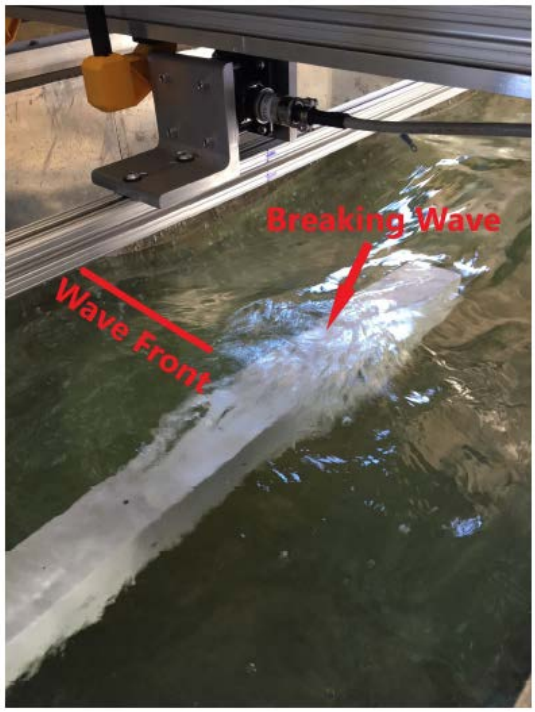

Figure 15. Waves breaking over a shallow body. Source: [10].

Velocity and pressure data were compared between the two models at specific locations. The locations chosen for comparison were three points halfway down the length of the body at 0.01 meter, 0.04 meter, and 0.06 meter above the upper surface of the body, as shown in Figure 16, with the center of the yellow crosshairs being the points and the blue contouring showing the water volume fraction. For this body position, the highest point located 0.06 meters above the upper body surface is above the still water height.

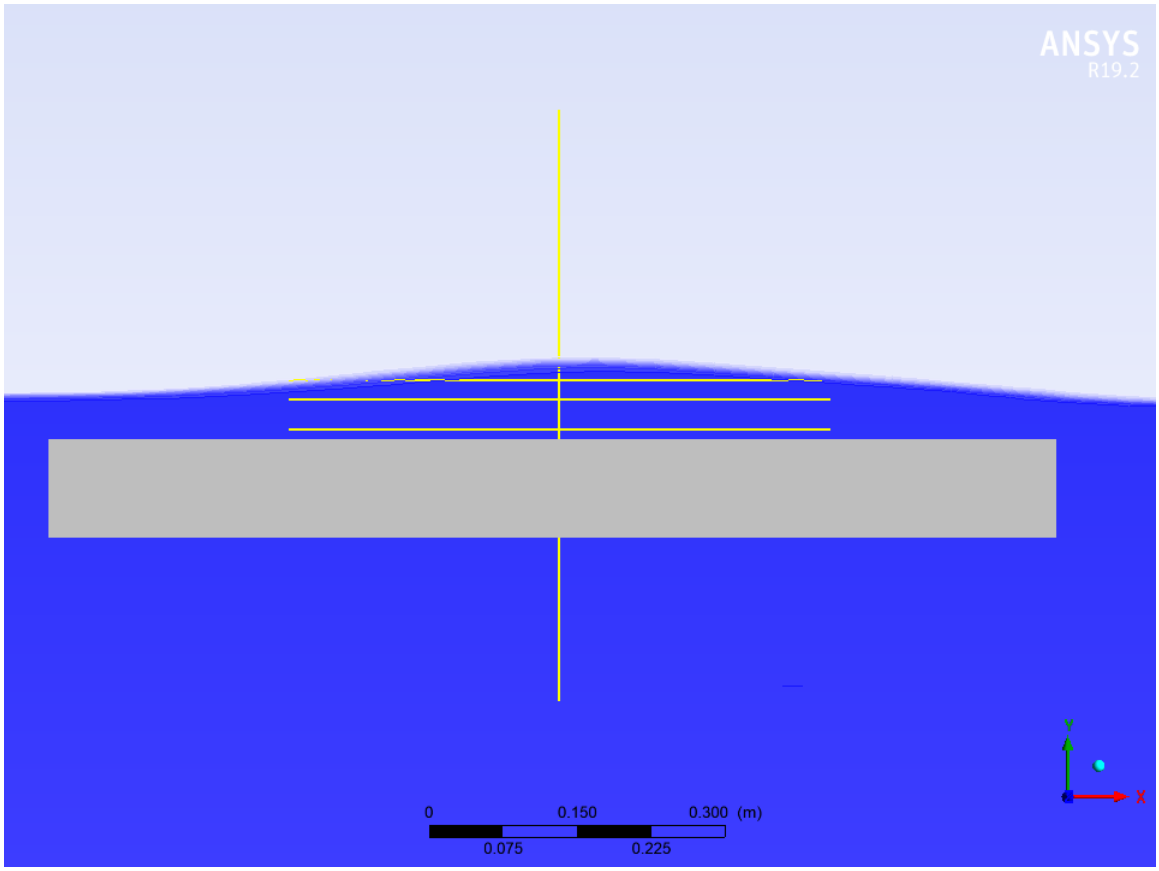

Figure 16. Location of data points used for comparison

Comparison of data at these points demonstrated that the immersed solid model exhibited smaller values for velocity and dynamic pressure behavior when close to the top surface of the body; but, as the distance from the top surface grew, the values for the immersed solid model grew faster than those for the rigid body model. At the larger distance from the body surface, the rigid body model exhibited larger values for velocity

and dynamic pressure. This can most clearly be seen by examining the x velocity, defined as the velocity down the length of the tank. Close to the upper surface of the body, the values for x velocity between the rigid body model and the immersed solid model maintained similar waveforms with the immersed solid model having lower wave amplitudes, shown in Figure 17.

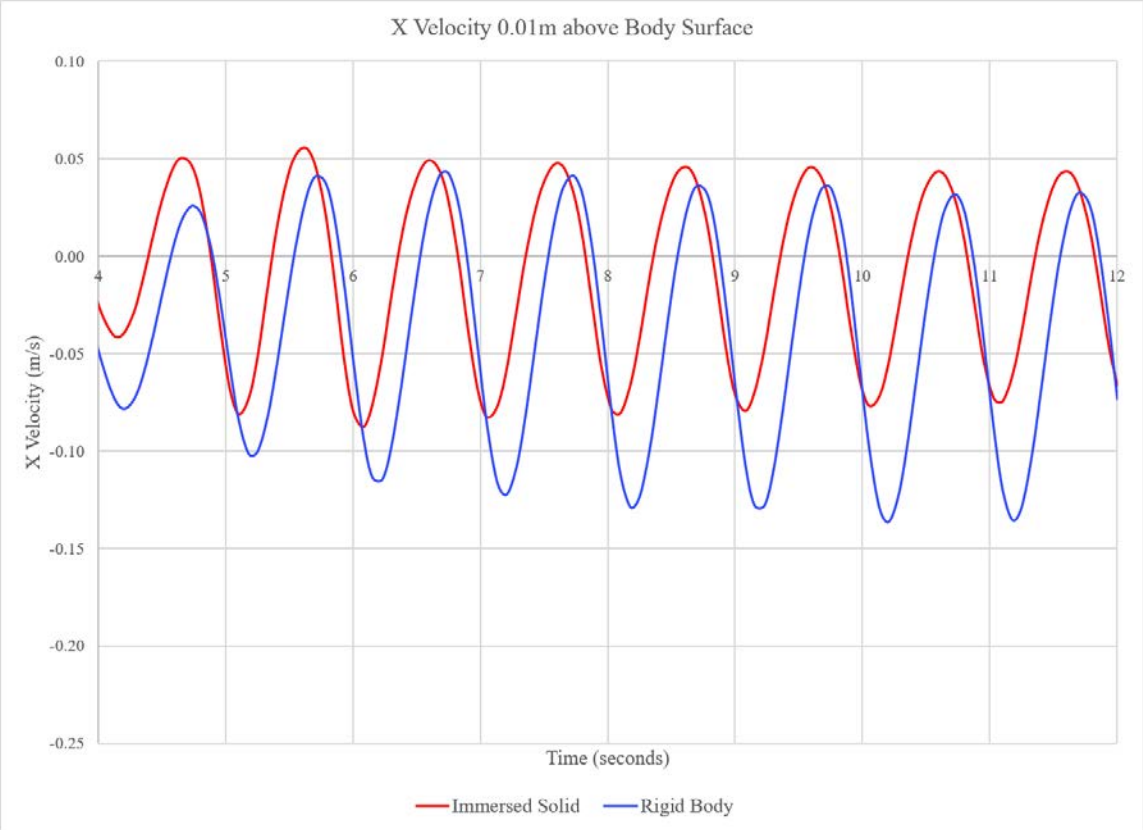

Figure 17. X velocity close to the body top surface, comparing models with body in high position

As the distance from the surface increased, the x velocity of the two models increased, with the immersed solid model growing faster. The immersed solid model exhibited non-standard waveforms with larger amplitudes than the rigid body model, as shown in Figure 18.

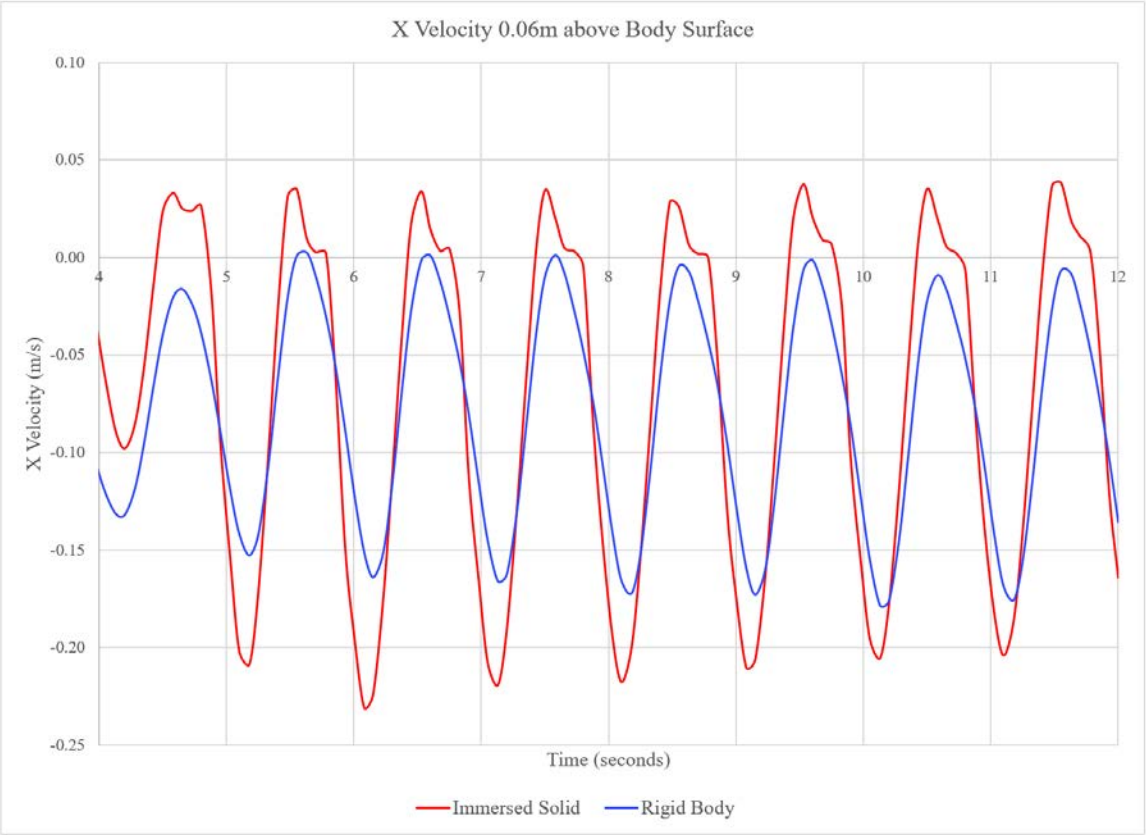

Figure 18. X velocity farther from the body top surface, comparing models with body in high position

Similar behavior was observed in comparison of the dynamic pressures between the two models. Close to the body, the dynamic pressures for the rigid body model were higher, as shown in Figure 19. Farther from the top surface of the body the dynamic pressures are larger overall, with the immersed solid model having the higher values, as seen in Figure 20. The dynamic pressures at the higher position shown in Figure 20 periodically drop to zero as the water height from wave motion drops below the monitoring point, exposing it to air. These dynamic pressures are also lower than values predicted by linear potential wave theory based on the incoming wave. However, as the wave height is rapidly decreasing over the body due to wave energy dissipation, it is expected that the pressure fluctuations from the passing wave will be small.

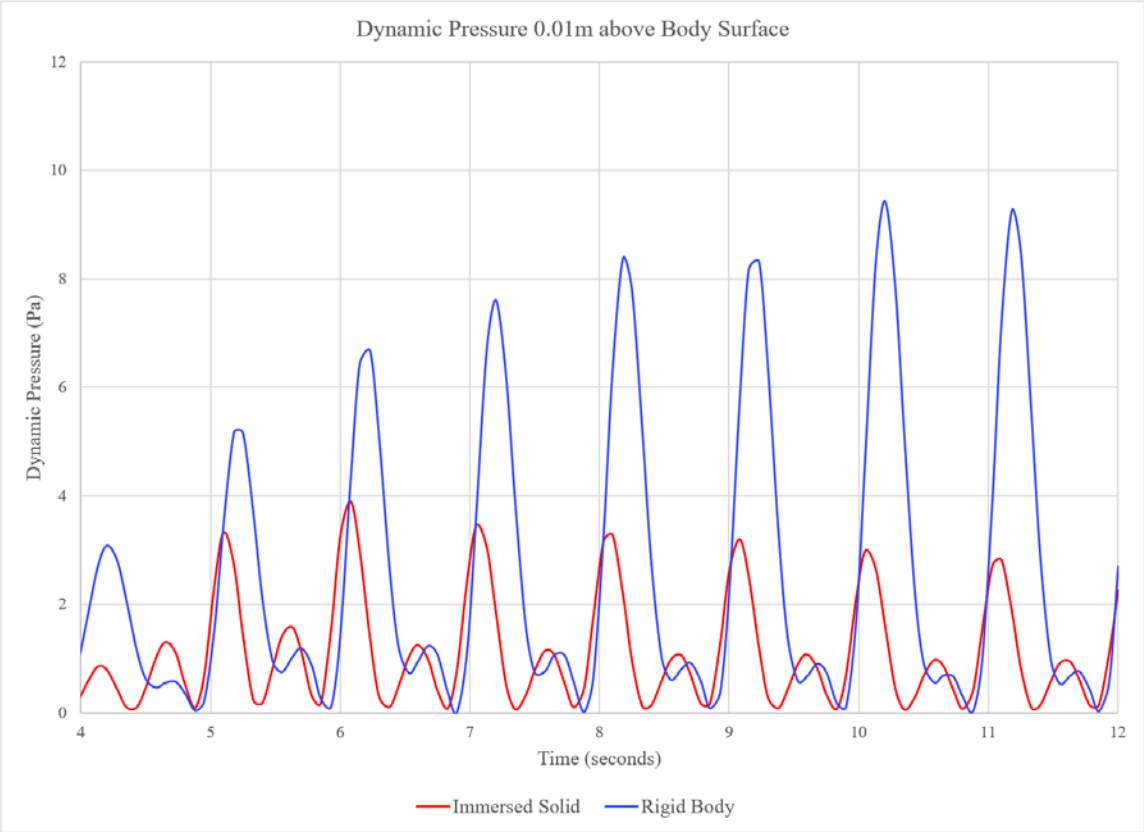

Figure 19. Dynamic pressure close to the body top surface, comparing models with body in high position

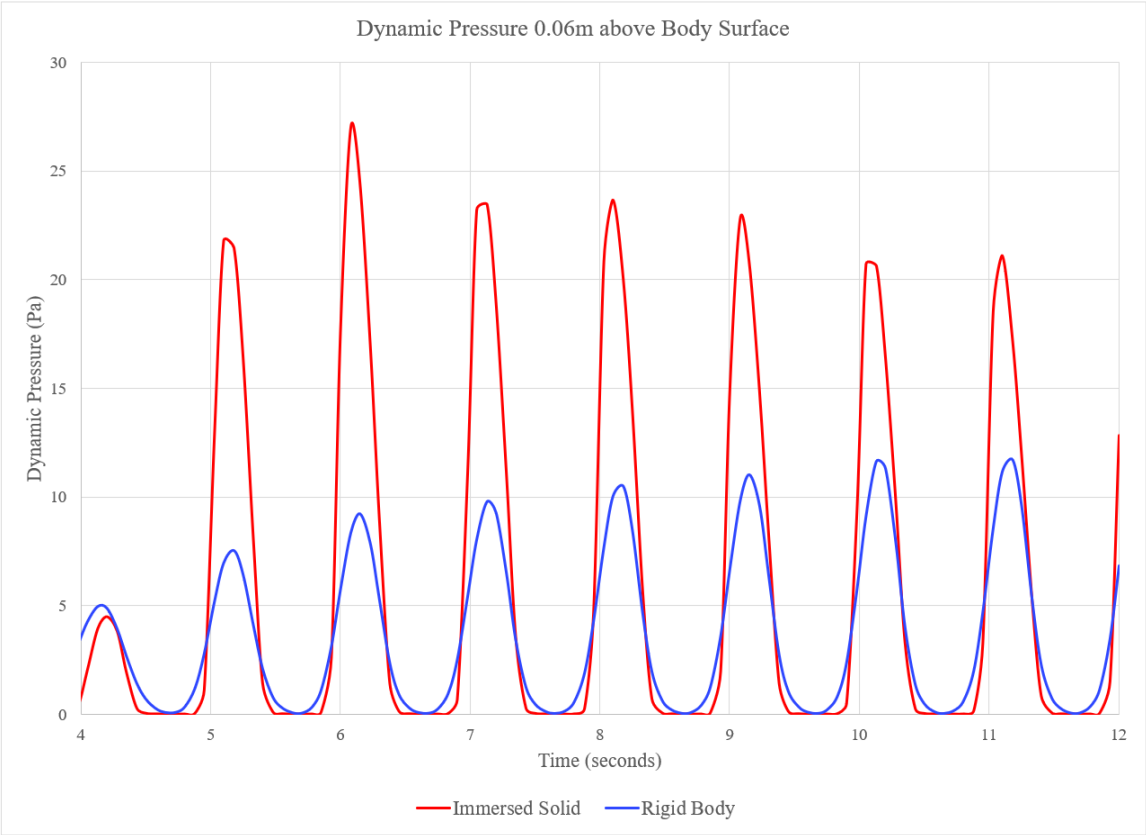

Figure 20. Dynamic pressure farther from the body top surface, comparing models with body in high position

As a final comparison between the two models, the force and moment on the body were analyzed. In order to perform this comparison, the force and moment must be non-dimensionalized. This was done using water density (ρ), gravitational acceleration (g), wave amplitude (a), body length (L_B) and body width (W_B). The non-dimensionalized drag and vertical forces (F_{ND}) are defined in Equation (2) and the non-dimensionalized moment (M_{ND}) is defined in Equation (3).

$$F_{ND} = \frac{F}{\rho g a L_B W_B} \tag{2}$$

$$M_{ND} = \frac{F}{\rho g a L_B^2 W_B} \tag{3}$$

The transient behavior for non-dimensionalized drag force, lift force, and moment on the body are shown in Figure 21, Figure 22, and Figure 23, respectively. The rigid body model computes peak body force and moment values that are lower than the immersed solid model.

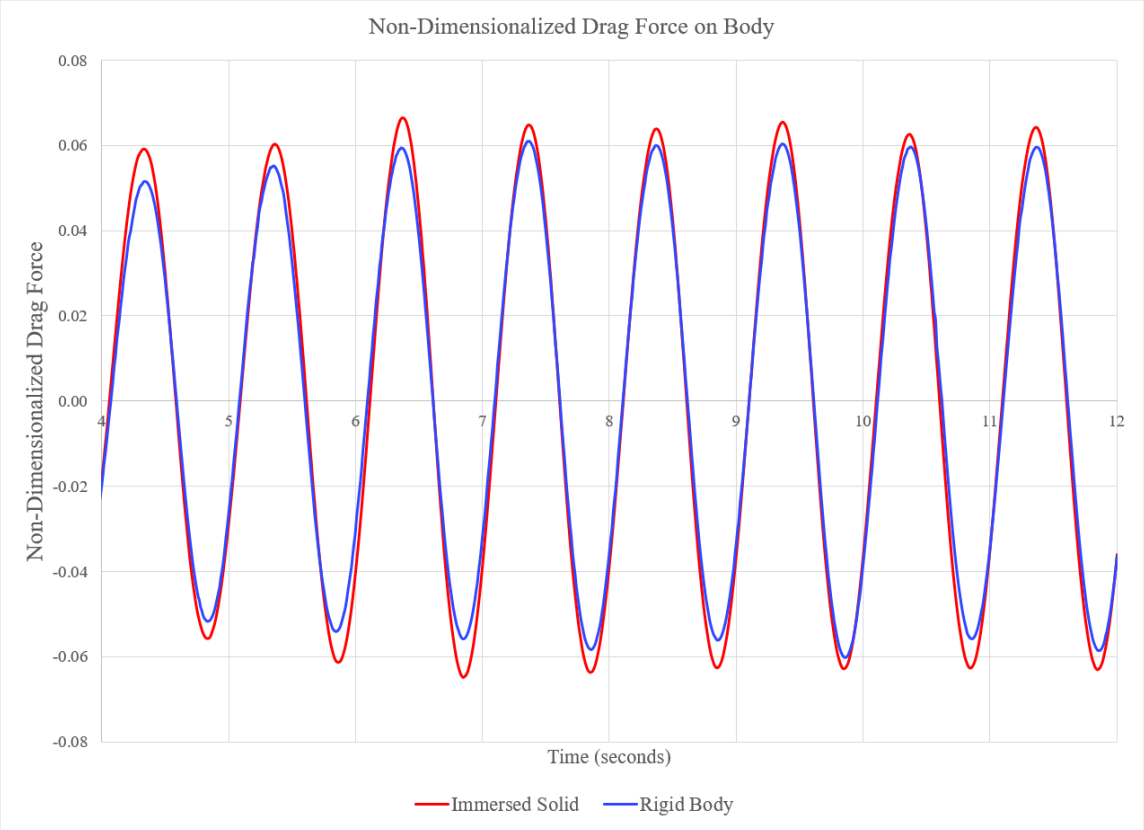

Figure 21. Non-dimensionalized drag force comparison for models with body in high position

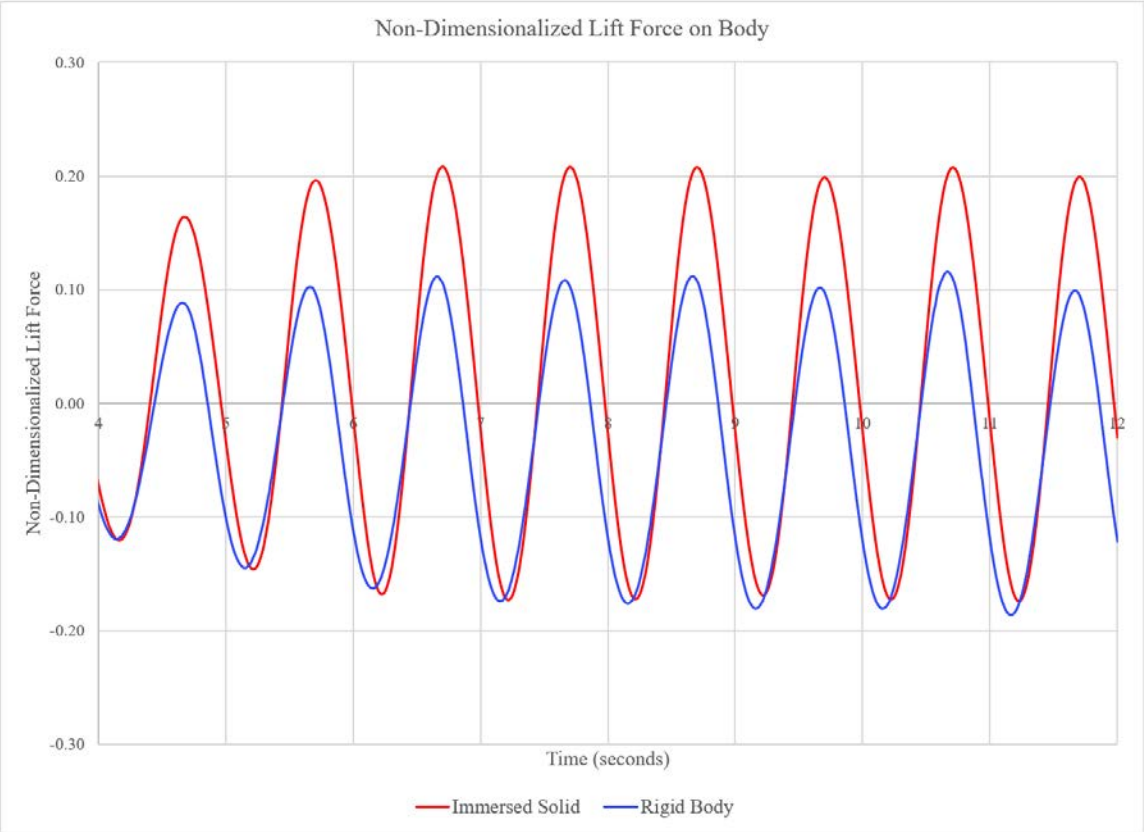

Figure 22. Non-dimensionalized lift force comparison for models with body in high position

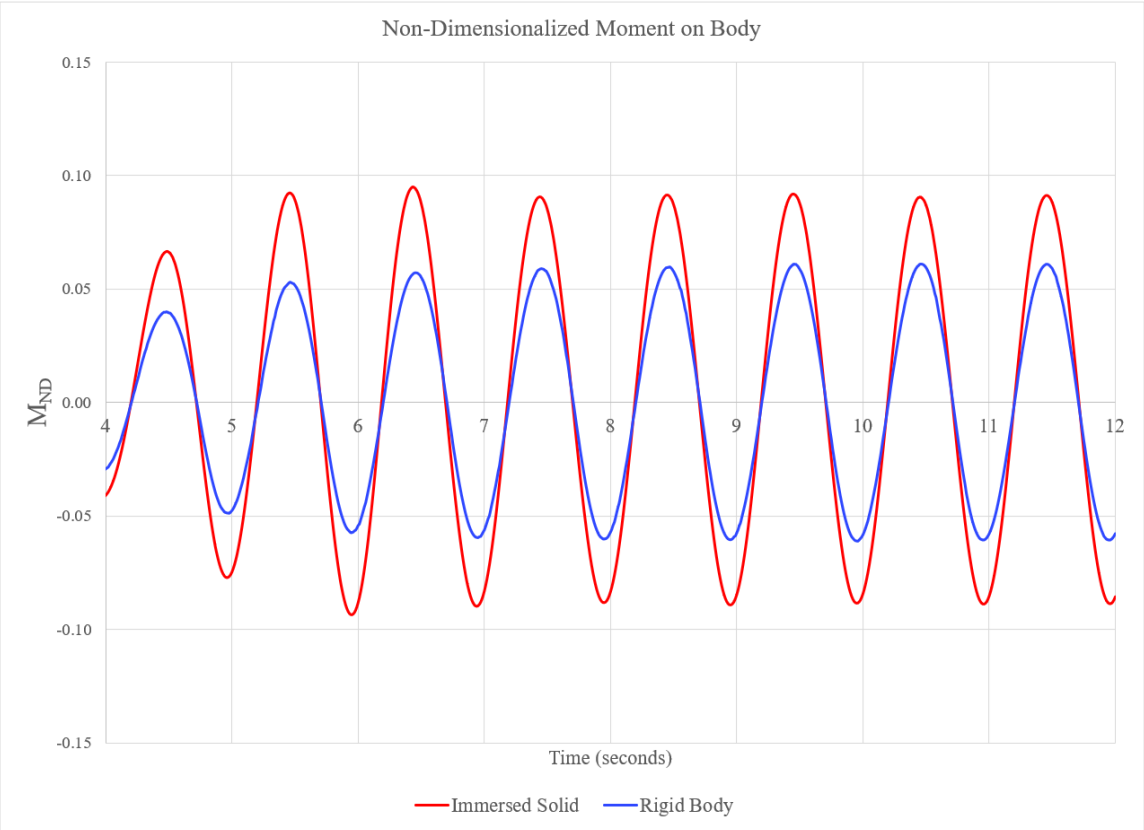

Figure 23. Non-dimensionalized moment comparison for models with body in high position

The comparison of these two models demonstrates that the rigid body modeling method and immersed solid modeling method can produce different results. However, due to the shallow nature of the body underneath the waves, it is not apparent if these inconsistent results are due to the different modeling method or lack of fidelity for complex body-wave interactions.

B. COMPARISON OF BODY FORMATION METHOD WITH BODY IN LOW POSITION

Once it was determined that the complex body-wave interactions may be impacting the two modeling results, a comparison was performed between the two methods of body formation at a lower position such that the body was farther beneath the wave surface. The wedge motion and generated waveform were maintained consistent with previous models. The two methods of modeling body formation, rigid body method and immersed solid

method, exhibited closer behavior at the lower depth. Figure 24 and Figure 25 show a comparison between the x velocity and the non-dimensionalized drag force on the body, respectively, between these two body formation methods with the body in the lower position. The comparison between the two methods of body formation provide evidence that the farther the body is from the wave action the more the solutions between the two methods of body formation converge.

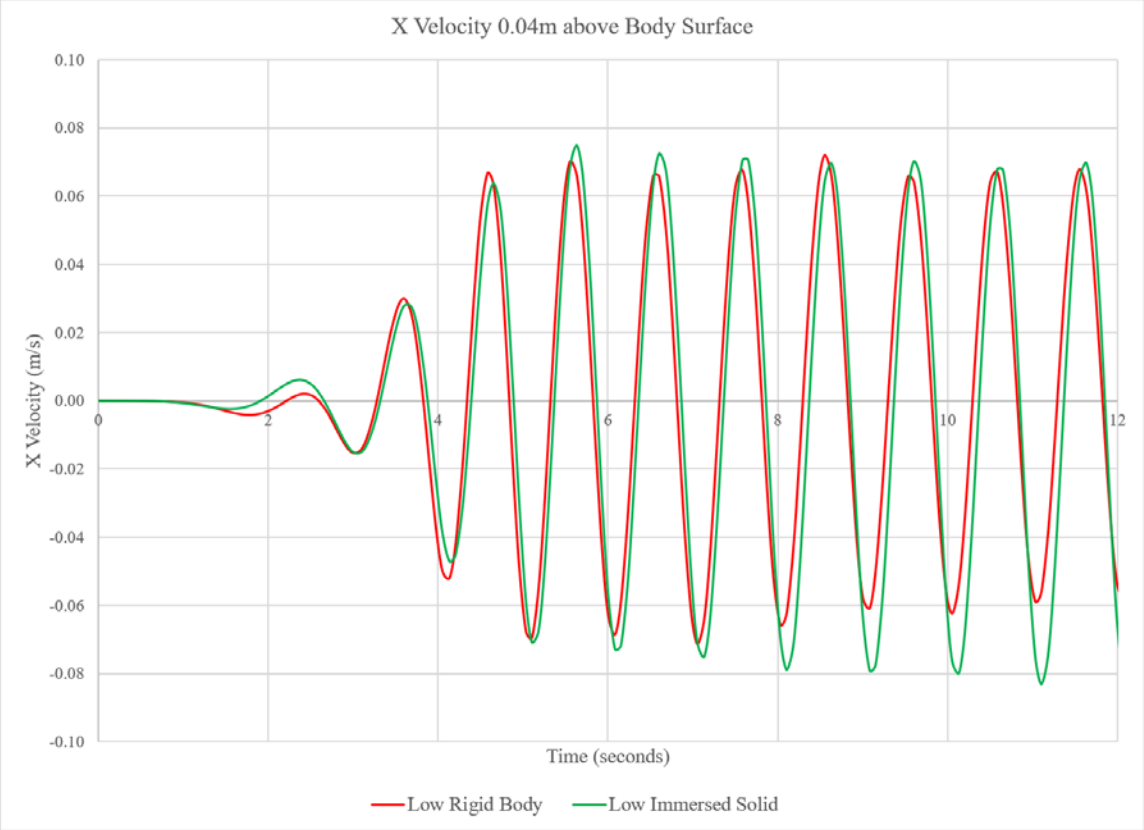

Figure 24. Comparison of x velocity with body in lower position

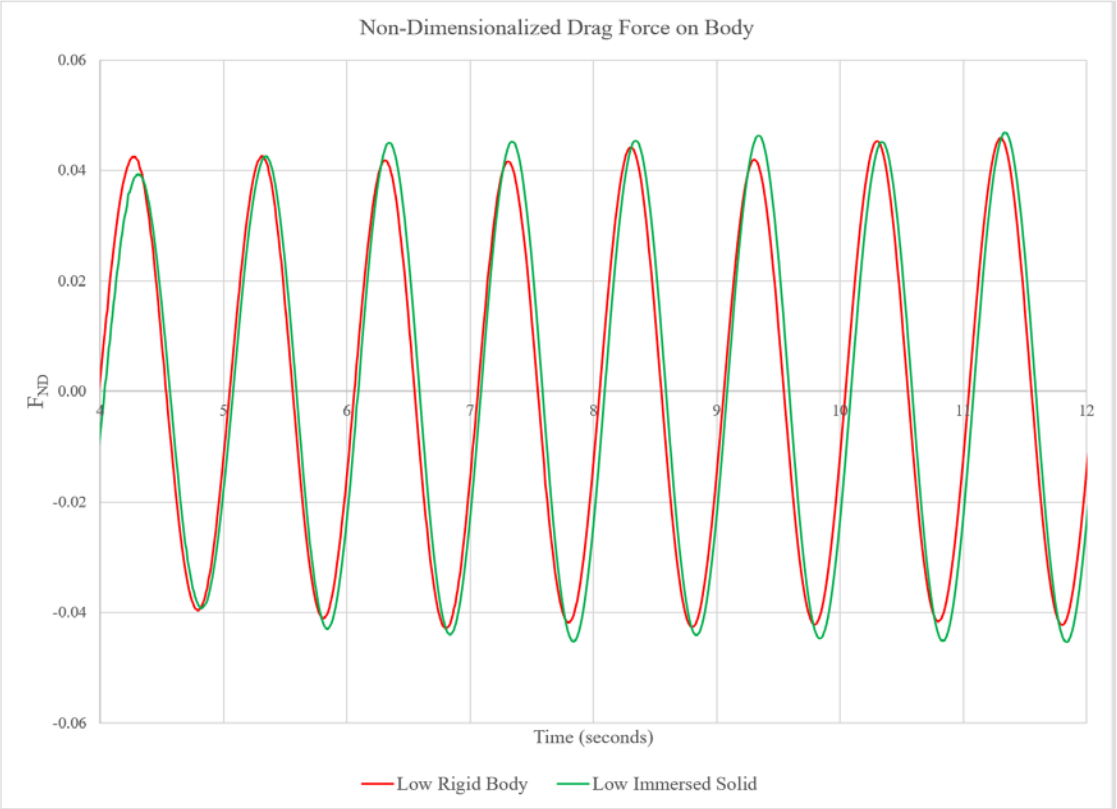

Figure 25. Comparison of non-dimensionalized drag force with body in lower position

A transient comparison of the velocity behavior between the two models was performed. The transient time was started at 6.00 seconds and progressed in 0.15-second increments until 7.05 seconds. These images are shown in Figure 26, Figure 27, and Figure 28 for the rigid body model and in Figure 29, Figure 30, and Figure 31 for the immersed solid model. In general, the velocity behavior between the two models is consistent. In both models, the flow over the top corner of the body exhibits a complete change in direction as the transient progresses. The biggest distinction between the models occurs at time 6.75 seconds, as the wave is over the front of the body. For the immersed solid model, the velocity vectors over the front of the body appears to evenly distribute between the top and bottom, flowing down the length of the body. For the rigid body model, the flow impinges against the front of the body, with some of the flow being reflected back against the direction of wave motion. This time step is shown in Figure 32 for the rigid body model and in Figure 33 for the immersed solid model.

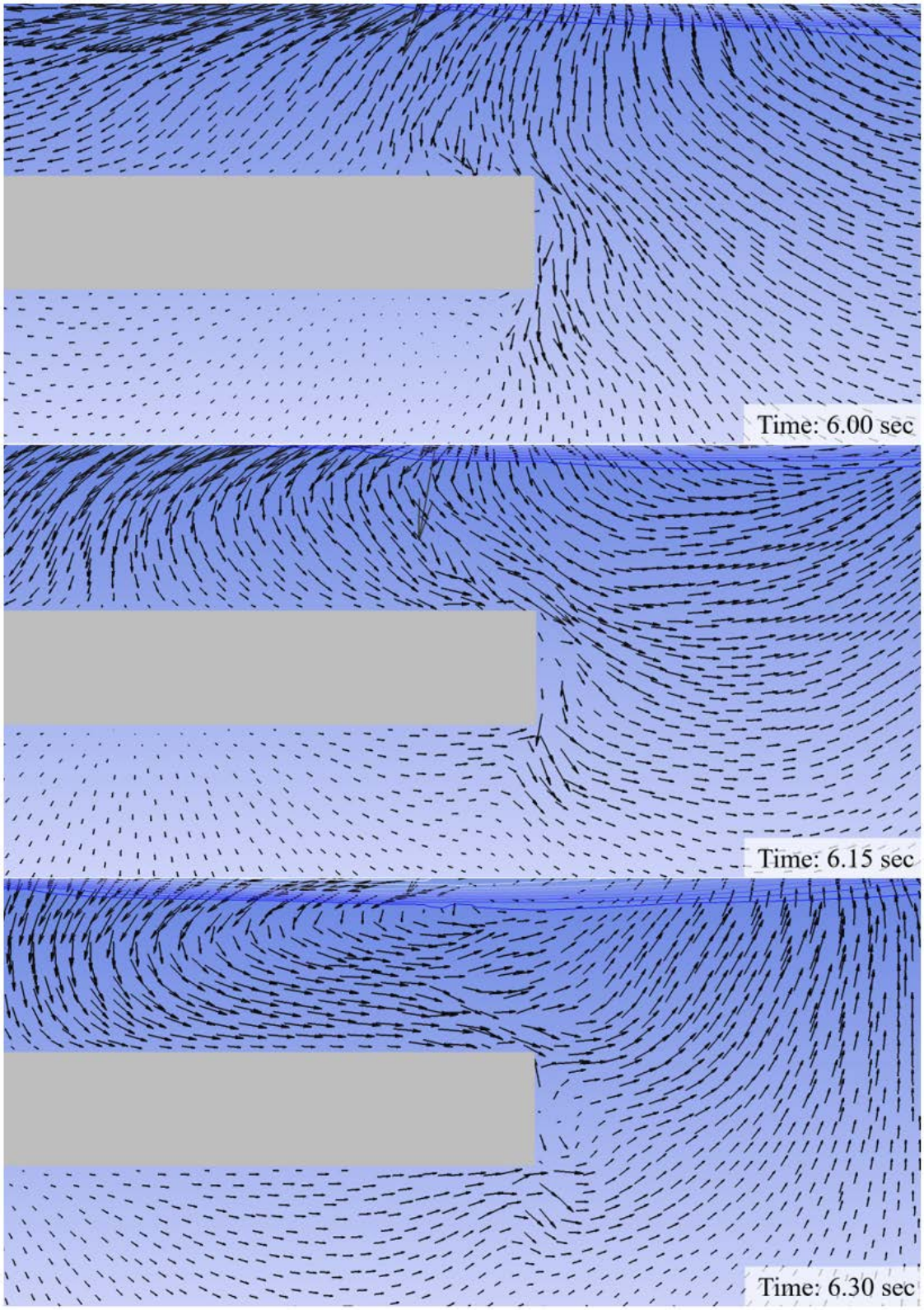

Figure 26. Transient velocity vectors for rigid body model in lower position (6.00 – 6.30 sec)

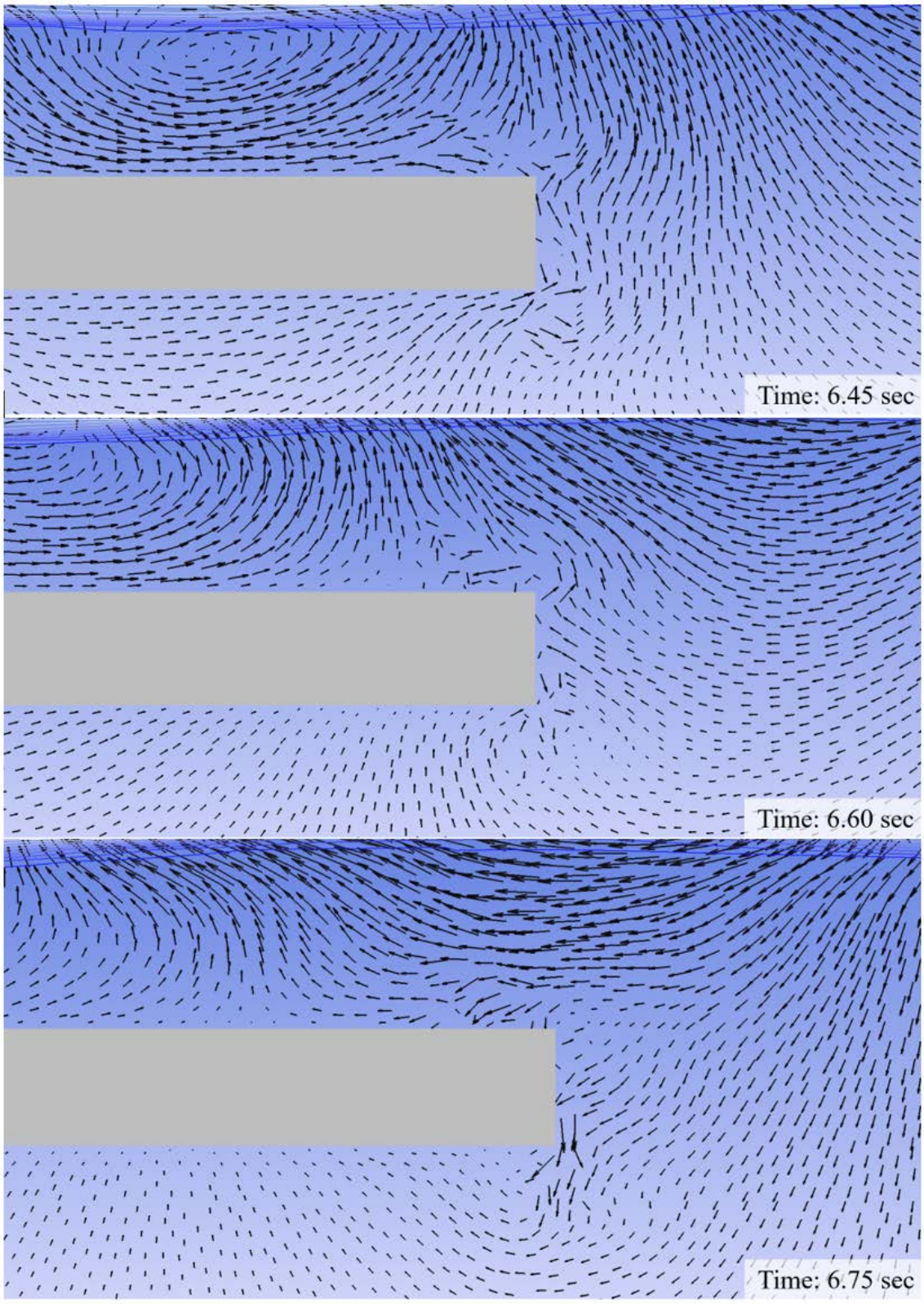

Figure 27. Transient velocity vectors for rigid body model in lower position (6.45 – 6.75 sec)

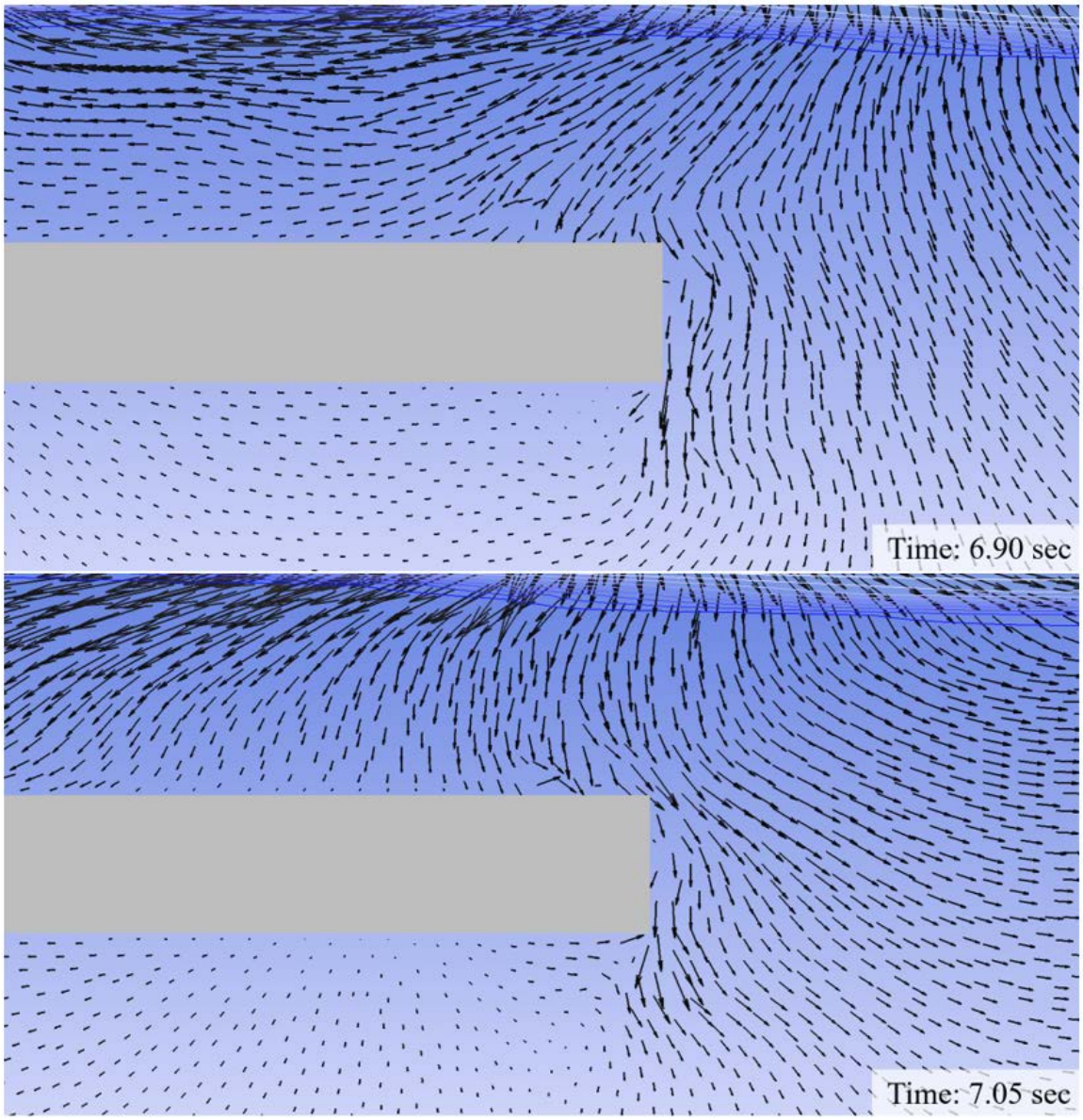

Figure 28. Transient velocity vectors for rigid body model in lower position (6.90 – 7.05 sec)

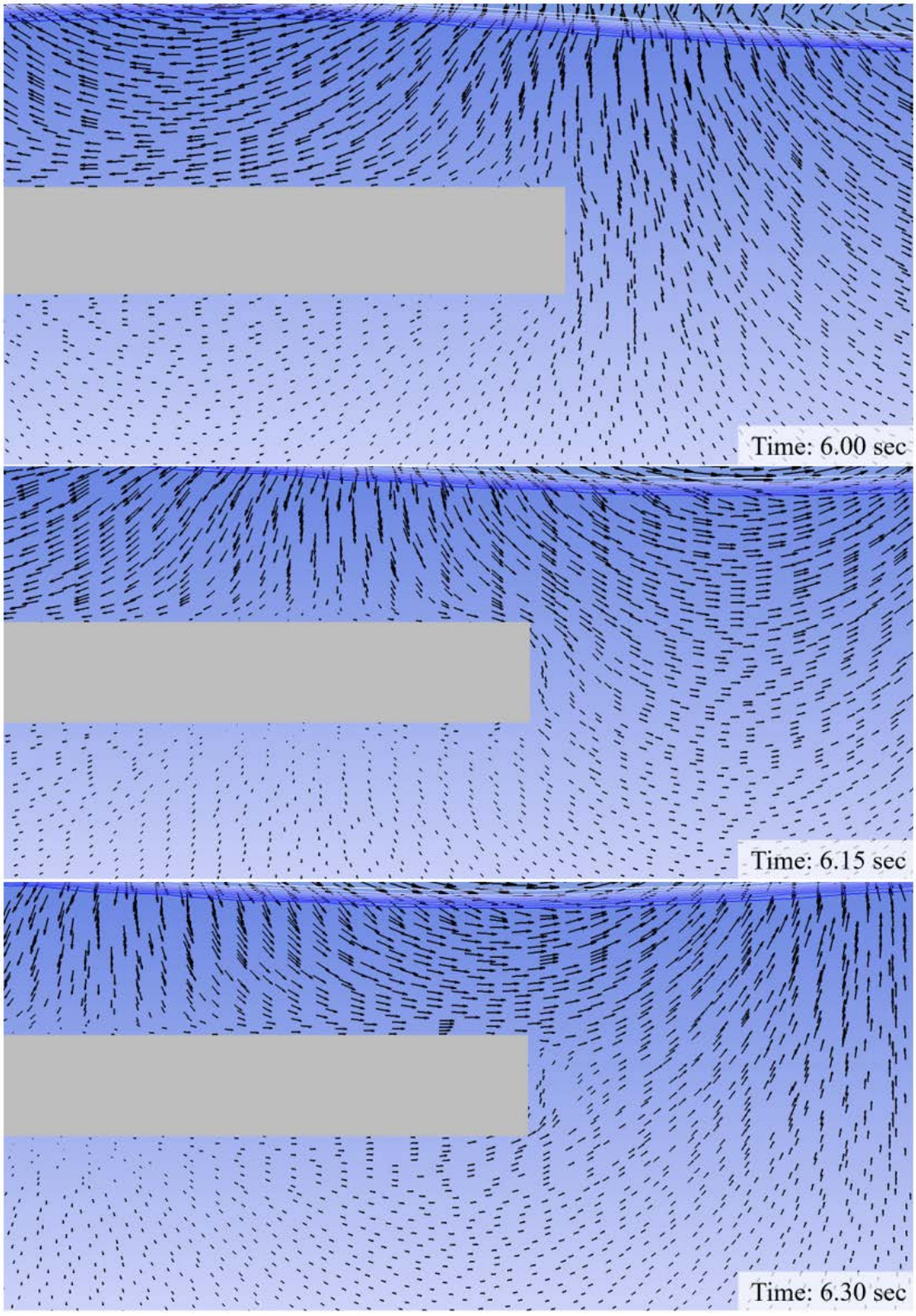

Figure 29. Transient velocity vectors for immersed solid model in lower position (6.00 – 6.30 sec)

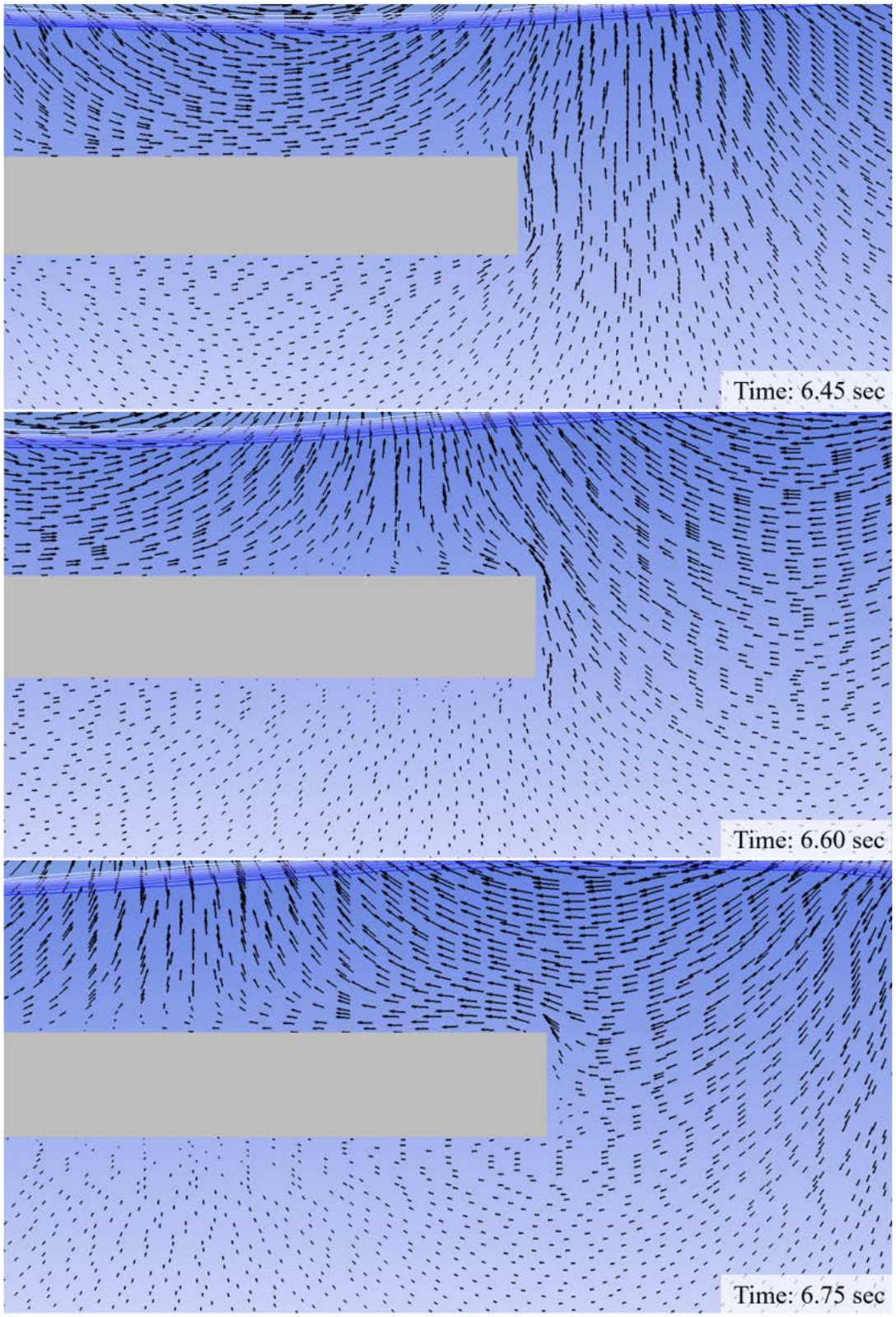

Figure 30. Transient velocity vectors for immersed solid model in lower position (6.45 – 6.75 sec)

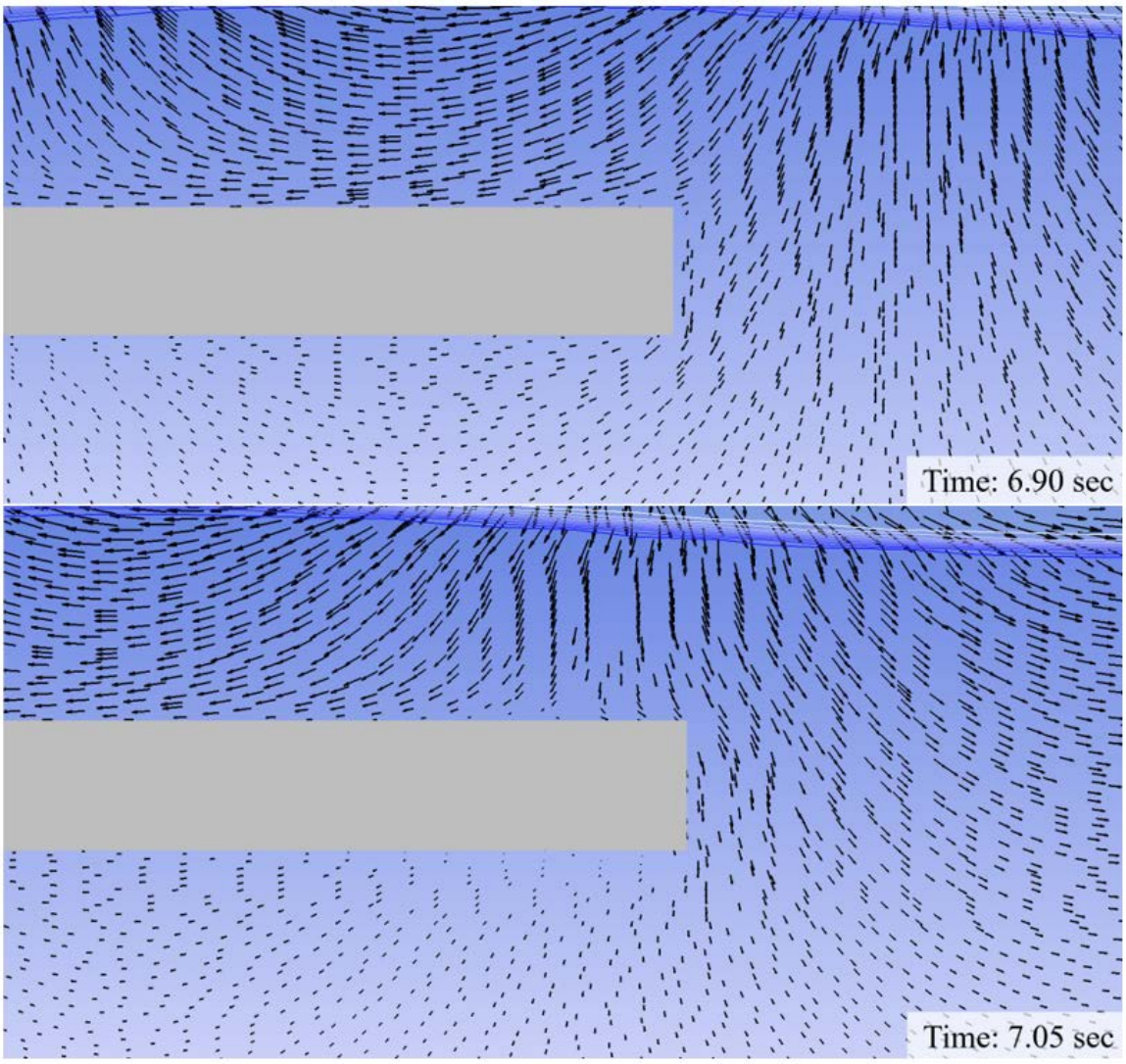

Figure 31. Transient velocity vectors for immersed solid model in lower position (6.90 – 7.05 sec)

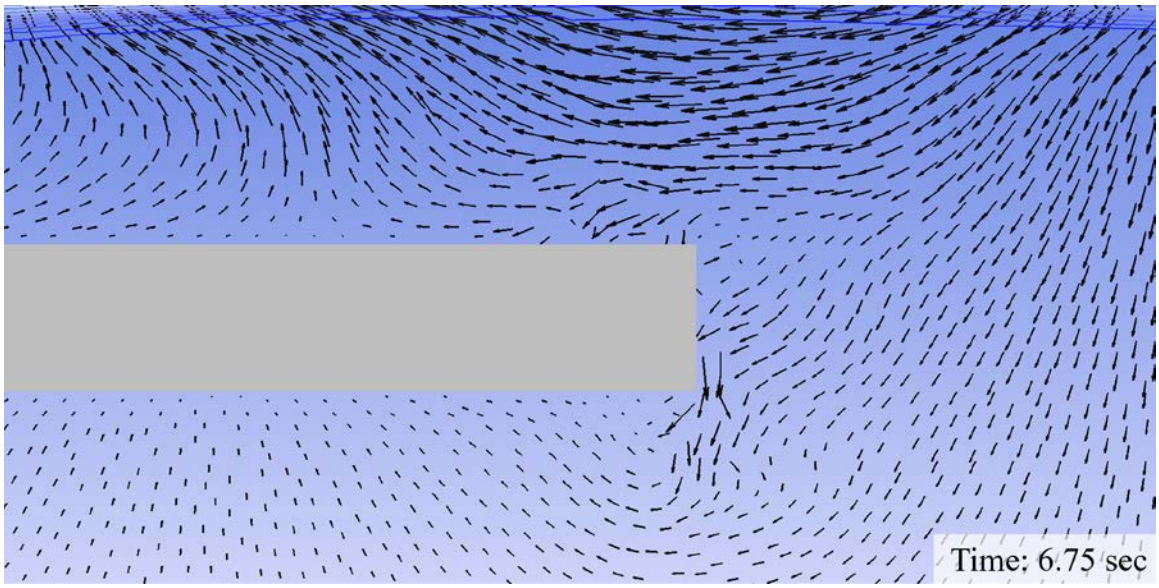

Figure 32. Velocity vectors at 6.75 sec for rigid body model in lower position

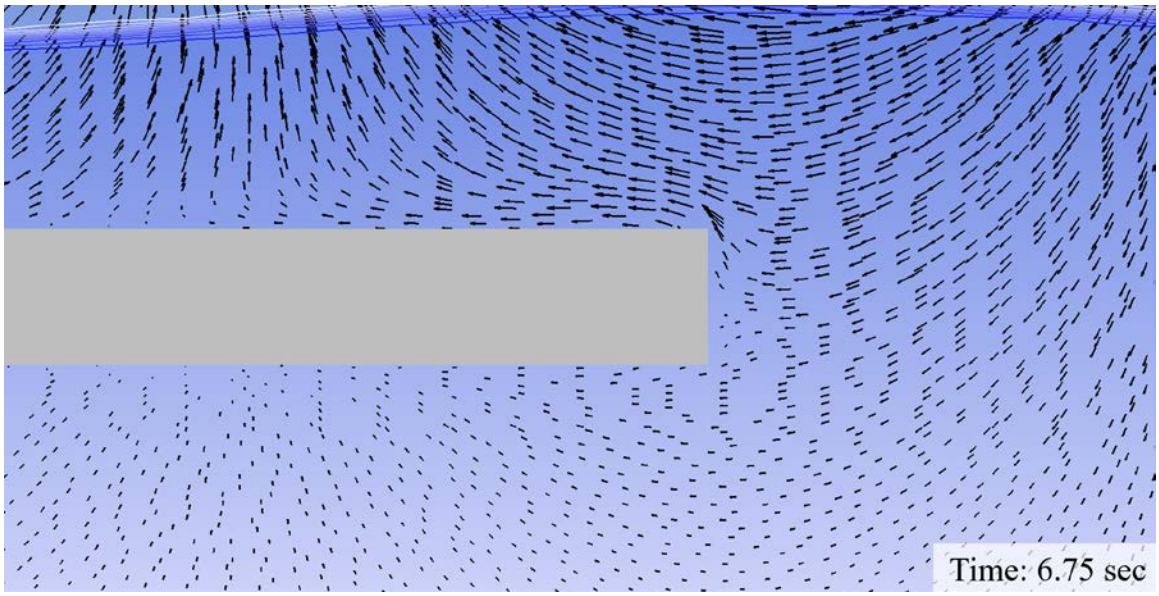

Figure 33. Velocity vectors at 6.75 sec for immersed solid model in lower position

A comparison of the transient dynamic pressure contour lines was also performed using the same time increments. Figure 34 and Figure 35 show the transient dynamic pressure behavior for the rigid body model and Figure 36 and Figure 37 show the behavior for the immersed solid model. Of note, the scale in the rigid body model is approximately double that of the immersed solid model.

The regions of lower dynamic pressure around the body appear to be consistent between the two models. For example, at time 6.60 seconds both models show two lower pressure bubbles on top of the body fore and aft. However, the contour lines for the immersed solid model are more continuous as a whole, while the rigid body model has more patchy dynamic pressure behavior. Also, the rigid body model exhibited higher dynamic pressures overall.

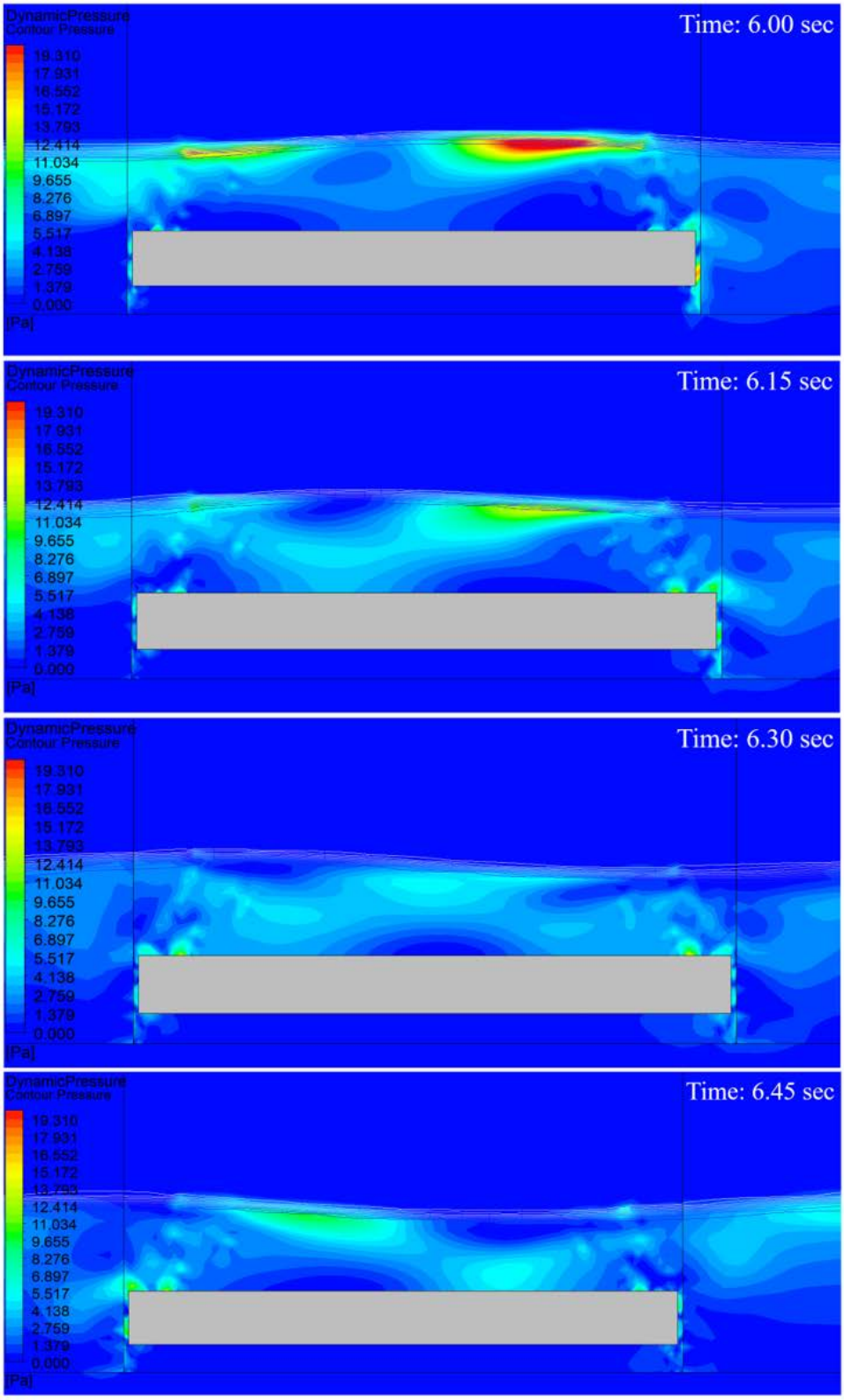

Figure 34. Transient dynamic pressure contours for rigid body model in lower position (6.00 – 6.45 sec)

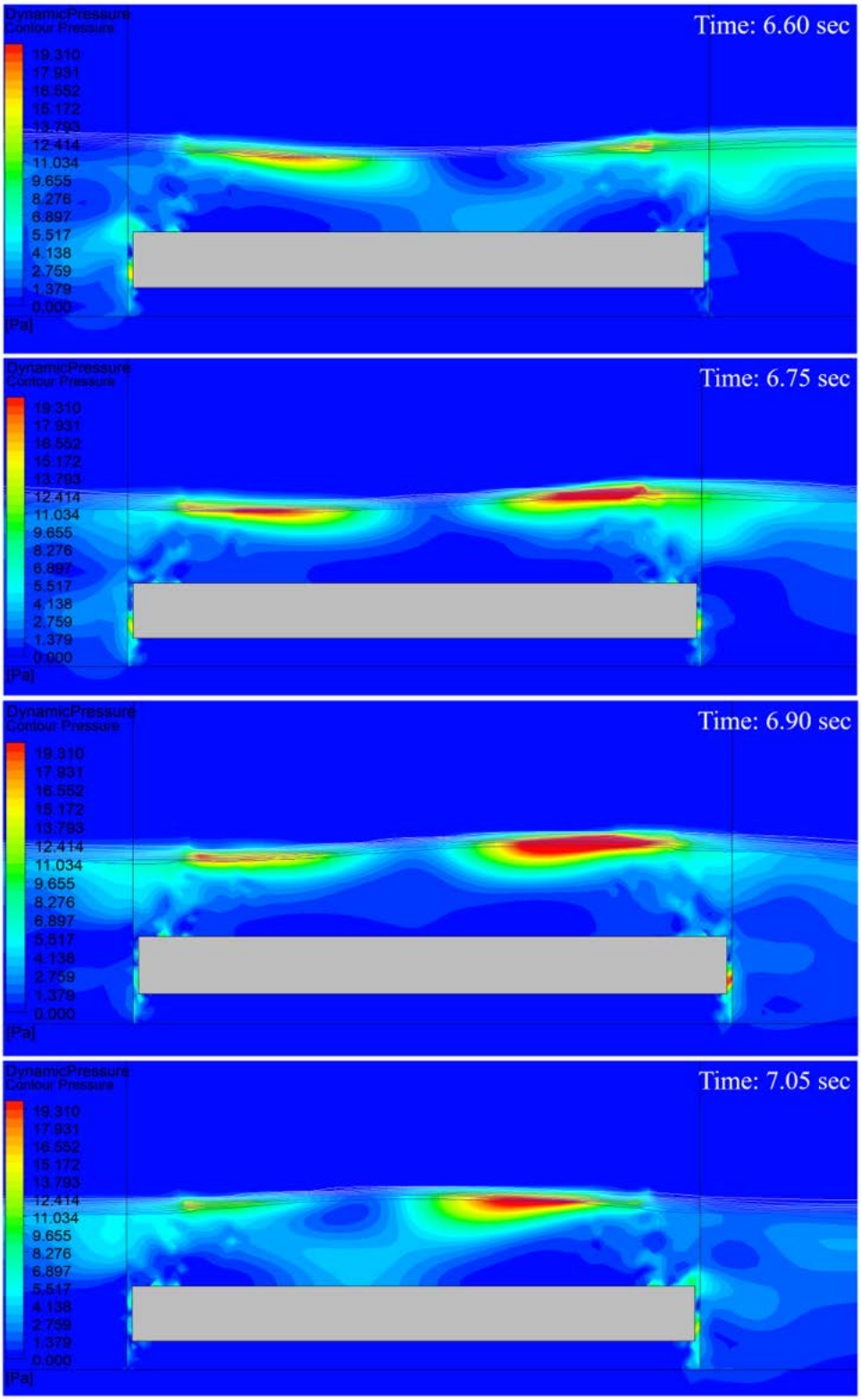

Figure 35. Transient dynamic pressure contours for rigid body model in lower position (6.60 – 7.05 sec)

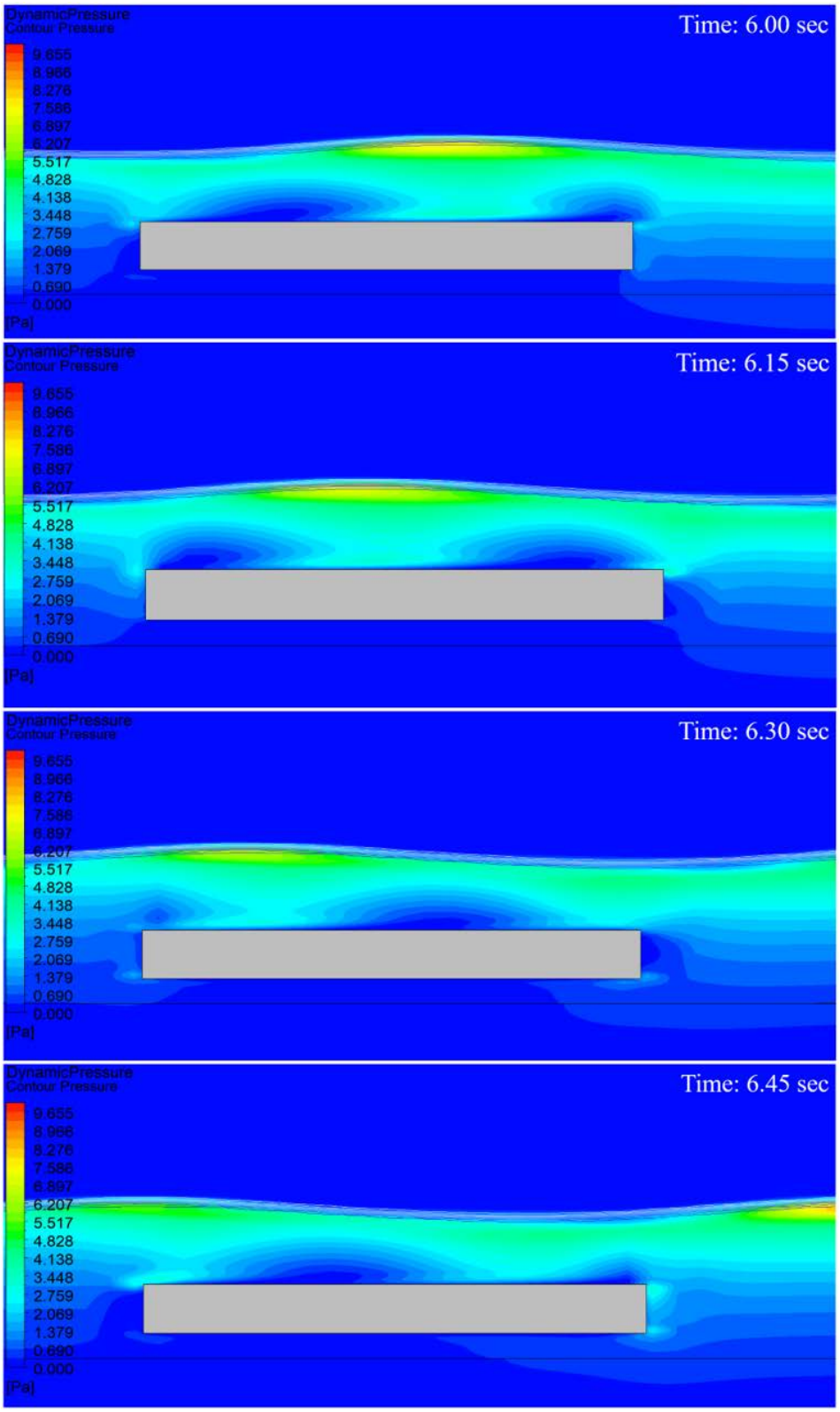

Figure 36. Transient dynamic pressure contours for immersed solid model in lower position (6.00 – 6.45 sec)

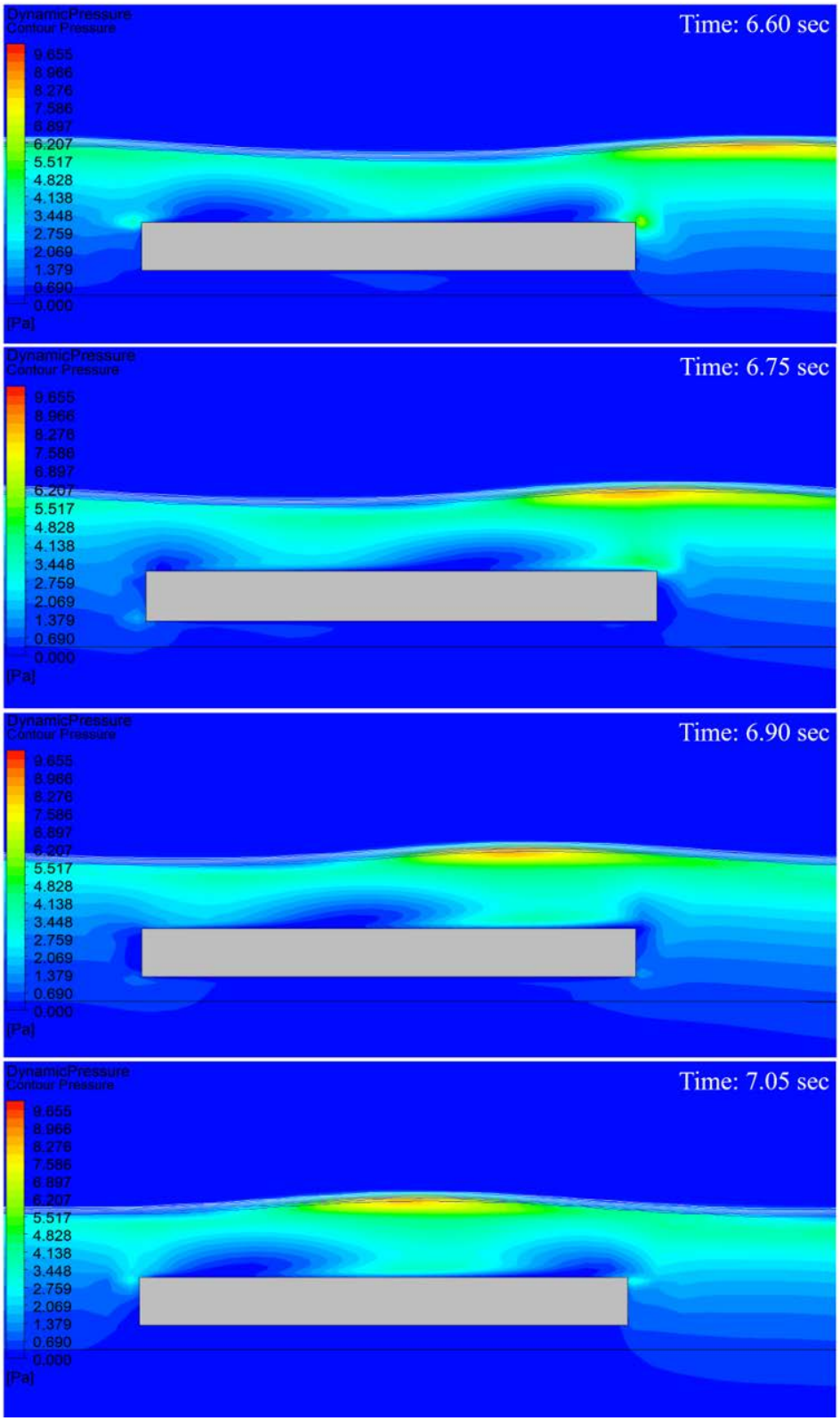

Figure 37. Transient dynamic pressure contours for immersed solid model in lower position (6.45 – 7.05 sec)

The next comparison was to assess the impact the position of the body has on the forces and moment exerted on the body by the wavefront. It is anticipated that the lower the body is beneath the waves, the smaller the forces and moments on the body will be. However, the appropriate decreasing behavior between the upper and lower positions was only exhibited by the immersed solid method of body formation. Figure 38, Figure 39, and Figure 40 show the non-dimensionalized drag force, lift force, and moment on the body, respectively, at the different depths and body formation methods. The drag forces show realistic behavior for both modeling methods where the body force in the high position is higher than the drag force in the lower position. However, while the immersed solid model shows a decrease for the lift force and pitch moment when moving from the high position to the low position, the rigid body model shows the lift force and pitch moment maintaining approximately constant.

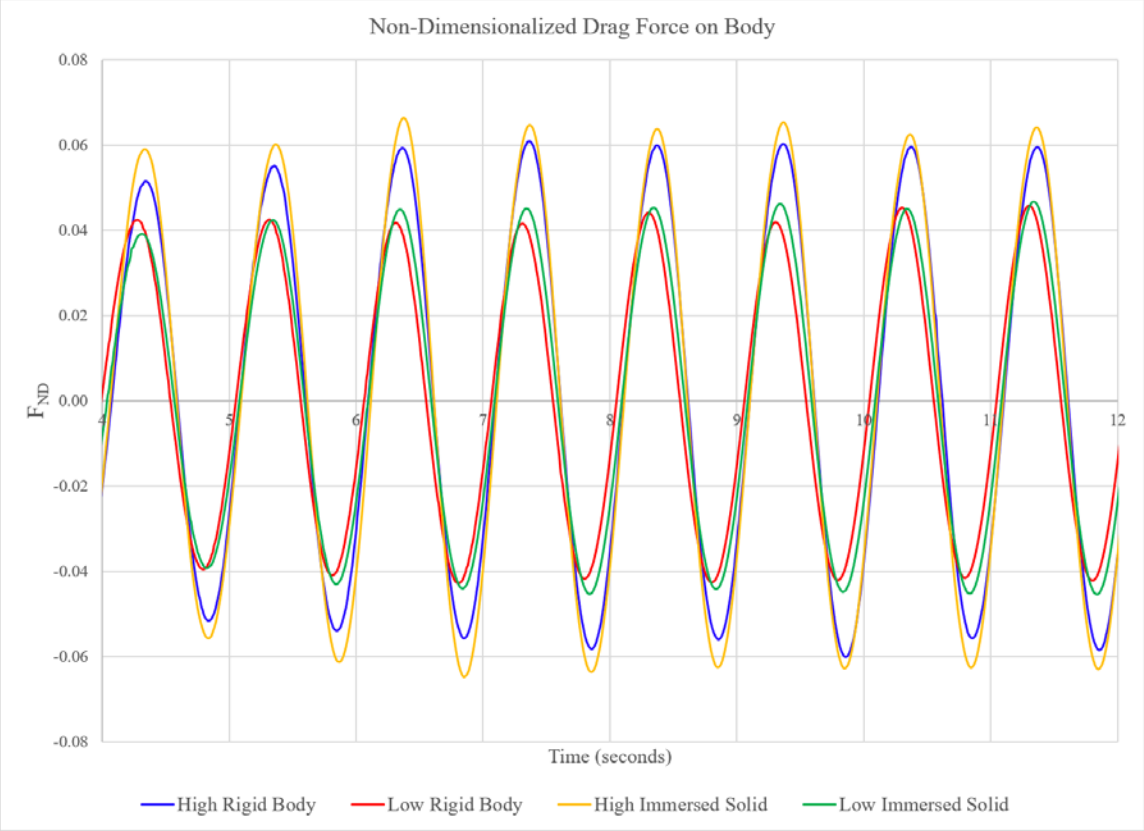

Figure 38. Non-dimensionalized drag force comparison between high and low body positions

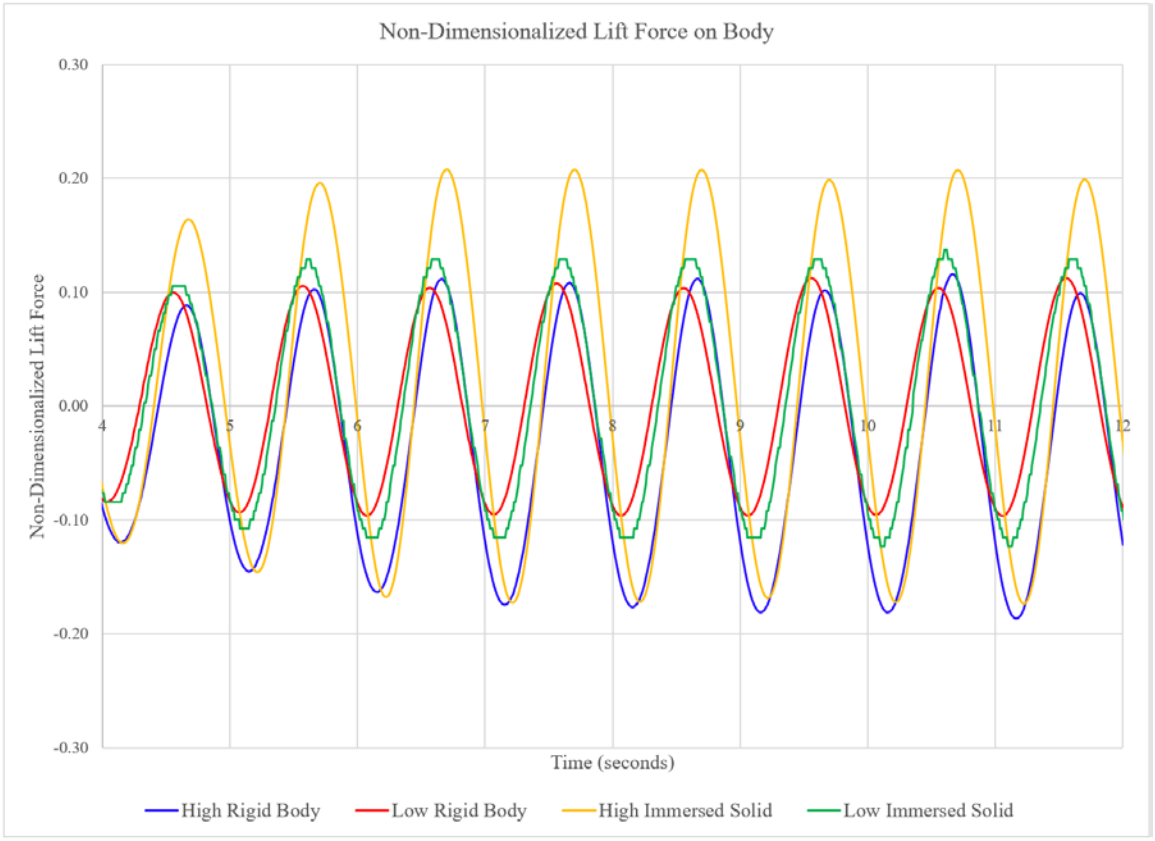

Figure 39. Non-dimensionalized lift force comparison between high and low body positions

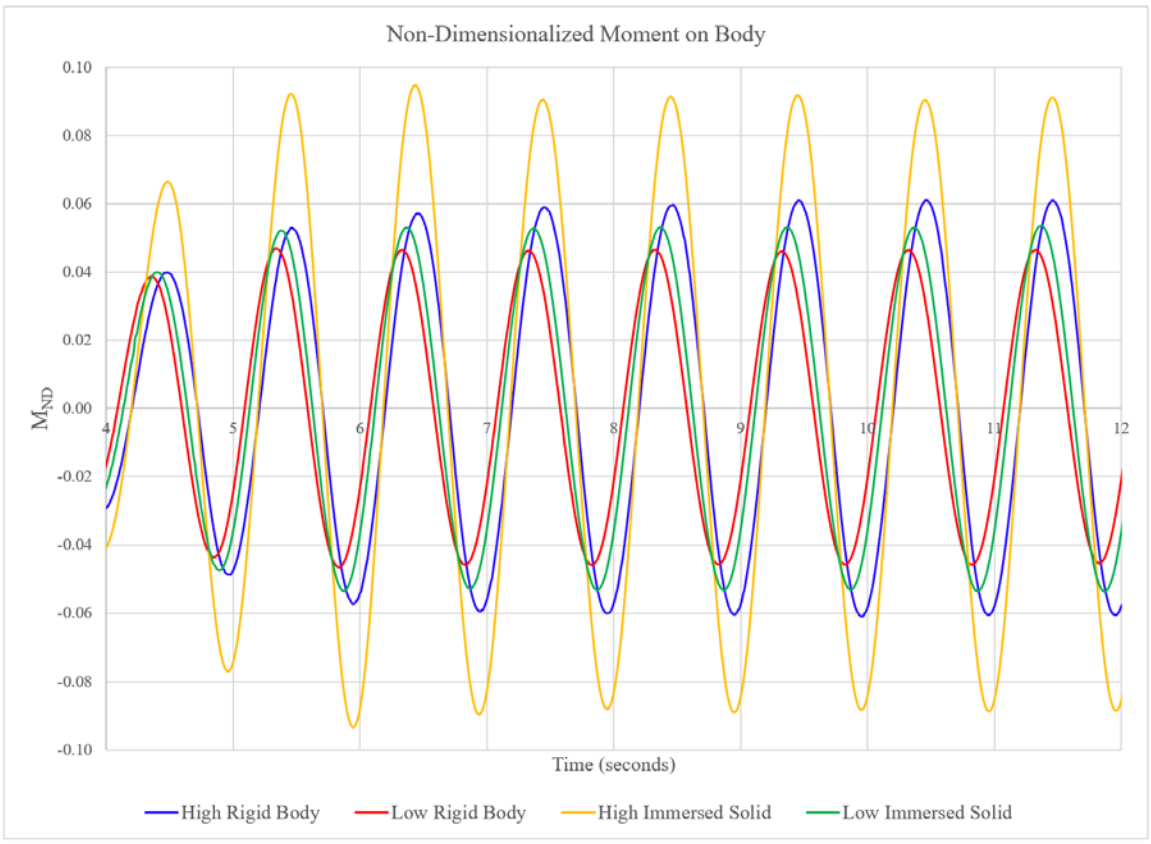

Figure 40. Non-dimensionalized moment comparison between high and low body positions

The rigid body model and immersed solid model both showed similar behavior for velocities, dynamic pressures, non-dimensionalized body forces and moment with the body in the lower position. Overall, this indicates that the two body formation modeling methods can be used interchangeably in situations with limited wave-body interactions.

C. WAVE ENERGY DISSIPATION

As it was determined the amount of fluid interaction with the body impacts the consistency of behavior between the body formation modeling methods, the amount of wave energy dissipated in the model was used to assess this interaction. In order to quantify the energy dissipation from the body, a wave amplitude analysis was performed. An NPS tow tank model without a body was used as the baseline. In this model, the transient wave amplitudes were monitored at locations 1 meter from the wedge and 4.25 meters from the

wedge, which would be located 1.25 meters in front of and 1 meter behind the submerged body, respectively, in the rigid body and immersed solid models. The baseline wave dissipation from the NPS tow tank model without a body is shown in Figure 41. Even without the body, there is a decent amount of wave energy dissipation, with the average value between these two stations being 14.6%.

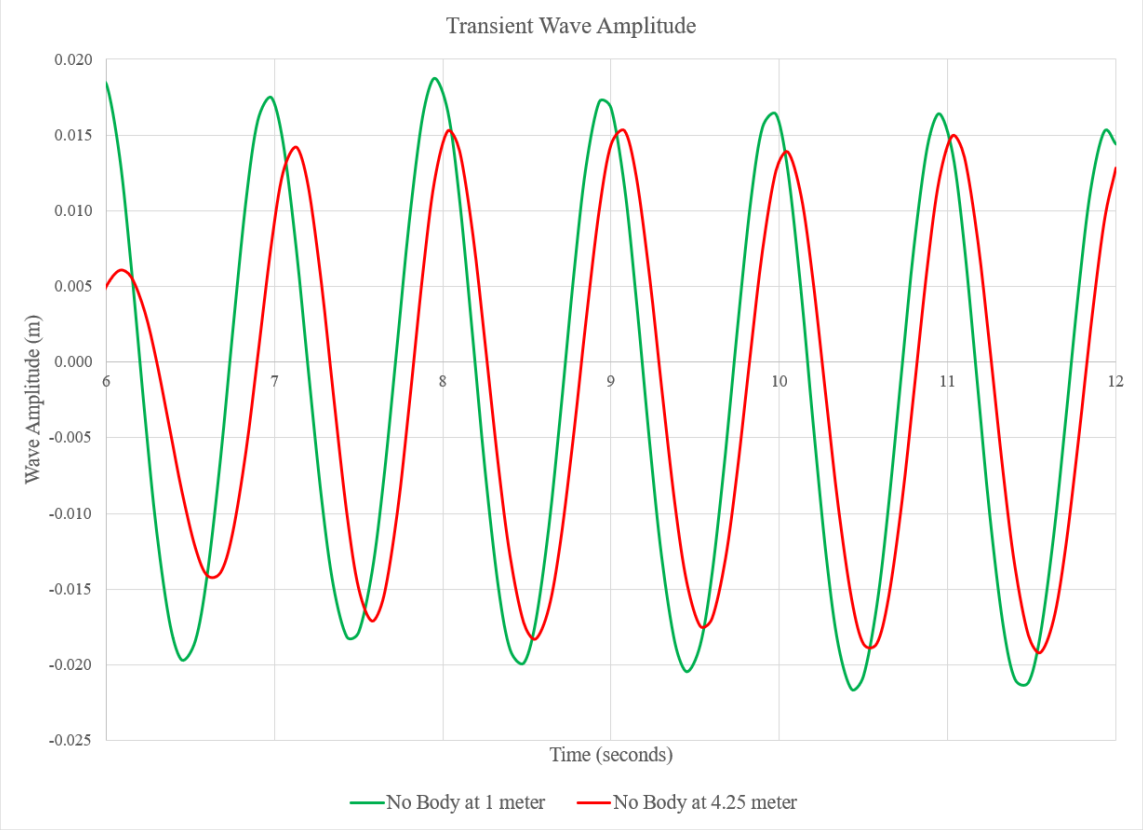

Figure 41. Transient wave amplitude for model with no body

This wave dissipation behavior was then compared to the model with the rigid body oriented with a 15° up angle, with results shown in Figure 42. The wave dissipation is significantly greater in the 15° up angle rigid body model, with average wave dissipation between the stations at 77.8%.

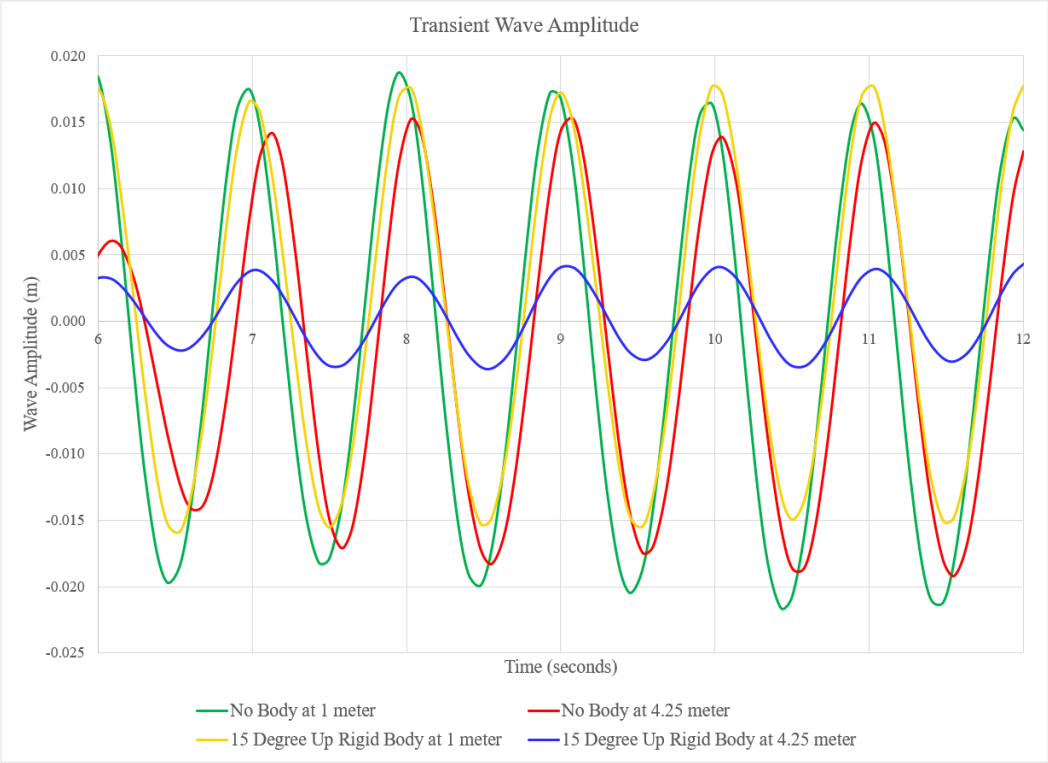

Figure 42. Transient wave amplitude comparison between model with no body and 15° up angle rigid body model

The process of determining wave energy dissipation was repeated for the horizontal and 7.5° up angle rigid body models and the horizontal and 7.5° up angle immersed solid models. Table 1 provides the results of this analysis with the models sorted from least dissipation to most dissipation.

Table 1. Average wave energy dissipation for various models

Body Model Type	Body Orientation	Average Wave Dissipation
None	N/A	14.6%
Rigid Body	0°	34.7%
Immersed Solid	0°	39.7%
Immersed Solid	7.5°	39.8%
Rigid Body	15°	77.8%
Rigid Body	7.5°	79.2%
Rigid Body	-15°	89.4%

All of the models with a submerged body show more wave energy dissipation than that of the model without a body. The horizontal rigid body, horizontal immersed solid, and 7.5° up immersed solid models have approximately the same amount of wave energy dissipation. The three rigid body models with the submerged body oriented at 7.5°, 15°, and -15° show a decrease in wave amplitude that is greater than 75% when comparing the waves before the submerged body to after the submerged body. This indicates that a significant amount of wave energy is being dissipated by the submerged body within the model.

D. BODY ORIENTATION COMPARISON

The final analysis was performed to compare the modelling behavior and forces on the body when the central axis of the body was placed at an angle while in the low position. This analysis, done in sections, includes rigid body models oriented with a 7.5°, 15°, and -15° angle as well as an immersed solid model angled at 7.5°. For all models, the body coordinate system and the corresponding orientation of the forces is maintained consistent with the horizontal bodies, meaning that the x-, y-, and z-, axes are maintained parallel to the global coordinate system. Additionally, the wedge motion and generated waveform were maintained consistent with previous sections.

Figure 43, Figure 44, and Figure 45 show the non-dimensionalized drag force, lift force, and moment on the submerged body modeled using the rigid body method, comparing the horizontal models at equivalent depth to when the body was angled at 7.5° and 15°. In all instances using the rigid body method, the forces and moment on the angled bodies were reduced when compared to the horizontal model, with the exception of the non-dimensionalized drag force on the body with a 15° up angle. The most likely cause for the reduction of forces is the high amount of wave dissipation discussed previously.

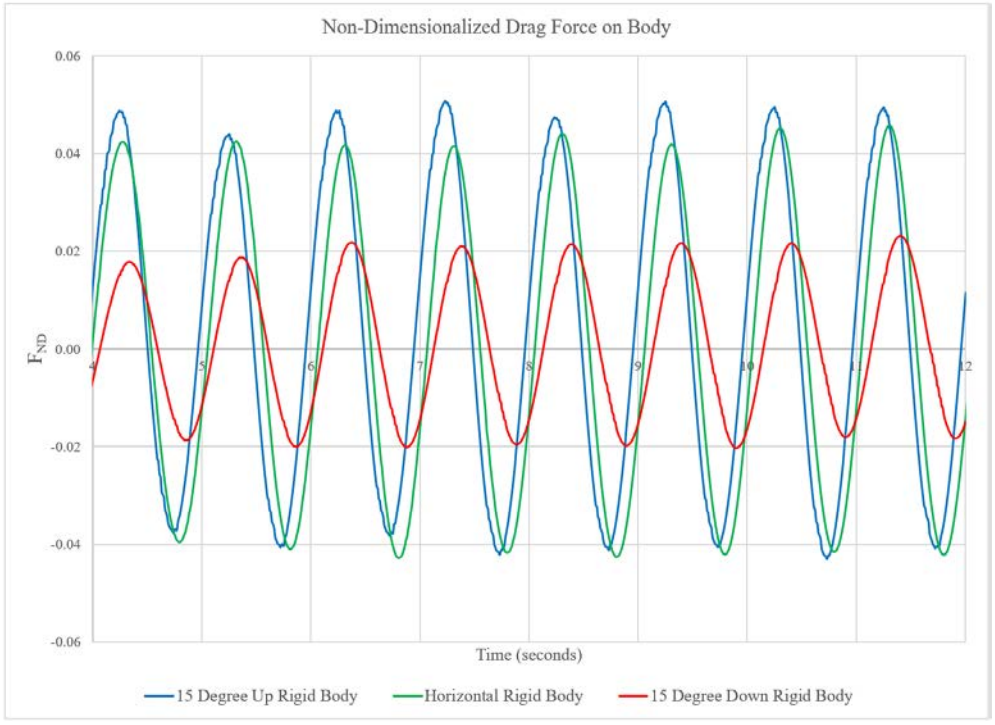

Figure 43. Non-dimensionalized drag force comparison for rigid body models with up angle

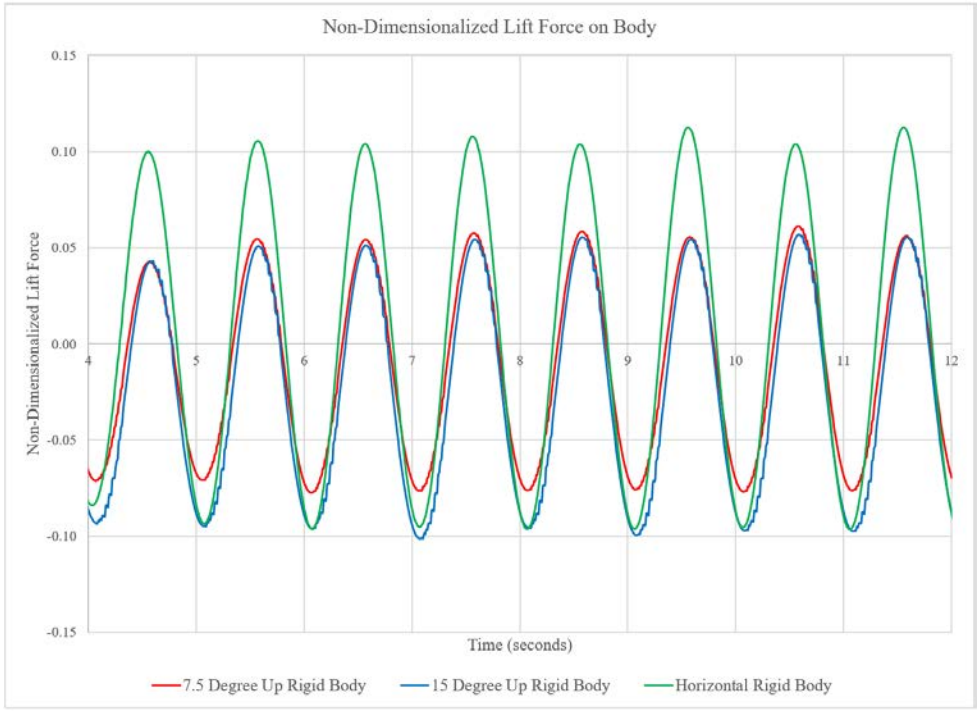

Figure 44. Non-dimensionalized lift force comparison for rigid body models with up angle

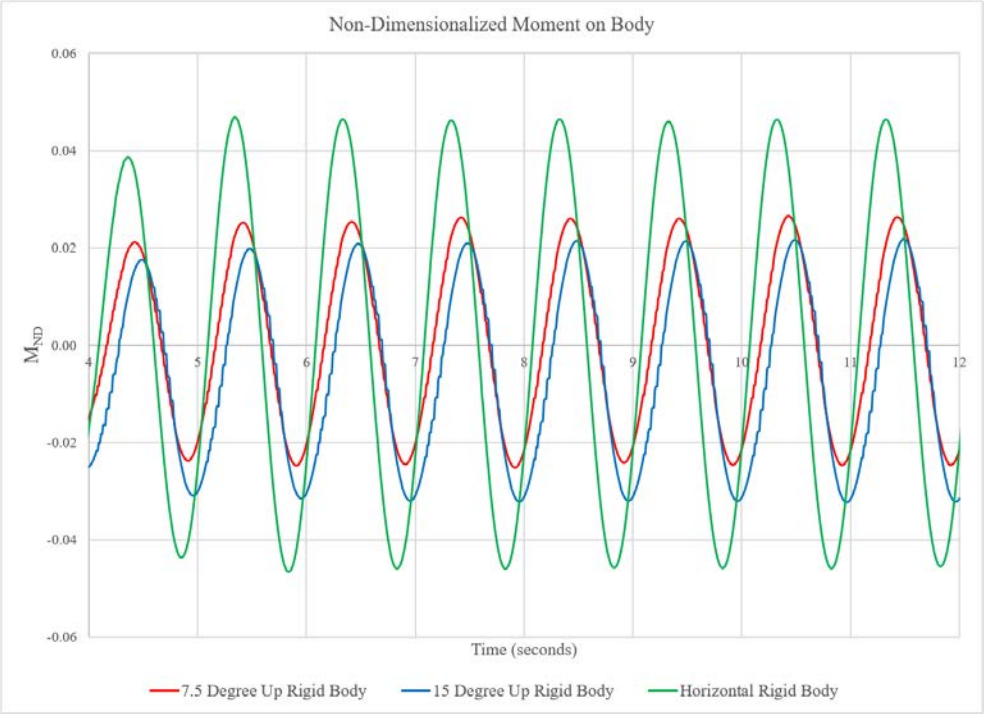

Figure 45. Non-dimensionalized moment comparison for rigid body models with up angle

Further investigation into the 15° up angle model provided evidence that the significant angle of the body as well as the position beneath the surface is causing the waveforms to be disrupted as it travels over the body. As shown in Figure 46, the wave shape is clearly disrupted by the body causing increased dispersion of the water on the water-air interface and less apparent sinusoidal behavior of the interface.

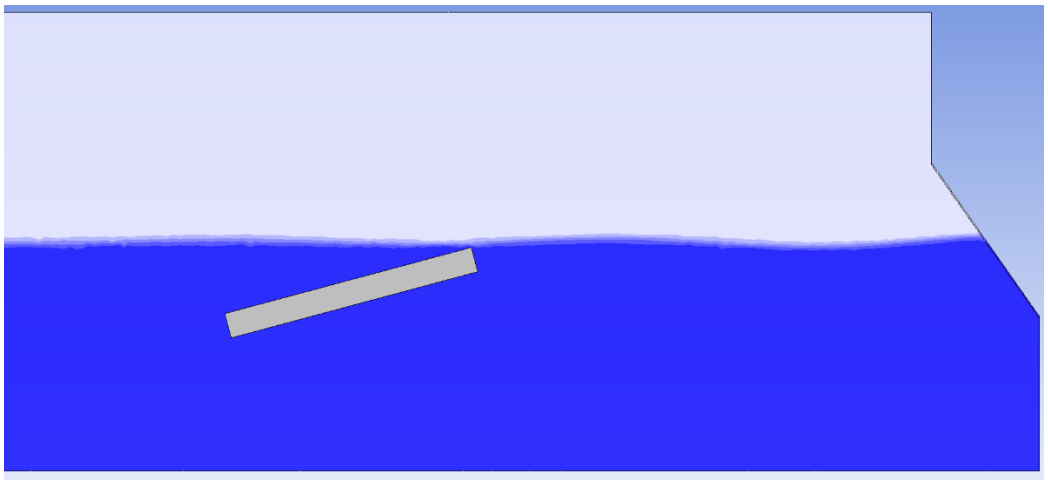

Figure 46. Waveform over rigid body with 15° up angle

Additional evidence of waveform interruption is shown by examining the velocity vectors of the model, shown in Figure 47. The black lines indicate the direction of fluid velocity and the blue bands with contour lines at the top of the image indicate the air-water interface. The velocity of the wave is clearly being disrupted by the submerged body. This will dissipate a significant amount of energy at the front of the body, resulting in waveform deterioration.

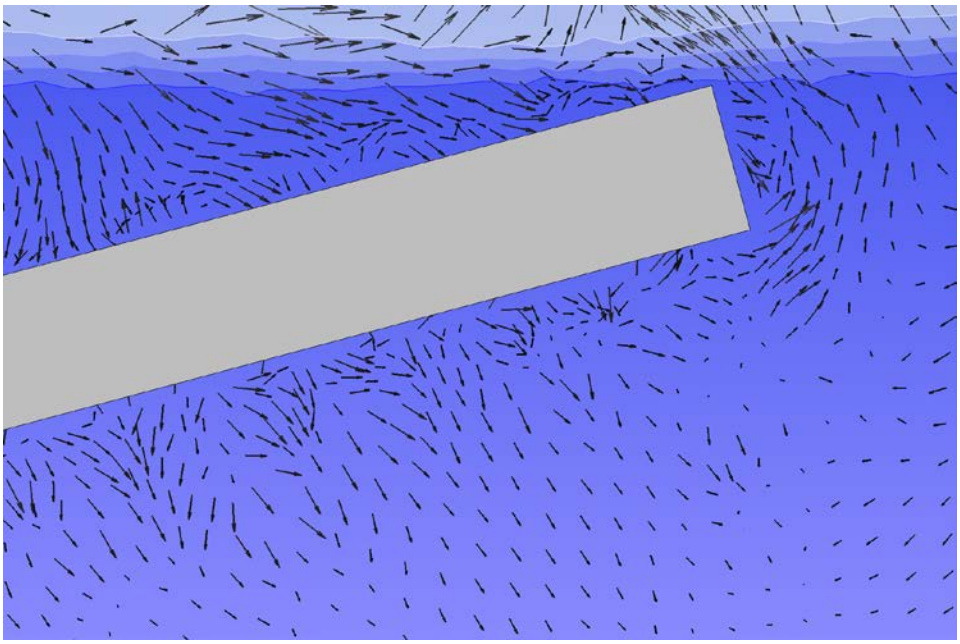

Figure 47. Velocity vectors around rigid body with 15° up angle

Additional comparisons were conducted with the rigid body at a 15° down angle. The non-dimensionalized drag force, lift force, and moment are shown in Figure 48, Figure 49, and Figure 50. The dynamic forces and moment imparted on the submerged body in this model are greatly reduced as compared to those from the horizontal models. The significant amount of wave energy dissipation shown Table 1 is the most likely cause. The rigid body model with a 15° down angle had the largest drop in wave amplitude when comparing the stations before the body and after the body. This amount of energy dissipation would result in less energy being imparted to the body from the wave, resulting in an overall reduction in body forces and moments.

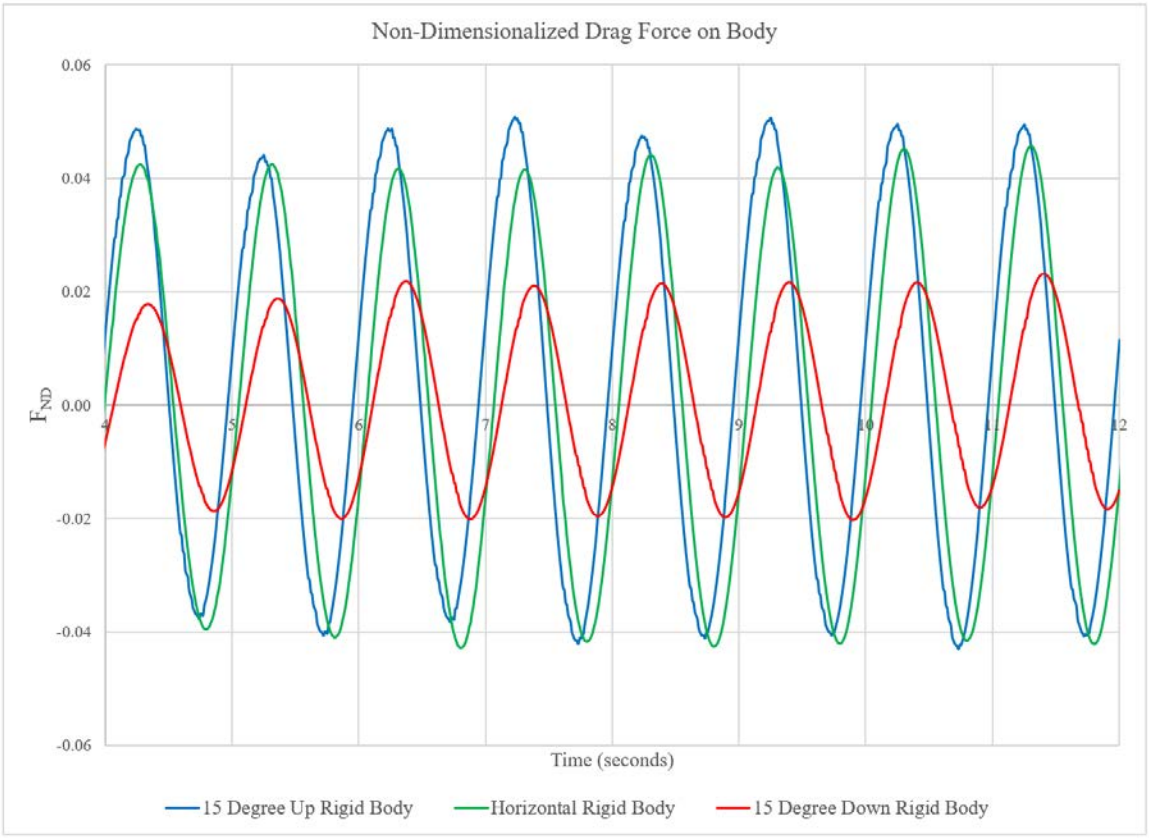

Figure 48. Non-dimensionalized drag force comparison for body with down angle

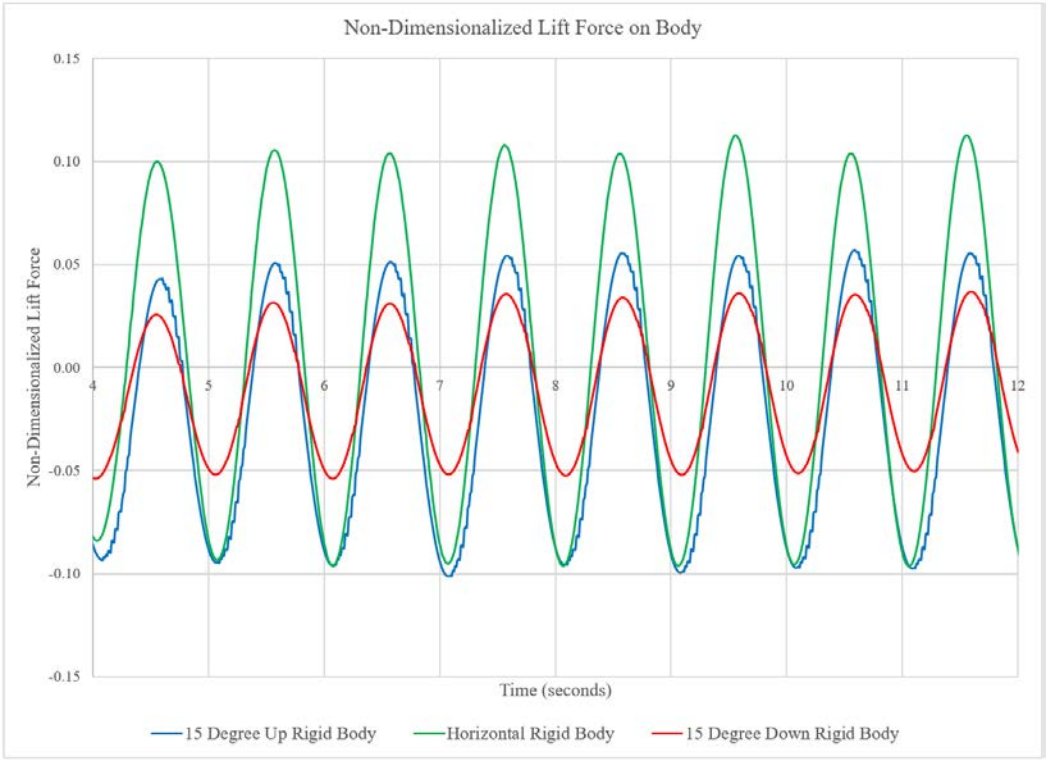

Figure 49. Non-dimensionalized lift force comparison for body with down angle

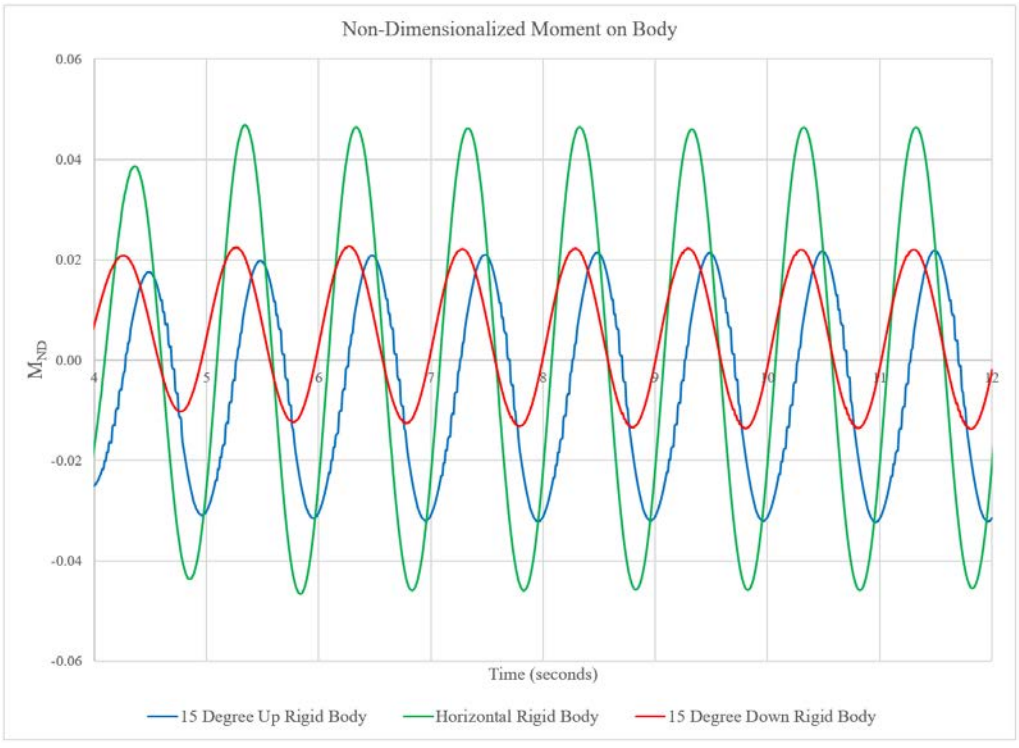

Figure 50. Non-dimensionalized moment comparison for body with down angle

An immersed solid model with a 7.5° up angle was then compared to the rigid body model with a 7.5° up angle to determine if the modeling techniques would produce similar results. Similar to the previous analysis, three points were used midbody at 0.01 meter, 0.04 meter, and 0.06 meter above the upper surface, shown in Figure 51. The total velocity behavior between the two models at these data points was very different as observed in Figure 52. This discrepancy prompted a comparison of the transient behavior of the velocity vectors in the vicinity of the forward nose of the body. The transient velocity vectors for the rigid body model are shown in Figure 53, Figure 54, and Figure 55 and for the immersed solid model are shown in Figure 56, Figure 57, and Figure 58.

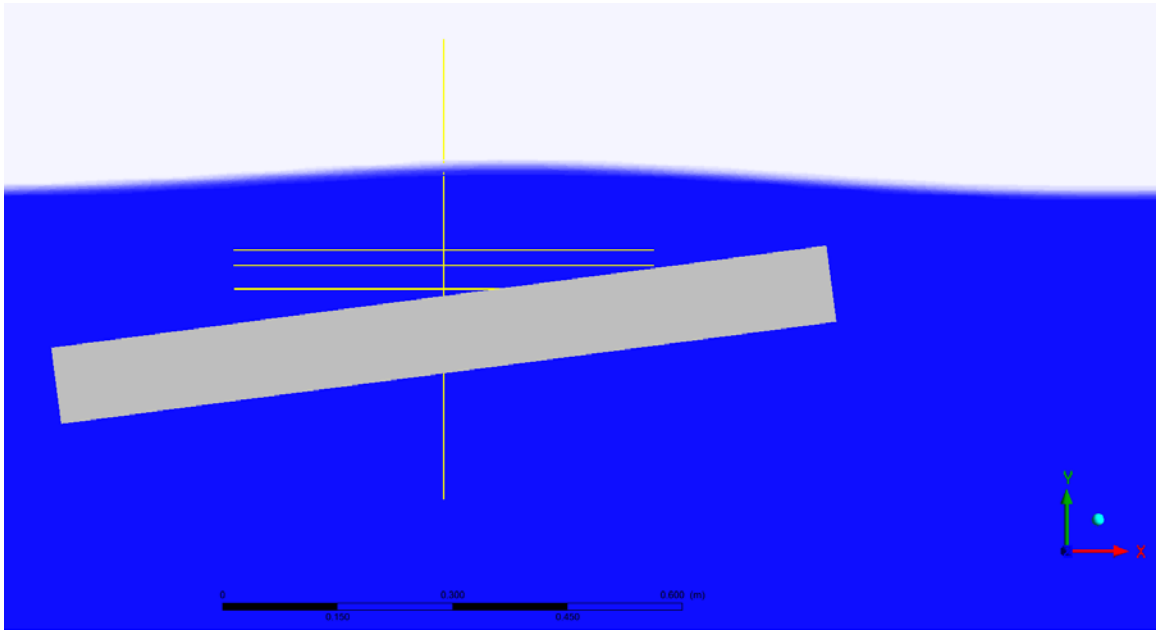

Figure 51. Location of data points used for 7.5° up angle comparison

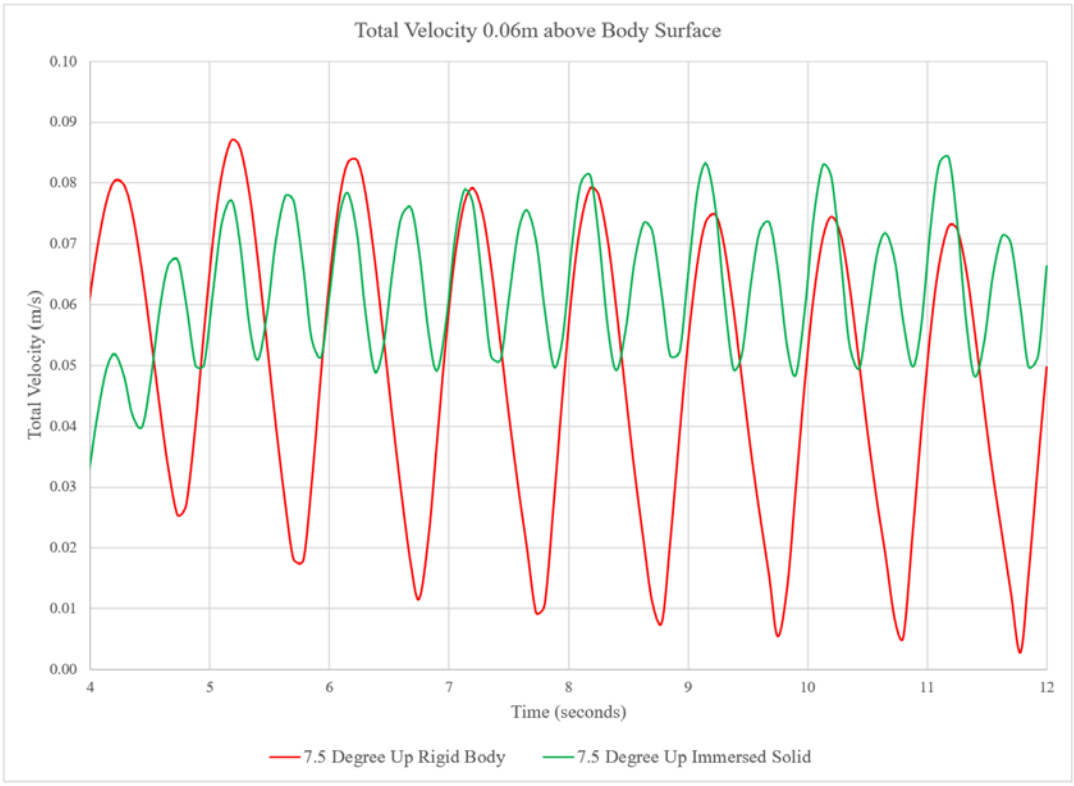

Figure 52. Total velocity comparison between models with 7.5° up angle

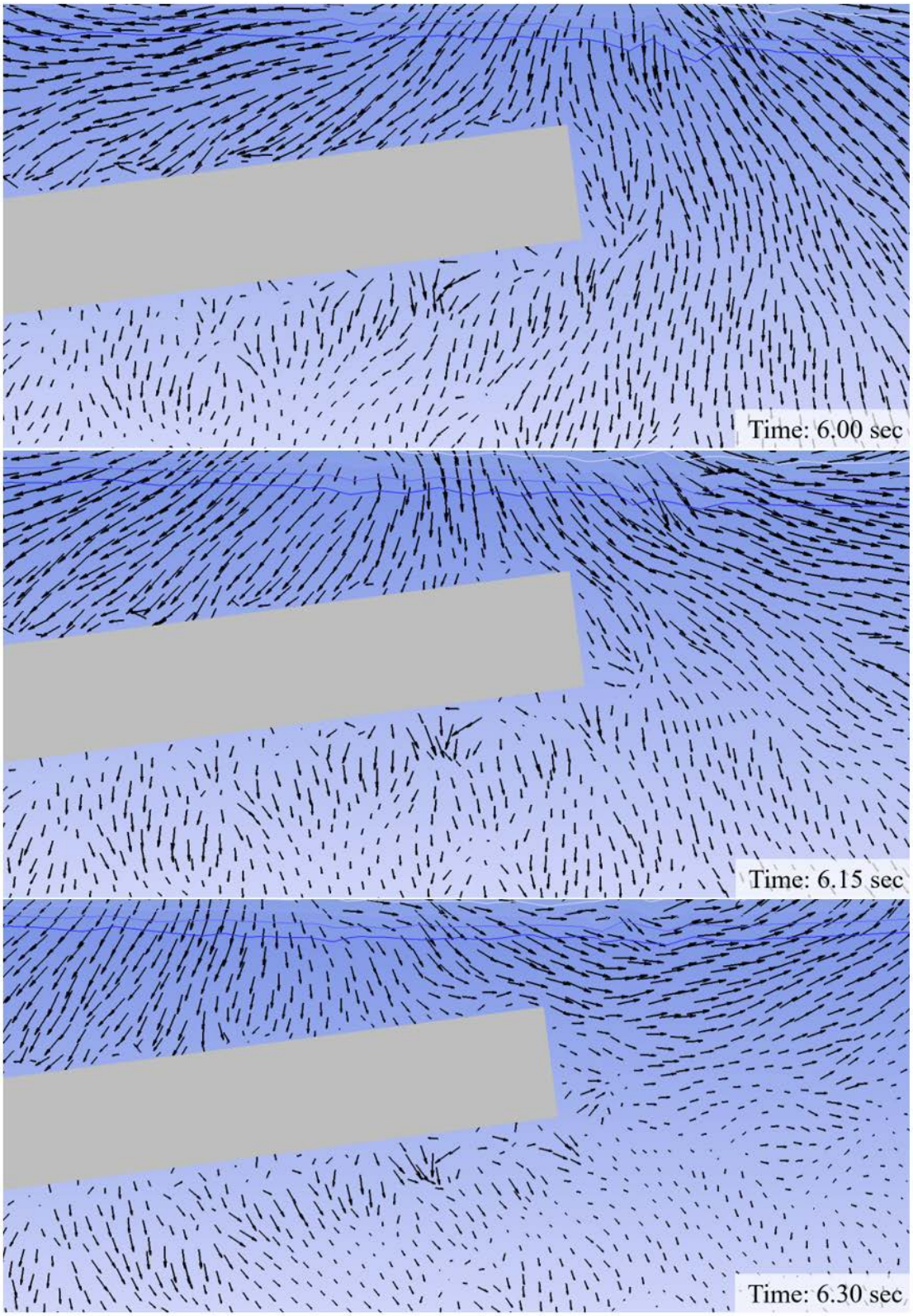

Figure 53. Transient velocity vectors for rigid body model with 7.5° up angle (6.00 – 6.30 sec)

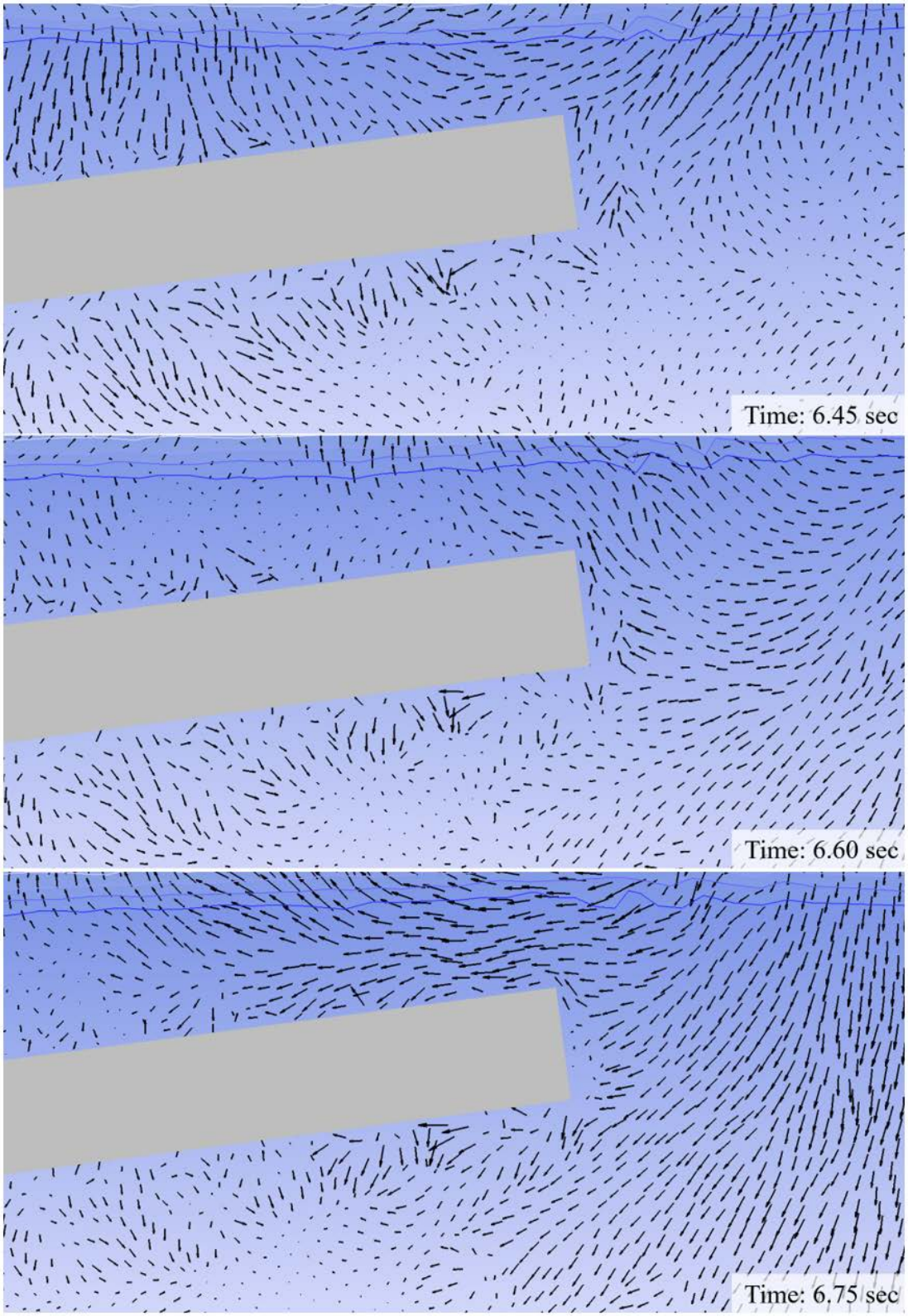

Figure 54. Transient velocity vectors for rigid body model with 7.5° up angle (6.45 – 6.75 sec)

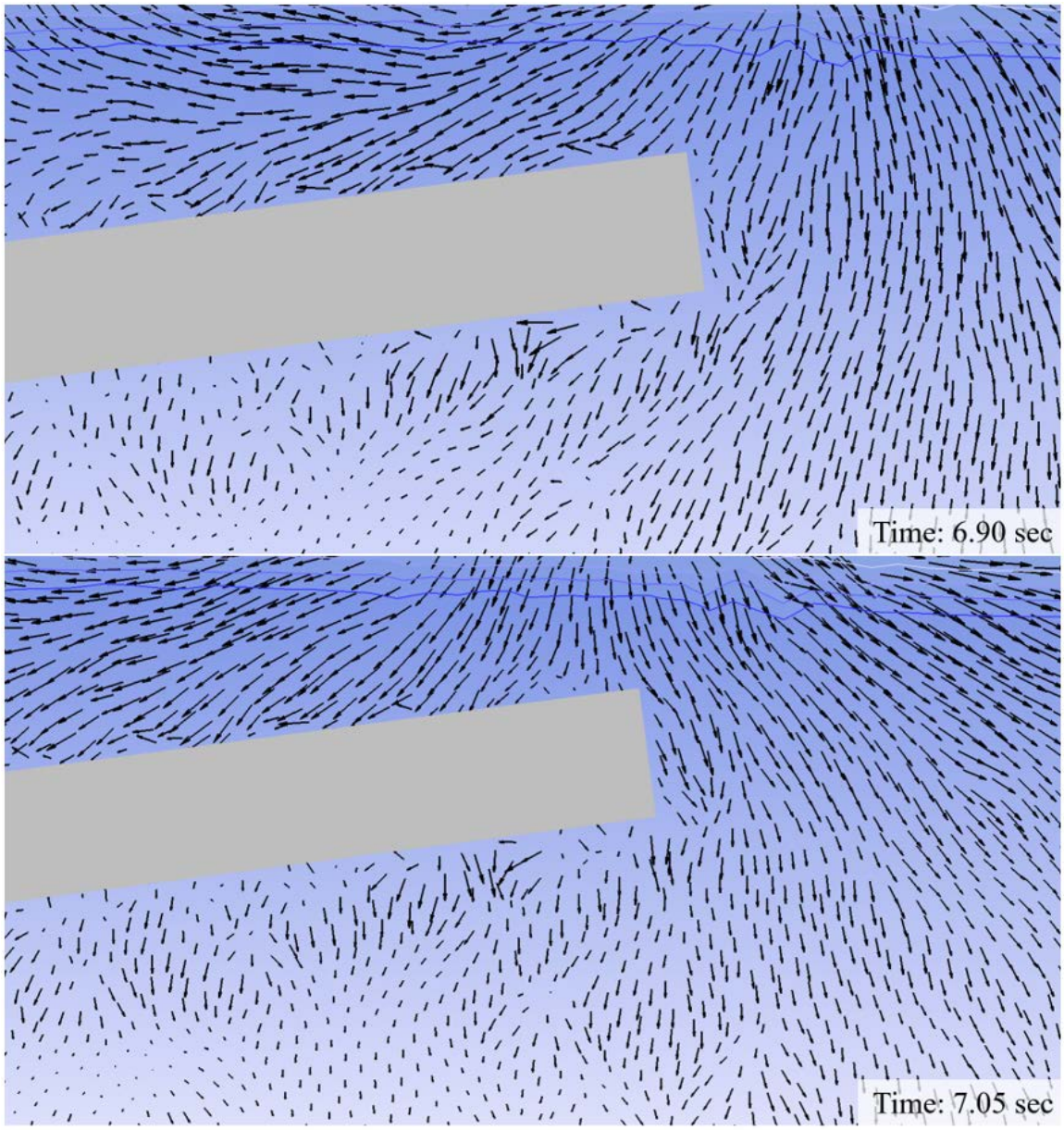

Figure 55. Transient velocity vectors for rigid body model with 7.5° up angle (6.90 – 7.05 sec)

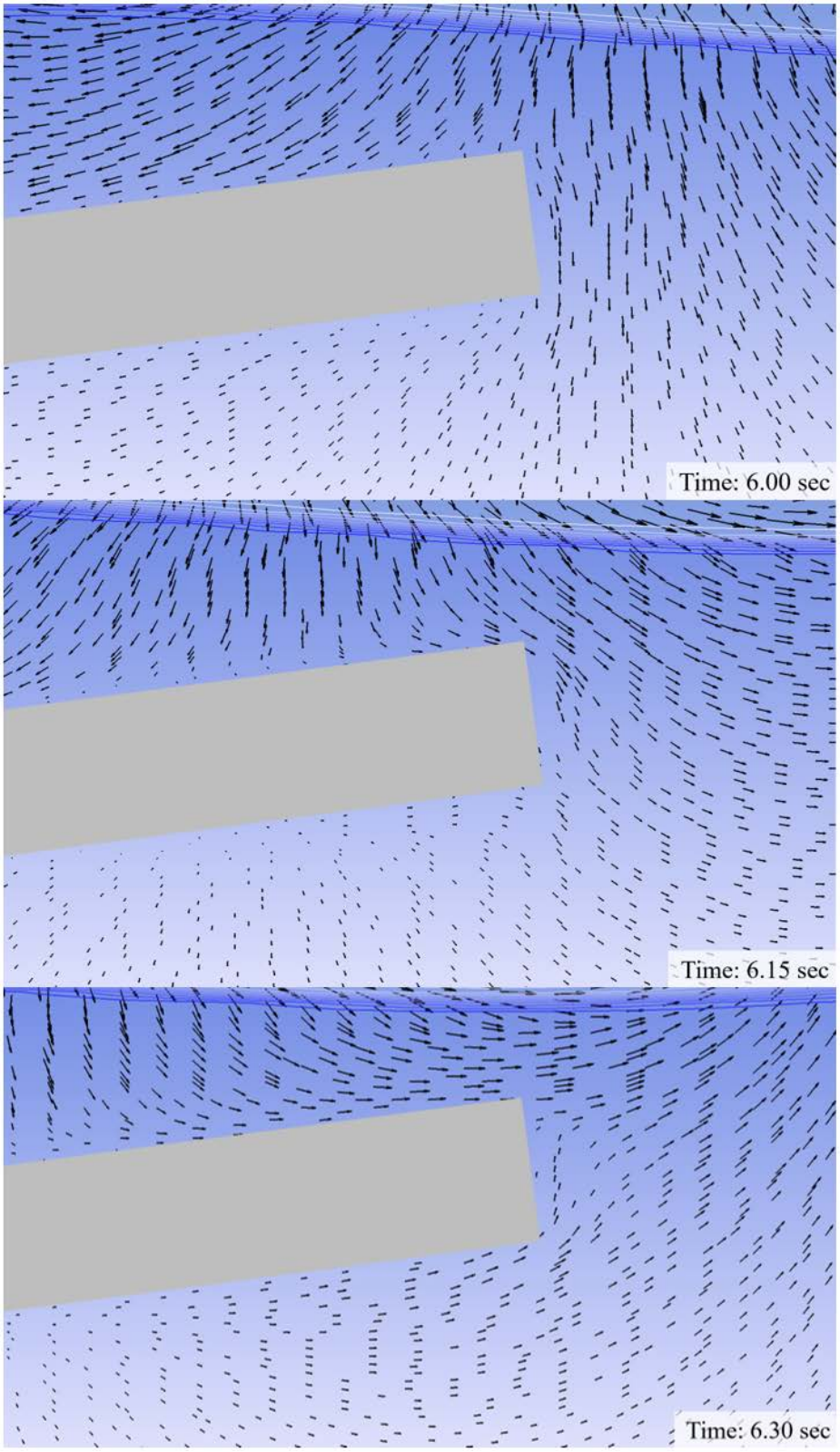

Figure 56. Transient velocity vectors for immersed solid model with 7.5° up angle (6.00 – 6.30 sec)

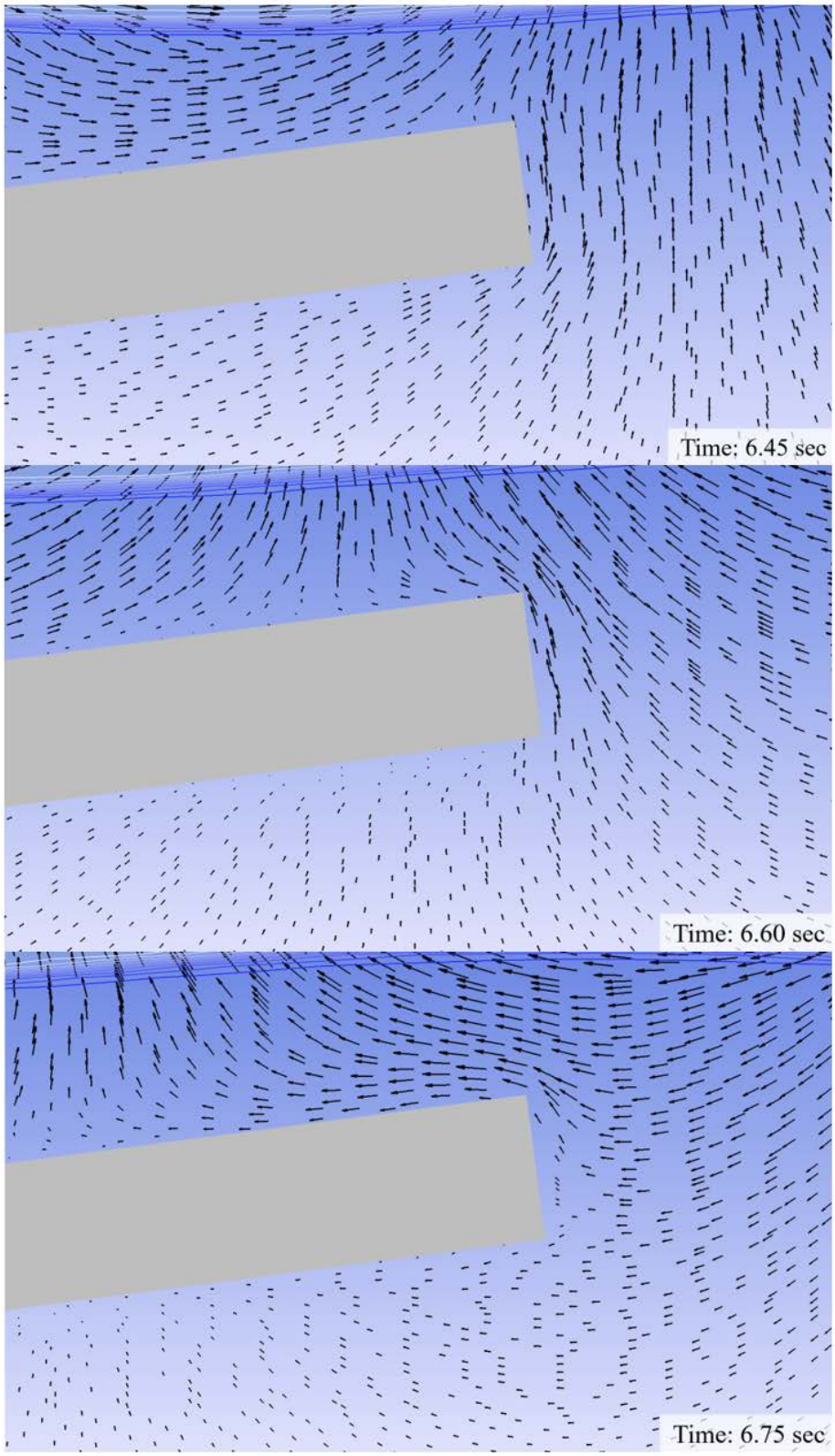

Figure 57. Transient velocity vectors for immersed solid model with 7.5° up angle (6.45 – 6.75 sec)

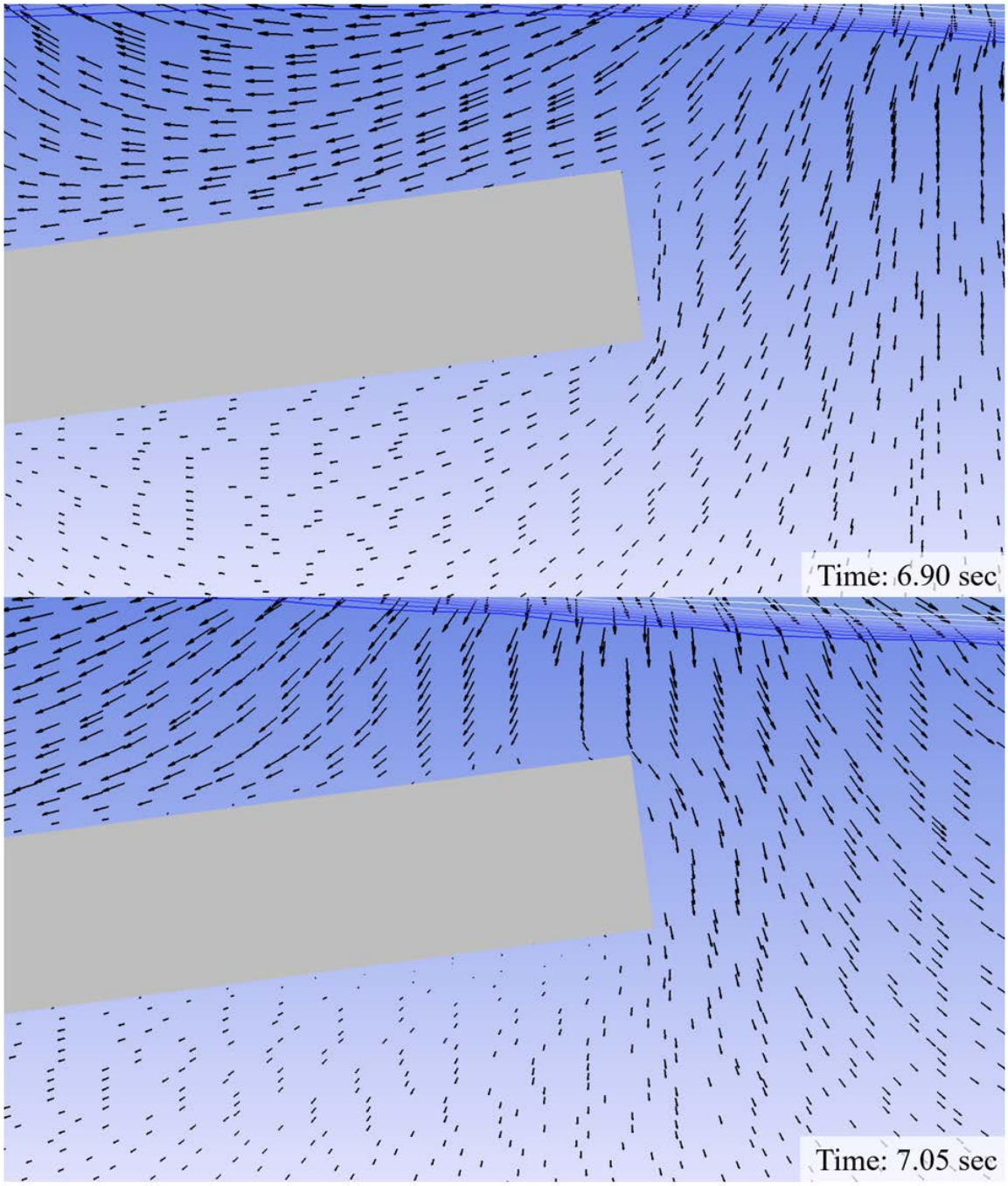

Figure 58. Transient velocity vectors for immersed solid model with 7.5° up angle (6.90 – 7.05 sec)

Similar to the behavior observed with the horizontal body in the lower position, the rigid body model shows the velocity vectors impinging on the body. This causes disturbances in the flow field in the immediate area of the body. Conversely, the immersed solid model does not have this interaction and the velocity vectors are significantly smoother around the body.

This distinction in body interaction is due to the difference in nature of the modeling methods. The immersed solid model does not allow particles to interact with the walls of the immersed solid. Instead, the particles along the immersed solid domain are tracked based on the fluid velocity which is driven to match the velocity of the immersed solid domain. In this model, the immersed solid domain is stationary, and so the fluid is driven to be stationary at the wall of the body. However, the particles cannot impinge upon the body as is being observed with the rigid body model. An enlarged view of this fluid particle-to-rigid body interaction is shown in Figure 59.

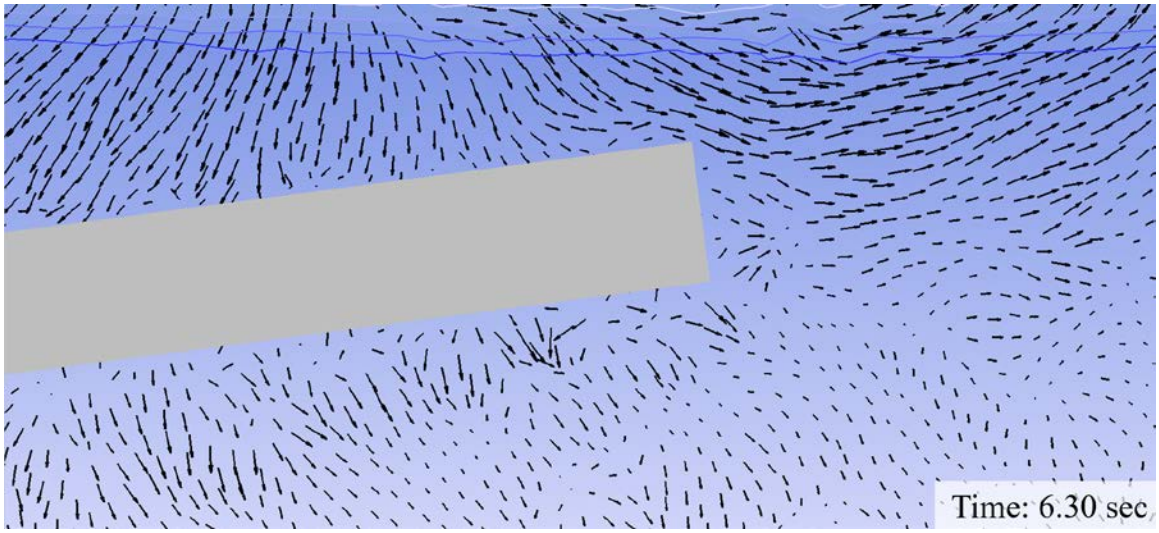

Figure 59. Rigid body velocity vectors showing fluid interaction with rigid body

An additional comparison of the two models was assessing the transient dynamic pressure behavior. Transient dynamic pressure contour lines for the rigid body model are shown in Figure 60 and Figure 61 and the dynamic pressure contour lines for the immersed solid model are in Figure 62 and Figure 63. In these contour lines, all figures have the same scaling. As seen previously, the immersed solid model produces dynamic pressure contours that are more continuous while the rigid body model results in patchy dynamic pressure contours. Additionally, unlike the previous model, the dynamic pressure pockets formed around the body are not consistent. All of the rigid body timesteps show pockets of higher pressure located underneath the rigid body, while the immersed solid model does not. The immersed solid model also shows a high dynamic pressure bubble forms along the upper tip of the body as the wave passes over it, while the rigid body does not show this high-pressure bubble.

As dynamic pressure is heavily dependent on velocity, it is likely that some of the discrepancy in behavior between the rigid body and immersed solid dynamic pressure contours is due to the difference in fluid to body interaction between the models described previously.

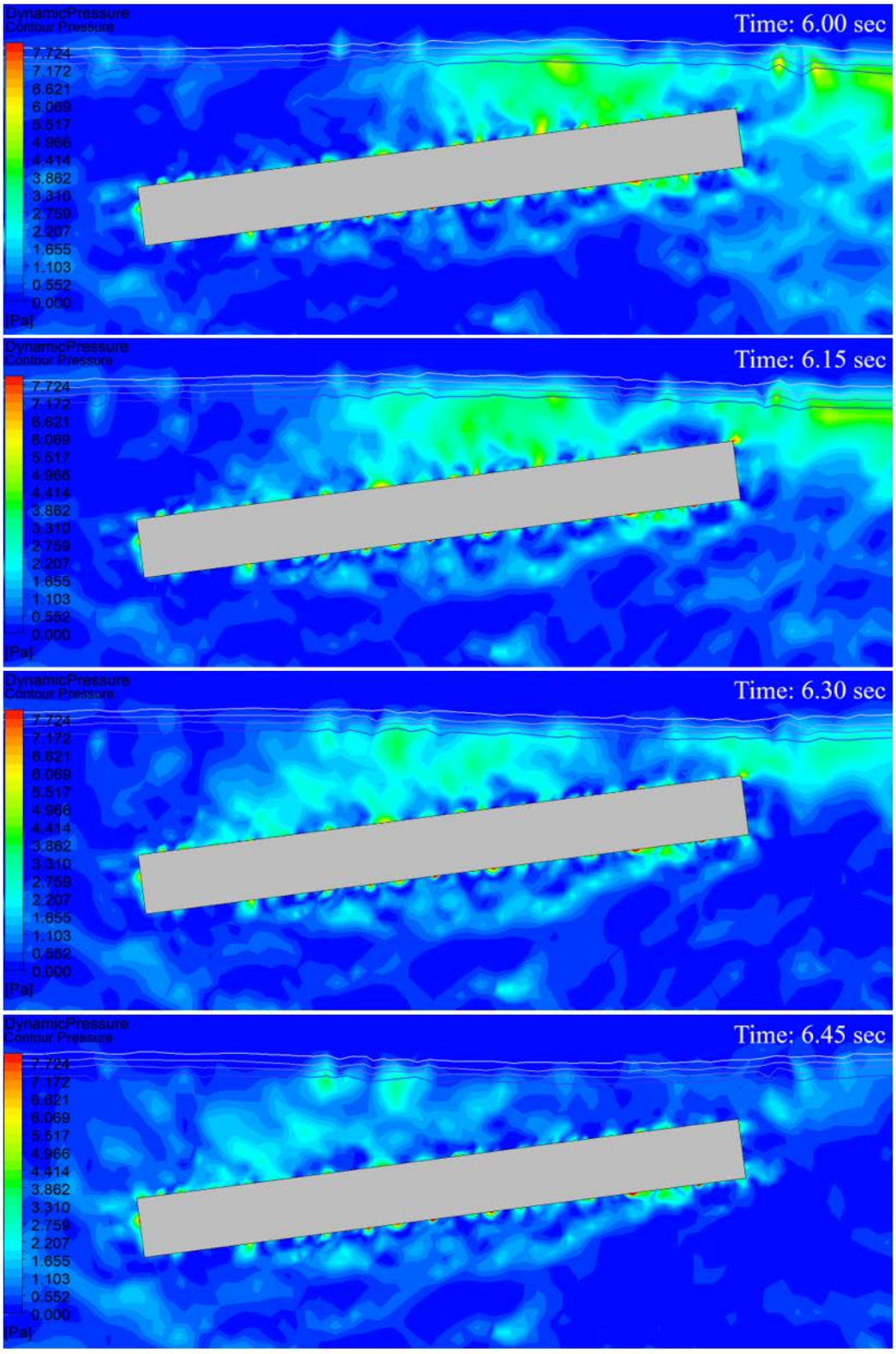

Figure 60. Transient dynamic pressure contours for rigid body model with 7.5° up angle (6.00 – 6.45 sec)

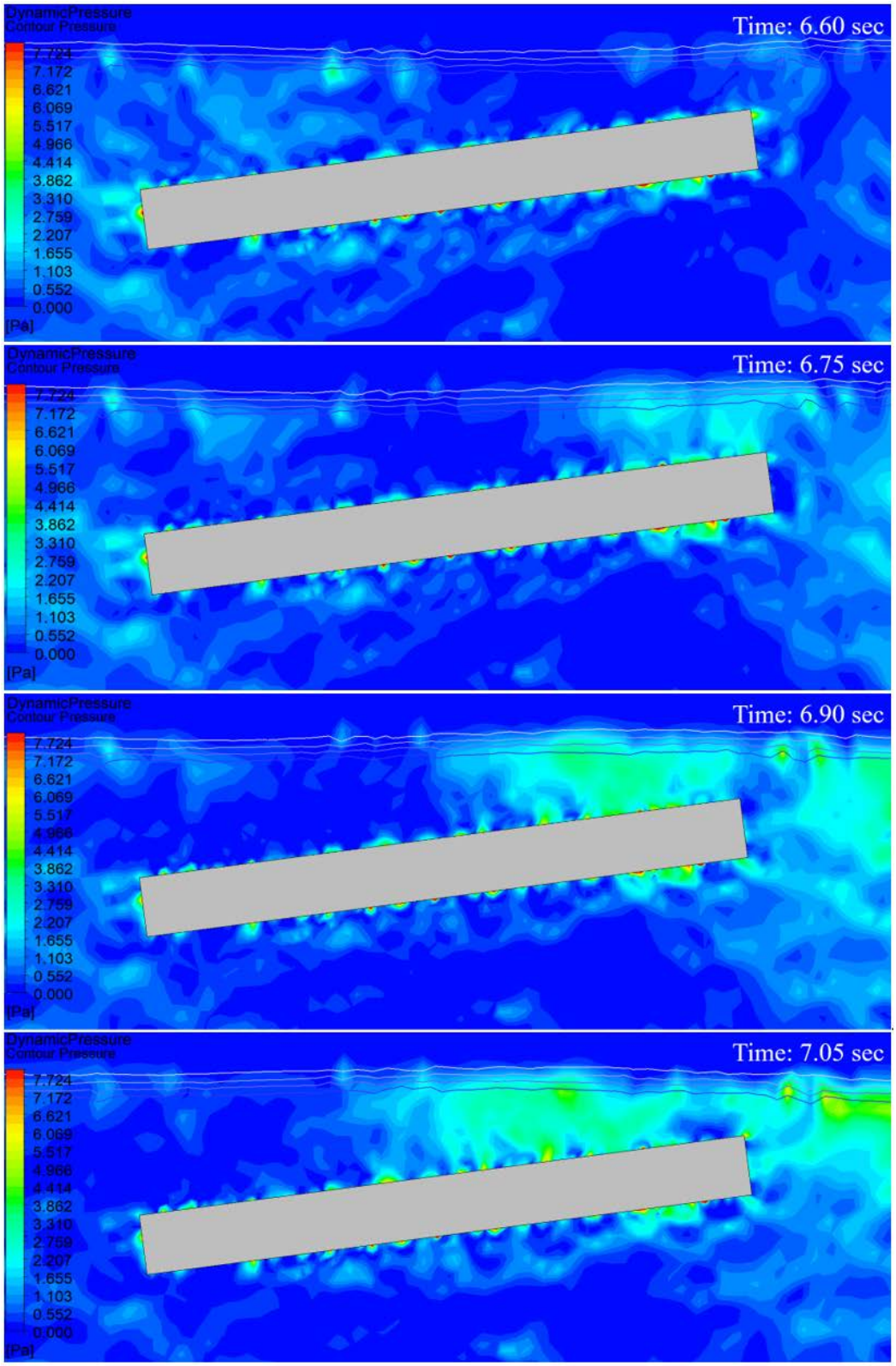

Figure 61. Transient dynamic pressure contours for rigid body model with 7.5° up angle (6.60 – 7.05 sec)

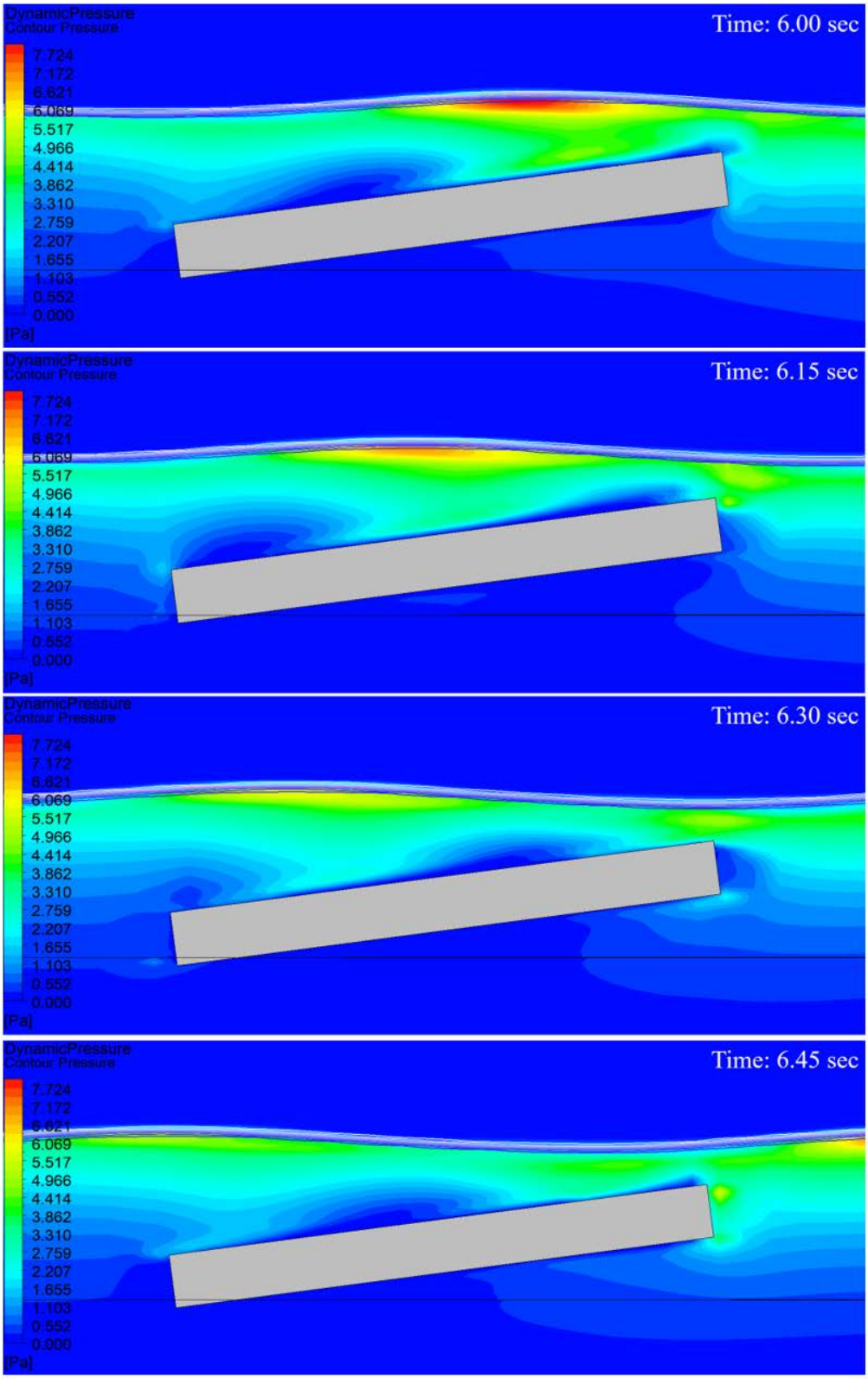

Figure 62. Transient dynamic pressure contours for immersed solid model with 7.5° up angle (6.00 – 6.45 sec)

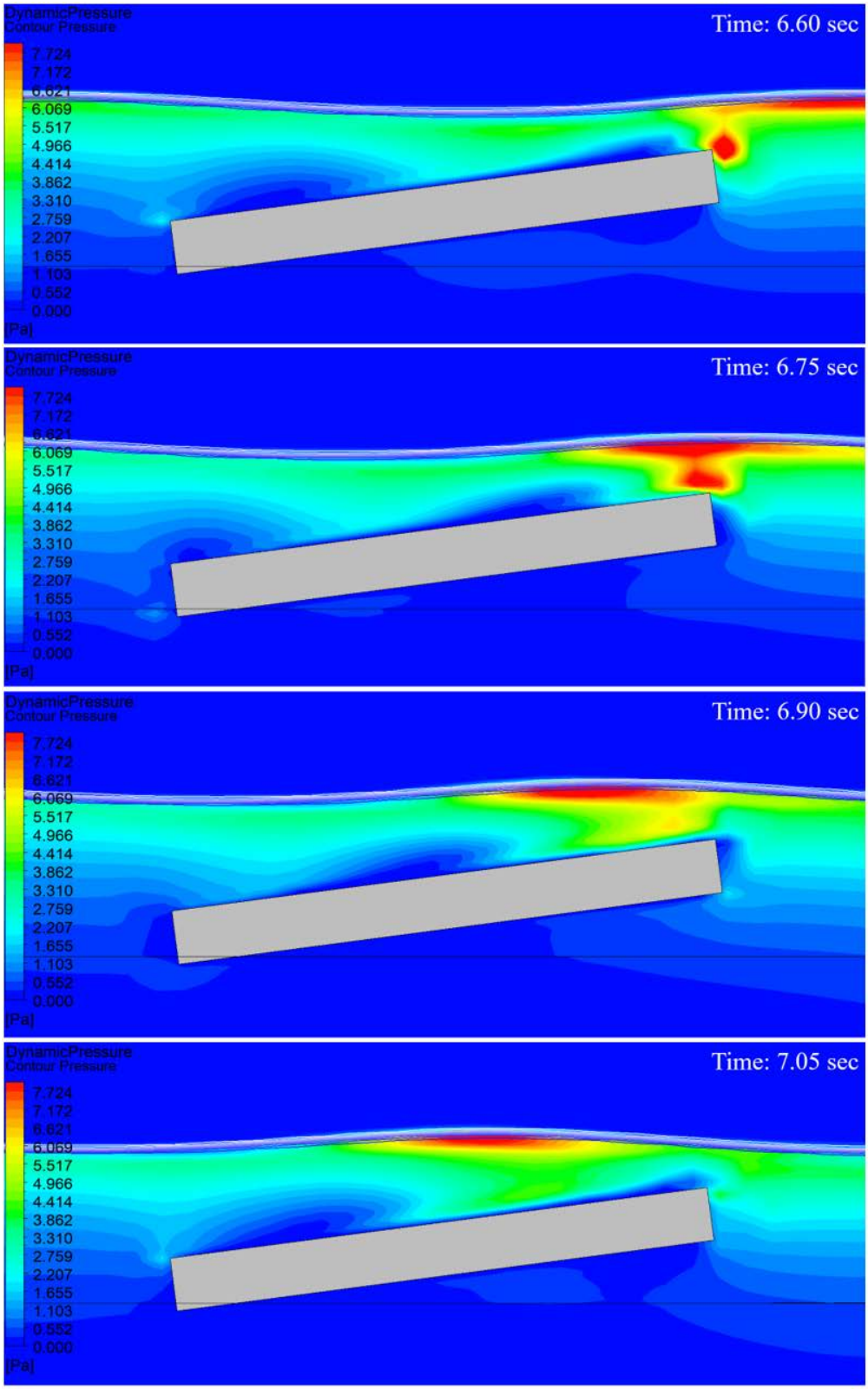

Figure 63. Transient dynamic pressure contours for immersed solid model with 7.5° up angle (6.60 – 7.05 sec)

The final comparison is to assess the impact on the submerged body using the non-dimensionalized drag force, lift force, and moment. The graphs of these values from the 7.5° up angled rigid body and immersed solid models as well as the horizontal rigid body and immersed solid models are shown in Figure 64, Figure 65, and Figure 66.

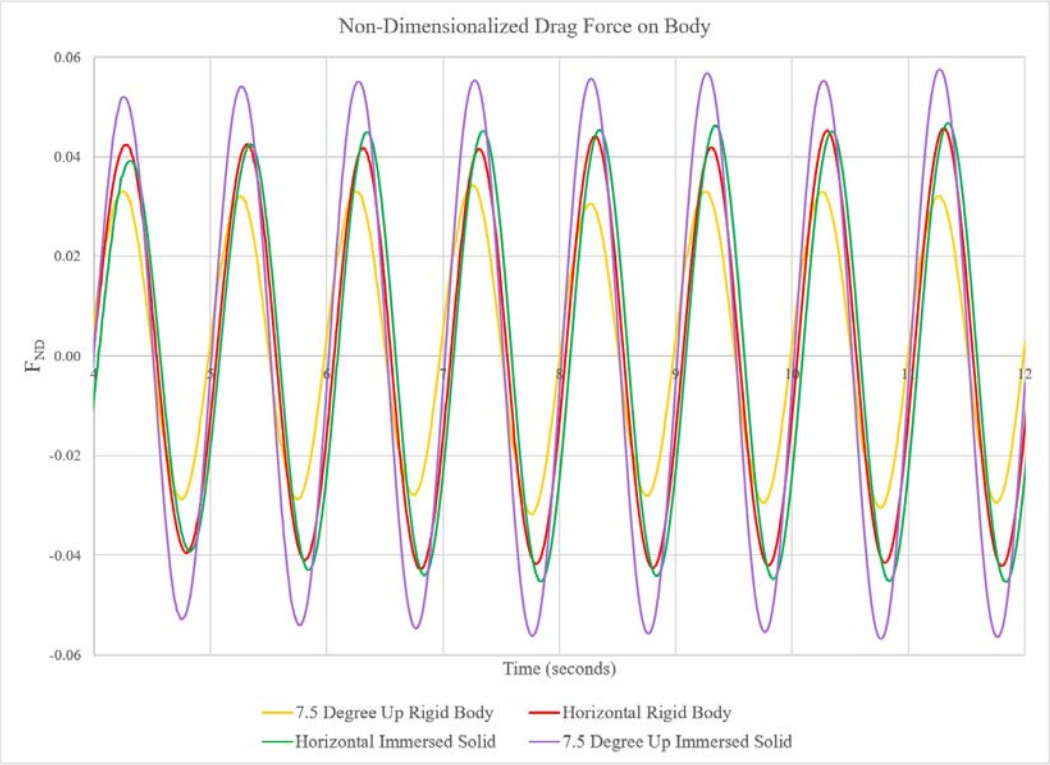

Figure 64. Non-dimensionalized drag force comparison for body with 7.5° up angle

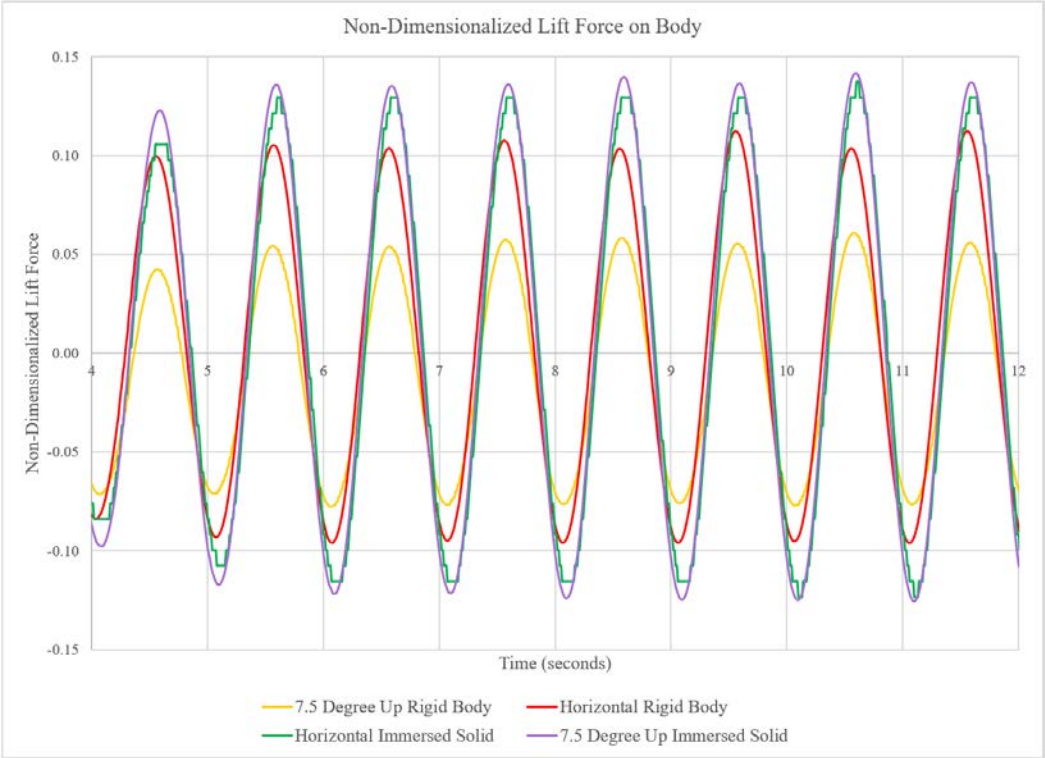

Figure 65. Non-dimensionalized lift force comparison for body with 7.5° up angle

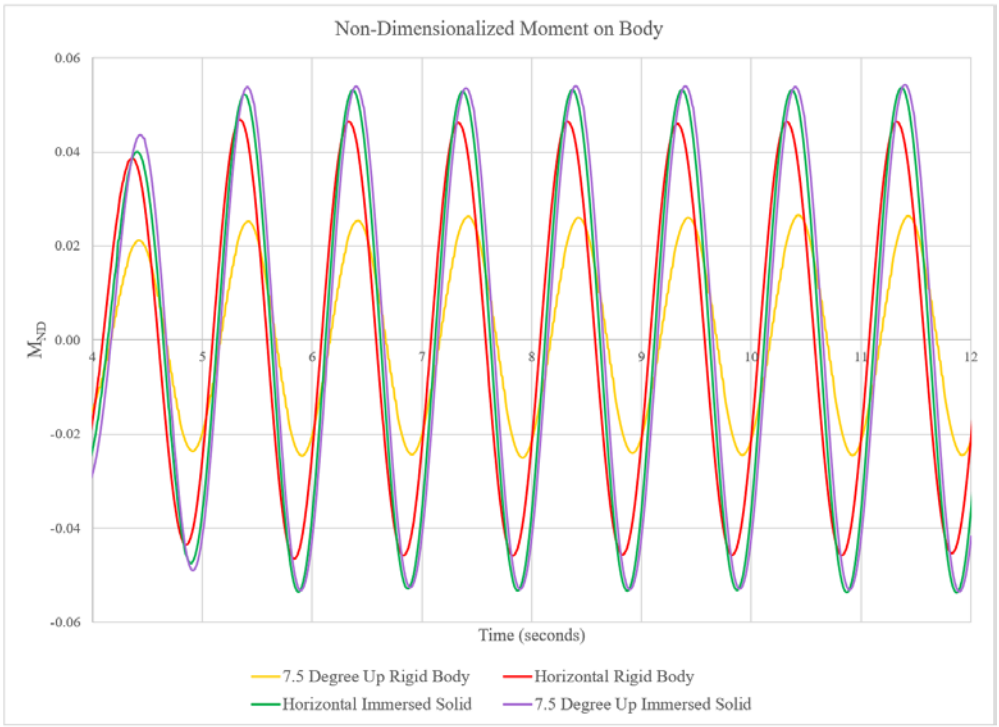

Figure 66. Non-dimensionalized moment comparison for body with 7.5° up angle

As already discussed, the rigid body model shows a decrease in body forces and moment when the body is angled as compared to the horizontal body. The immersed solid model actually shows a slight increase in body forces and moment when the body is angled. The reason for this discrepancy is due to the difference in wave energy dissipation between the rigid body model at 79.2%, and the immersed solid model at 39.8%. It is likely the different methods of modeling fluid-body interaction is what is causing this difference in energy dissipation despite the bodies being oriented in the same manner.

IV. CONCLUSIONS AND RECOMMENDATION

CFD modeling has the potential to decrease development costs by providing a mechanism to perform assessments and trade-off analyses without requiring significant physical experimentation. In order to support this, accurate FEA models must be developed. Additionally, it would be beneficial for the models to be simple to modify and be small enough to support quick runtimes while maintaining fidelity to provide realistic results.

In support of these goals, a model of the NPS tow tank with wave generation and a submerged body was created in commercial CFD software, ANSYS CFX. The goal was to determine if a different method of modeling the submerged body could result in improved ease of modification while maintaining accurate results. The two methods of body formation investigated were the rigid body method and the immersed solid method. The rigid body method has been used in the past with accurate results; however, the immersed solid method is much easier to modify by the user.

The comparison of the two different methods of body modeling showed different results depending on the situation. When the case being modeled had less higher energy fluid to body interaction, as was the case in the horizontal model at a lower position, the rigid body model and the immersed solid model produced similar results for velocities and forces and moment on the body. However, when the environment being modeled resulted in higher energy fluid to body interaction, as was the case with the horizontal model at a higher position and the angled models, the velocity, dynamic pressure, and body forces and moment produced by the two models was significantly different.

An analysis of the transient behavior between the two models shows that in the rigid body model, the fluid is interacting with the body occasionally resulting in flow reversal that significantly impacts velocity and dynamic pressure distribution along the body. The methodology of the immersed solid model does not allow this fluid body interaction. Instead, the immersed solid forces the fluid that touches the solid to be at the same velocity as the solid. The difference in modeling results in smoother velocity vectors

with no localized flow reversals from fluid-body interactions. With different velocity profiles and dynamic pressure contours, the body forces and moment between the two models will also be different.

Although the difference in behavior between the two modeling techniques can be explained, the accuracy of a CFD model using immersed solid body formation methodology is undetermined. As this method of CFD modeling within ANSYS has the potential to increase the speed and ease with which changes are made to body within the model, additional efforts should be made to assess and improve the accuracy of this modeling method. Additionally, more work should be performed to refine the delineation of choice between the two modeling methods within the field of submerged body modeling, as both may be better suited for specific situations.

LIST OF REFERENCES

[1] D. Arthur, F. M. Woodward, and Congressional Budget Office, "Long-term implications of the 2019 future years defense program," Washington, DC, USA, 2019. [Online.] Available: www.cbo.gov/publication/54948

[2] B. Phillips, S. Apgar, L. Levin, T. Koch, T. Cianciolo, and Defense Business Board, "Best practices for the business of test and evaluation," Washington, DC, USA, DBB Report No. DBB FY17-01, 2016. [Online.] Available: dbb.defense.gov/Portals/35/Documents/Reports/2017/DBB%2017-01%20Test%20%20&%20Evaluation%20Study%20(Complete)%20Final%20v2.pdf

[3] B. N. Mandal and S. De, *Water Wave Scattering*. Hoboken, NJ, USA: CRC Press, 2015.

[4] A. Constantin, "The trajectories of particles in Stokes waves," *Inventiones mathematicae*, vol. 166, no. 3, pp. 523–535, Dec. 2006.

[5] W. Finnegan and J. Goggins, "Numerical simulation of linear water waves and wave–structure interaction," *Ocean Engineering*, vol. 43, no. C, pp. 23–31, Apr. 2012.

[6] D. Prasad, M. Ahmed, Y. Lee, and R. Sharma, "Validation of a piston type wave-maker using numerical wave tank," *Ocean Engineering*, vol. 131, pp. 57–67, Feb. 2017.

[7] S. H. Bolstad, "Hydrodynamic response of a composite structure in an Arctic environment," Master's thesis, Dept. of Mechanical and Aerospace Engineering, NPS, Monterey, CA, USA, 2015. [Online.] Available: http://hdl.handle.net/10945/45817

[8] R. M. Tran, "Evaluation of composite-hull ships operating in Arctic ice," Master's thesis, Dept. of Mechanical and Aerospace Engineering, NPS, Monterey, CA, USA, 2016. [Online.] Available: http://hdl.handle.net/10945/49404

[9] A. R. Whitmer, "Predicting wave-induced loads in complex seaways on shallowly submerged vessels," Master's thesis, Dept. of Systems Engineering, NPS, Monterey, CA, USA, 2018. [Online.] Available: http://hdl.handle.net/10945/59622

[10] L. M. Jones, "Development of a numerical tow tank with wave generation to supplement experimental efforts," Master's thesis, Dept. of Mechanical and Aerospace Engineering, NPS, Monterey, CA, USA, 2017. [Online.] Available: http://hdl.handle.net/10945/56736

[11] L. M. Jones, J. T. Klamo, Y. W. Kwon, and J. M. Didoszak, “Numerical and experimental study of wave-induced load effects on a submerged body near the surface.” *Proceedings of the ASME 2018 37th International Conference on Ocean, Offshore and Arctic Engineering. Volume 7B: Ocean Engineering*, 2018. [Online.] doi: 10.1115/OMAE2018-77624

[12] A. R. Whitmer, J. T. Klamo, and Y. W. Kwon, “On the Validity of Predicting Wave-induced Loads on a Submerged Body Using the Superposition of Regular Wave Results,” in *OCEANS 2019 MTS/IEEE SEATTLE*, 2019, pp. 1–11.

[13] T. M. Turner, “Analyzing UUV hull cross-sections for minimizing wave loads when operating near surface,” Master’s thesis, Dept. of Systems Engineering, NPS, Monterey, CA, USA, 2018. [Online.] Available: http://hdl.handle.net/10945/59606

[14] T. M. Turner, J. T. Klamo, and Y. W. Kwon, “Comparison of wave-induced loads on a near surface slender body from inviscid flow linear solution and an experimental modal test.” *Proceedings of the ASME 2018 37th International Conference on Ocean, Offshore and Arctic Engineering. Volume 7A: Ocean Engineering*, 2018. [Online.] doi: 10.1115/OMAE2018-77760

[15] K. Suriben, “Study of wave-induced load effects on a submerged body near the surface,” Master’s thesis, Dept. of Mechanical and Aerospace Engineering, NPS, Monterey, CA, USA, 2019. [Online.] Available: http://hdl.handle.net/10945/62748

INITIAL DISTRIBUTION LIST

1. Defense Technical Information Center
   Ft. Belvoir, Virginia

2. Dudley Knox Library
   Naval Postgraduate School
   Monterey, California